Fundamental and Applied Studies using *de novo* peptide inhibitor targeting gliding motility of *Plasmodium falciparum*

Thesis submitted to Jawaharlal Nehru University

for the award of the degree of

DOCTOR OF PHILOSOPHY

ZILL-E-ANAM

SPECIAL CENTRE FOR MOLECULAR MEDICINE

JAWAHARLAL NEHRU UNIVERSITY

NEW DELHI

2020

SPECIAL CENTRE FOR MOLECULAR MEDICINE
JAWAHARLAL NEHRU UNIVERSITY
NEW DELHI – 110067, INDIA

CERTIFICATE

The research work in this thesis entitled **"Fundamental and Applied Studies using *de novo* peptide inhibitor targeting gliding motility of *Plasmodium falciparum*"** has been carried out by Ms. Zill-e-Anam under my guidance at the Special Centre for Molecular Medicine, Jawaharlal Nehru University, New Delhi, India. The work presented here is original and has not been submitted in part or full for any other degree or diploma of any university/institution elsewhere.

Z. Anam

Zill-e-Anam
(Candidate)

Prof. Anand Ranganathan
(Supervisor)

Date: 28/12/2020

Prof. Suman K. Dhar
(Chairperson)

To Ammijaan, from whose womb the writing started

and Abbajaan, whose chai shots brought me here

ACKNOWLEDGEMENTS

As I write this thesis, it is my pleasure to express my gratitude to the following individuals and organisations for making me the human being I am today. Some have contributed towards this directly, others indirectly; in small and big ways; instantly or consistently; some within the time-frame of this doctoral study while others' much beyond. Whatever way it might be, each one has left and continues to leave an impression of themselves on me. I am grateful -

To my primary teacher Mr. **Shadab Siddiqui**, for instilling me with curiosity and happiness for doing Mathematics and Sciences.

To Prof. **Gobardhan Das**, I'm indebted for directing me to this lab (even though I knew nothing of it), and helping me make the best decision for myself.

To Prof. **Anand Ranganathan,** I realise that my learning and development under your mentorship has been much broader than just the boundary of the lab. If I was to start summing them up, I would end up writing another huge document! In the interest of this thesis, I would just say it has been one of my biggest privileges to be a part of this lab. Thank you for taking the gamble!

To Dr. **Shailja Singh** for never saying no to anything, always emitting passion for the work we did, and being a go-getter. It helped me stay motivated during tough times.

To Prof. **Suman K. Dhar** for teaching me the first lessons after being admitted to PhD and constantly being a source of inspiration (even though I was not directly supervised by you), as I crossed you in the corridors.

To Prof. **Vibha** for wishing me back good morning/afternoon. I have shamelessly wished you. The response made my day, always.

To all other SCMM faculty members (Prof. **Rakesh**, Prof. **Chimay**, Dr. **Souvik**, Dr. **Saima** and Dr. **Dipankar**) for having the doors of your labs open for scientific discussions.

To Dr. **Neha** for saving me from mental breakdowns, sharing experiences, giving re-assurances and correcting the manuscript draft avoiding me from faux-paus!

To Dr. **Bhumika** for being by my side when I felt I was all alone, listening to me and sharing insights.

To **Satarupa** for all the drives – long and short, uncountable chats, laughs and lab blurbs.

To Dr. **Jhalak** for teaching me organisational and time management skills.

To Dr. **Pooja** for her sense of humour and the power of perspectives.

To Dr. **Amandeep** for her sincerity and deep desire to learn and re-learn.

To **Ayushi** for her diligence and persistence. You saved me from uncountable blunders.

To Mr. **Sushil** for his resentment and warmth.

To Dr. **Prem** for teaching the easiest and most logical scientific practices.

To Dr. **Niharika** for her relaxed and chilled out attitude.

To **Shikha** for her questions, answers and silences.

To **Manisha** for all the midnight walks and hostel room chats.

To **Mukesh** for his curiosity.

To **Pallavi** for her politeness.

To **Ajay** who devotedly provided all the glassware and plastic ware before experiments.

To SCMM office staff (Mr. **Nandkumar**, Ms. **Niti**, Ms. **Daya**, Ms. **Priyanshu,** Mr. **Naresh**) for patiently helping with the administrative work.

To all **SCMM colleagues** for shedding utmost kindness; be it to allow me use centrifuge before you, without booking; sharing salts and last moment autoclaved glassware; softwares; teaching how to use them or instruments, or just exchanging a smile as we walked pass by each other in the corridors. Being in here around you made life and experiments easier.

To **University Grants Commission,** for providing bread n butter and helping fund this research.

To **Jawaharlal Nehru University**, for being my academic home for the past seven years.

To **IndiaBioscience** (Dr. **Smita**, Dr. **Shreya**, Dr. **Shantala**) for mentoring out of lab, helping me learn to communicate effectively and showing me the multi-disciplinary nature of this degree.

To **Science Policy Forum** (Dr. **Chagun**, Dr. **Nimita**, Dr. **Aditya**, Dr. **Suryesh**, Dr. **Jenice**, Dr. **Divya**) for making lockdown much more than thesis writing, breaking me out of my science silo, and opening up my mind to Science Policy.

To Dr. **Karishma** for being a gushing fountain of enthusiasm and helping me understand the scope and hope of talking to your favourite scientists.

To **Sudesh,** for taking me off to travel trips, they filled me with fascination and re-filled me with energy to carry out experiments when I returned back to lab.

To **Anuradha** for all the chai-time terrace exchanges; and Science, Education and SciEd discussions.

To Dr. **Jaishree** and **Paksh** for being my emotional warehouse and backup during free fall.

To Dr. **Sunita** for always keeping her stethoscope ready when my heart beat went up or down.

To **Sumaiya** for being by my side for the past 25 years.

To **Nawaz** for dragging me out of the lab for a bit and being my best thereafter.

To my sister, **Aakriti**, my weekends are bright because of you.

To my better-bitter half, **Sapna** mom for helping me be in shape.

To my **extended family** making me the social bee.

To my brothers, **Ansab** and **Yashab,** for being the most annoying yet supportive siblings.

To my parents, Dr. **Zill-e-Huma** and Dr. **Shahid Husain** for having me.

And to innumerable others' whom my forgetful brain fails to capture!

Zill-e-anam

CONTENTS

FIGURES AND TABLES

List of Figures

List of Tables

ABBREVIATIONS

RBC	Red Blood Cell
Pf	*Plasmodium falciparum*
IMC	Inner Membrane Complex
PV	Parasitophorous Vacuole
ART	Artemisinin
ACT	Artemisinin-based Combination Therapy
MyoA	Myosin A (tail)
MTIP	Myosin A Tail Interacting Protein
PPI	Protein-protein interaction
RT	Room temperature
pI	Isoelectric point
GRAVY	Grand average of hydropathy
bp	base pair
rpm	revolutions per minute
DDW	double distilled water
kb	kilo - base pair
µl	micro-litre
ng	nanogram
mg	milligram
mol	mole
mM	milli-molar
nM	Nanomolar
kcal	kilocalorie
mm^2	milli-meter squared
µM	micro-molar
sec	seconds
min	minutes
M	Molar
N	Normal
kDa	kilo Dalton
PCR	Polymerase Chain Reaction

For	Forward primer
Rev	Reverse primer
LB	Luria-bertani Broth
LA	Luria-bertani Agar
E.coli	*Escherichia coli*
PBS	Phosphate-buffered saline
PBST	Phosphate-buffered saline with tween
PIC	Protease Inhibitor Cocktail
PMSF	Phenylmethylsufonyl floride
SDS	Sodium dodecyl sulphate
PAGE	Polyacrylamide gel electrophoresis
BSA	Bovine serum albumin
IPTG	Isopropyl-β-D-thiogalactopyranoside
Ni-NTA	Nickel-Nitrolotriacetic acid
ESAT-6	Early secretory antigen target – 6 kDa
CFP-10	Culture filtrate protein – 10 kDa
X-gal	5-bromo-4-chloro-3-indolyl-β-D-galactopyranoside
ITC	Isothermal Titration Calorimetry
T	Temperature
ΔH	Enthalpy change
ΔS	Entropy change
K_d	Dissociation constant
K_a	Association constant
N	Stoichiometry
ELISA	Enzyme-linked Immunosorbent Assay
Anti-His	Antibody recognising 6X histidine tag
OD_{450}	Optical density measured at 450 nm
HRP	Horseradish Peroxidase
SPR	Surface Plasmon Resonance

INTRODUCTION

1 INTRODUCTION

1.1 Origin and history of malaria

The origins of malaria date back to the origins of human civilization, with its first impressions found in ancient Chinese medical records of Nei Ching dating back to 2700 B.C. Soon after, the disease got its name from Hippocrates' theory describing evaporating swamps as the causative agents due to 'bad air' or *mal aria* in 4th century B. C. [1].

The Indian Sanskrit text *Sushruta Samitha* has a mention of malaria dating back to 6th century B.C. [2]. India occupies a pivotal position in early malaria studies. Ronald Ross became the front runner in understanding the biology behind malaria while he was posted in Secunderabad in India. Ronald explained the role of vector Anopheles in malaria transmission (Figure 1.1). Thereafter, Charles Louis observed the parasites in the RBCs of infected patients for the first time in the 1880s.

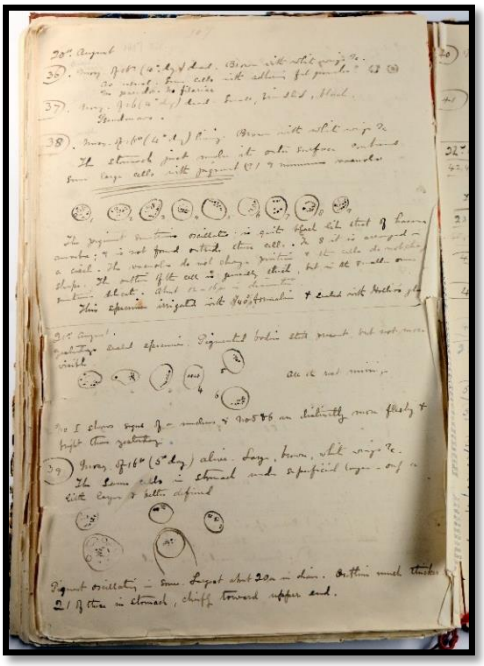

Figure 1.1: Image of the page from Ronald Ross's notebook where he describes the mosquito to be the culprit of malaria transmission, on August 20 1897 (London School of Hygiene and Tropical Medicine).

The ancient history of malaria, leading to a huge economic and mortality burden has kept malaria based research aimed at improving diagnosis, surveillance, and elimination at the forefront for decades. The result of which has been the award of five Nobel prizes in malaria related areas to date. (Table 1.1).

S. No.	Laureate	Year of award	Awarded for
1	Ronald Ross	1902	Discovery and role of mosquitoes in malaria
2	Charles Louis Alphonse Laveran	1907	Role of protozoa in malaria
3	Julieus Wagner-Juaregg	1927	Therapeutic value and use of malaria inoculation for dementia paralytica
4	Paul Mueller	1947	Discovery of dicholorodiphenyltricholoroethane (DDT)
5	Youyou Tu	2015	Isolating active compound artemisnin from *Artemisia annua*

Table 1.1: List of malaria related Nobel Prizes

1.2 Current status of malaria

Concerted efforts in malaria research have resulted in a steady decline of malaria incidence and mortality rates starting from the 1990s up until 2015, after which the

decline rates have reduced drastically [3,4]. This is a serious cause of concern because increased incidence can revert years of hard work and progress made in malaria elimination.

As per the latest figures for 2019, malaria incidence is 228 million and 405000 deaths worldwide [3]. The endemic regions remain Africa, South-East Asia, and Eastern Mediterranean region with pregnant women and children being in the high-risk group (Figure 1.2). WHO has warned, that if malaria elimination is not paid enough attention, the 2025 milestone and 2030 elimination goal will be a distant dream [3].

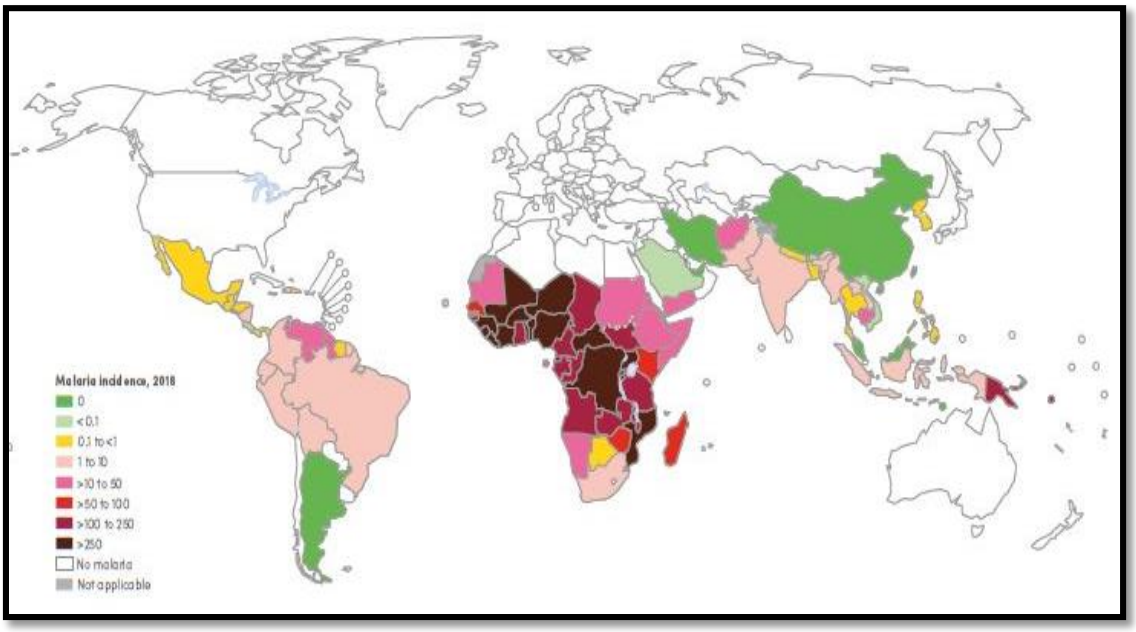

Figure 1.2: Country wise incidence of malaria (per 1000 population) (Adapted from WHO World Malaria Report 2019) [3].

To add to this, there are reports from South East Asia [5] – India [6], Myanmar, Cambodia [7,8], Vietnam, Thailand [9] and some African countries [5] identifying mutations and delayed parasite clearance resulting in resistance against first line drugs namely; Artemisinin, Artemisinin Combined Therapies (ACT), Mefloquine and Lumefantrine. The primary mutations identified in ACT resistant parasites are in Kelch13 propeller region [9] among other point mutations leading to parasite non-

responsiveness. Novel approaches for combating drug resistant parasites that are under development use RNAi, nanotechnology and stem cells [10]. Apart from this, antimalarial peptides extracted from naturally occurring sources or chemically synthesised show huge chemotherapeutic potential.

1.3 Parasite biology

The parasite harbours triple genomes: nuclear, mitochondrial and apicoplast genomes [11] that collectively help in disease pathogenesis and survival.

Six *Plasmodium* species are human invasive: *P.ovale curtisi, P.ovale wallikeri, P.malariae, P.knowlesi, P.vivax, P.falciparum.* Of these, *Pf* and *Pv* are the most common and deadly at the same time [12]. *Pf* is unique among all *Plasmodium* species in removing RBCs from blood circulation for nearly half of the asexual cycle. It does so by promoting adhesive phenotype that sticks RBCs to the endothelium. *Pv* on the other hand, is uniquely reticulocyte infecting [12].

Phylum	Apicomplexa
Class	Aconoidasida
Order	Haemosporida
Family	Plasmodiidae
Genus	*Plasmodium*
Species	*P. falciparum*

Table 1.2: Taxonomy and Classification

1.4 Life-cycle of *Plasmodium*

The 48 hour life-cycle of *Plasmodium* results in more than ten different morphological states [12] within two-highly species-specific hosts: the female Anopheles and humans. Two blood meals with fever and chills is the essence of *Plasmodium's* life-span.

At one end, it commences with setting of the migratory mode of the parasite 'on' when *Plasmodium* sporozoites are injected in dermis and parasite transversal happens in order to find a suitable hepatocyte and transitioning to the invasive mode. Invasion in the hepatocyte is assisted by CSP (Circumsporozoites Protein) that covers the sporozoite as a dense coat, and HSPG (Heparin Sulphate Proteoglycans) binding and is a silent feature of the disease with no symptoms [13]. CSP binds hepatocytes through a repeated sequence and Type I Thrombospondin Repeat (TSR). For invasion to occur in hepatocytes, the TSR domain of CSP is exposed by HSPGs cleaving their N-terminal domain thereby activating CSP [14]. The hepatocytes house parasites for 2-10 days, this stage is called the exo-erythrocytic form. The liver stage culminates through the release of tens to thousands of daughter merozoites in the vasculature ready to find their next house in erythrocytes. The clinically silent disease, upsurges with symptoms showing up in the erythrocytic stages (Figure 1.3). The blood or the erythrocytic stage of the parasite life-cycle is also fatal and shows extreme disease pathology.

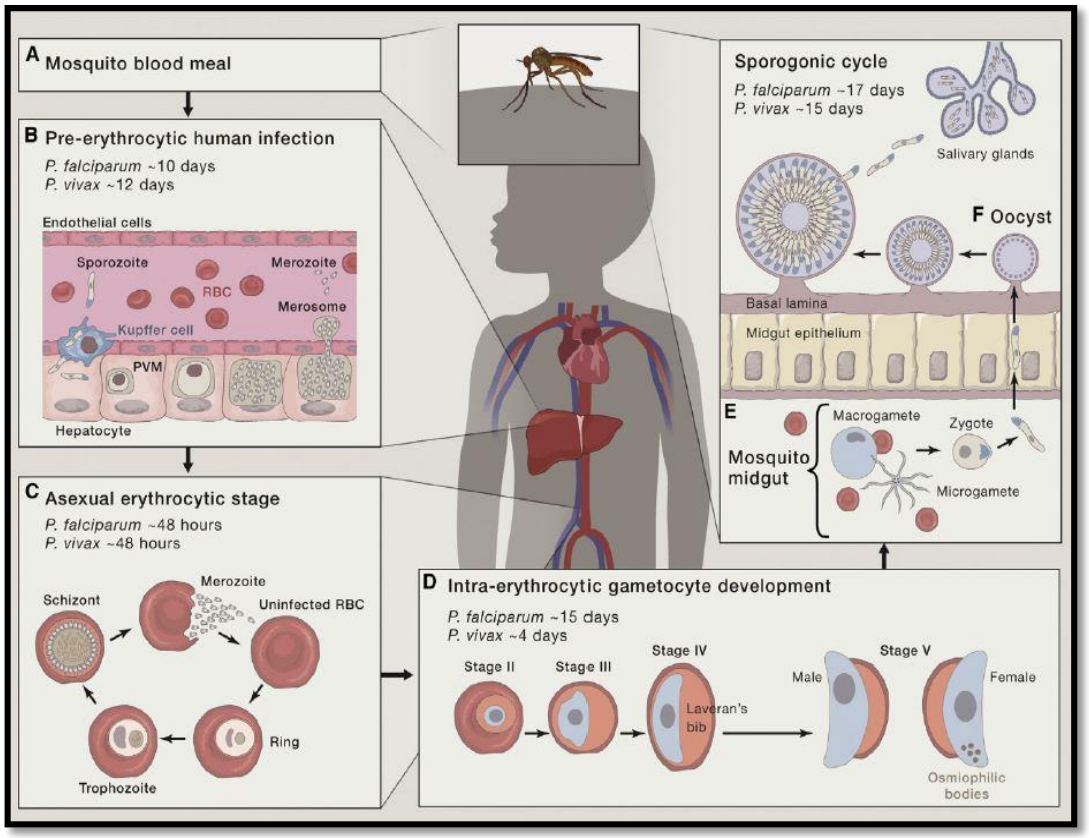

Figure 1.3: Life-cycle of *Plasmodium* (Adapted from Cowman et al., 2016) [15].

1.5 *Plasmodium* invasion machinery

1.5.1 Glideosome and its components

The erythrocytic cycle of *P. falciparum* is a muti-step coordinated event occurring over a short time frame of 2 minutes [15]. The junctures include pre-invasion, post-invasion and echinocytosis (Figure 1.4).

The first encounter of merozoite with erythrocyte is called pre-invasion. At the molecular level, there are grey areas surrounding this step. Some players like MSP1 (Merozoite Surface Protein) are known to act as a stage on which large complex formation occurs [16]. Pre-invasion results in actinomysin motor driving erythrocyte deformation [17]. The rise in calcium levels leads to the release of proteins in membrane-bound microneme namely, EBL. *Pf*EBL, *Pf*Rh proteins are responsible for

the initiation of signalling cascade for invasion, specifically through EBA-175. Following EBA-175-Glycophorin A interaction, calcium levels decline, triggering Rhoptry release [18]. Microneme and Rhoptry release are sequential steps and cannot be reversed.

The deformation of RBC also runs parallel with Rh5-Basigin interaction [15,19] and apical reorientation of merozoite. This leads to a lasting and an irreversible interaction between host RBC and the parasite. This step is also mediated by parasite AMAI-RON2 interaction that sets the stage for propeller motion by forming a moving junction complex. The moving junction is universally conserved along with the mechanism of invasion in all Apicomplexan parasites despite different host cell types[20].

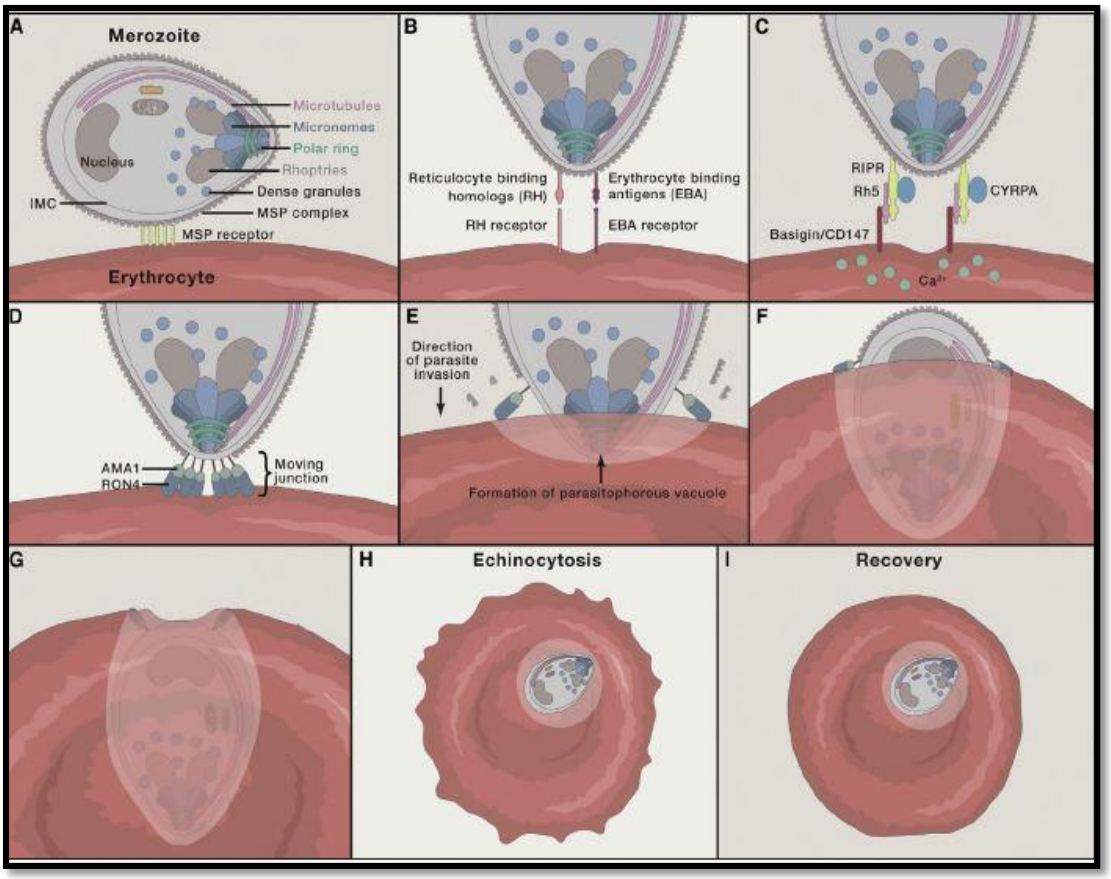

Figure 1.4: Molecular events surrounding merozoite invasion in host RBC (Adapted from Cowman et al., 2016) [15].

Eventually, the post-invasion cascade follows during which the parasite penetrates in the RBC directed by the force that is generated by its actinomysin motor. The actinomysin motor is present in the inner membrane complex (IMC). As the parasite moves on the RBC, the membrane behind is sealed, leading the parasite in the parasitophorous vacuole (PV) within RBC. A result of this invasion is the formation of a safe room PV for the parasite where it resides hidden from the host immune system and attacking compartments like the lysosome. The parasite is also able to replicate unimpeded in the PV forming daughter merozoites ready to transmit the infection exponentially wherein again actinomyosin system helps in motility [21]. The housing of *Plasmodium* in a null-organelle cell requires a myriad of proteins to be exported out on the cell surface and exhibit antigenic variation. *Pf*EMP1 is the well-characterised set of proteins along with var genes that enable chronic *Plasmodium* infection [15].

The transmission of the parasite is ensured by the development of gametocytes from some of the merozoites that are released when RBC bursts open. This fraction gets committed to gametogenesis. The gametes are taken up by the Anopheles in the blood meal that completes the life-cycle. The other fraction contributes to progression in human host as naïve uninfected RBCs are infected and parasites rise exponentially in number.

1.5.2 Molecular players of invasion machinery

Apicomplexan parasites namely *Plasmodium* and *Toxoplasma* lack locomotive structures like flagella, cilia, and pseudopodia. Still, the movement remains one of the most integral and crucial activities in the parasite life-cycle. Movement of parasites in these organisms is termed as ‘gliding motility’ which typically denotes no change in

the shape of the parasite while moving [22]. This function is enabled with the help of a multi-layered and multi-complex structure called 'glideosome' (Figure 1.5). Apart from crossing biologically impermeable surfaces (migration), glideosome also helps in Apicomplexan entry (invasion) and exit (egress) [23]. The importance and relation between gliding motility and infectivity by the parasite is directly related. The glideosome allows substrate-dependent motility of the parasite thereby directly contributing to its virulence. The structure underlines the parasite plasma membrane within the triple later membranous structure called the inner membrane complex. IMC is triple-layered in vesicular sacs, flattened one above the other. The IMC is connected to microtubular proteins through a network of alveolin that are filamentous proteins [22]. This network apart from a role in motility and invasion, aids in maintaining the overall structure of the parasite.

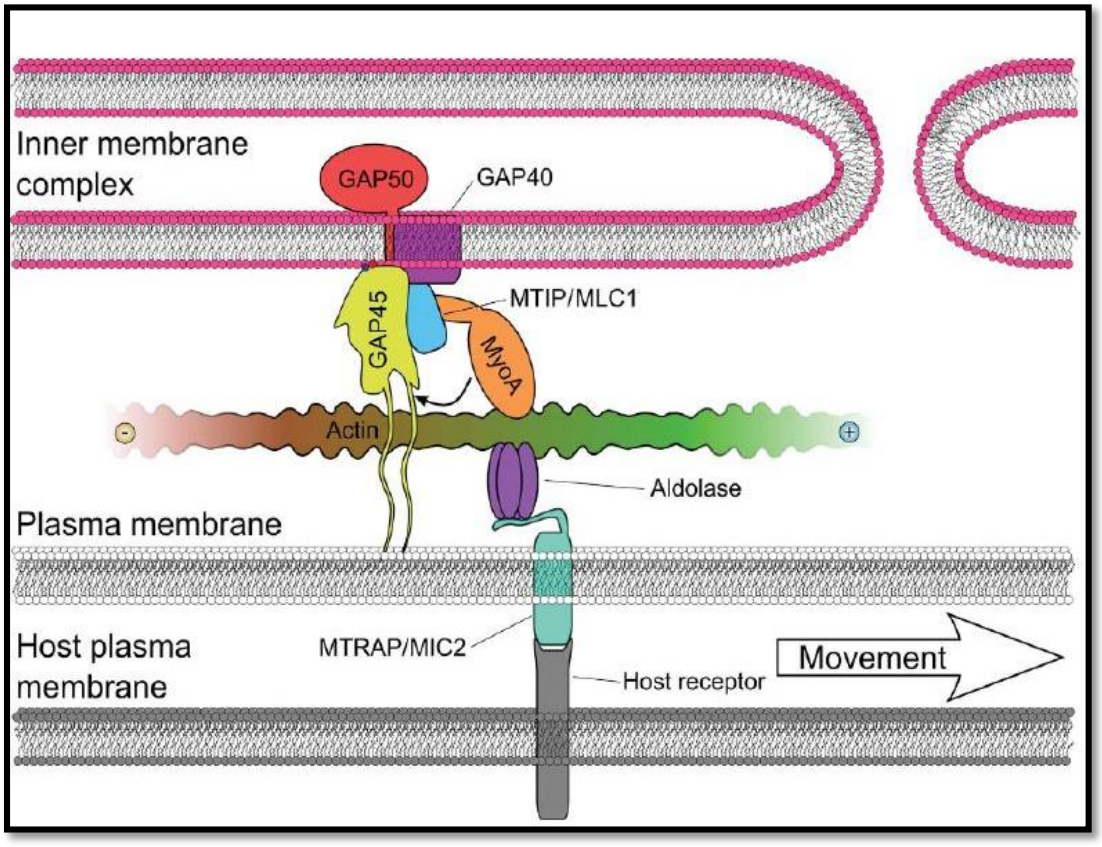

Figure 1.5: Model for *Plasmodium* invasion machinery/glideosome (Adapted from Kumpula et al., 2015) [23].

The *P. falciparum* invasion is governed by energy transmission within the parasite that allows the concerted action of all the proteins in glideosome. The invasion machinery or glideosome comprises three categories of proteins: motor–receptor bridging proteins, motor complex proteins, and IMC proteins. The following table lists the individual proteins in each category and highlights their specific role.

Category	Protein	Function
Motor-receptor bridging proteins	Aldolase	At one end binds actin, at the other binds TRAP [23,24].
	GAPDH	Binds Rhoptry proteins, crystal structure not known.
Motor-complex proteins	Actin	Forms a linear repeated track via polymerization on which myosin walks [23]
	Myosin A	Central force generating component of glideosome. Myosin A pulls actin filament back and forth generating mechanochemical force using ATP. Myosin is found majorly on periphery towards apical end of the parasite [25]. Myosin is a stationary motor that swings its lever arm on F-actin.
	MTIP	Allows anchorage of Myosin A to IMC through direct interaction in a charge dependent manner, first one of the light chain.

	ELC	Second light chain that binds Myosin A upstream to where MTIP/MLC binds [26,27].
IMC proteins	GAP 40	Possess nine trans-membrane domains, hence may act as anchor [25].
	GAP 45	Post translationally modified: palmitoylated, myristoylated, and phosphorylated helping in plasma membrane anchorage and localization. GAP 45 forms a pre-complex with MTIP- Myosin A [24,28].
	GAP 50	IMC bound, interacts with GAP 45 [24].

Name	**Protein**	**Function**
Adhesins: extracellular membrane receptors of parasites that enable specificity in host.	TRAP	Interacts with Aldolase in a charge dependent manner by linking intracellular motor to extracellular substrates [24,29].
	AMA	Binds to RON that is secreted from Rhoptries of the parasite and goes on host cell surface to bind AMA [30].

Table 1.3: Components and function of glideosome proteins

1.5.3 Structural features of Myosin A and its light chains

P. falciparum possess in all six myosins (*Pf*Myosin A- *Pf*Myosin F)[31], of which Myosin A is the most crucial and central to parasite biological processes. Myosin B is the second of the two-class XIV myosins known in *Plasmodium* species. Despite sharing structural similarity with Myosin A, Myosin B is distinct in its sub-cellular localization, function, and interacting partners. It is found in all invasive stages of *Plasmodium* but is not a member of glideosome complex [32]. Myosin B interacts with Myosin light chain that is distinct from MTIP. Further studies are needed to shed light on this unconventional myosin.

Among Apicomplexans, Myosin A was first discovered in *P. falciparum* [33]. A motor protein found to be majorly present in schizonts and merozoites, the direct role of Myosin A was first discovered in *Toxoplasma gondii* through conditional gene knockout studies that showed decreased parasite invasive capacity [34]. In *Plasmodium* gene knockout studies of Myosin A have been performed recently [35] thus confirming the direct role and molecular mechanism underlying the force generation during parasite movement. Myosin A belongs to an atypical class of myosins (XIV) that are present only in Apicomplexans. Class XIV has an unusually short tail and neck, lacks the typically conserved residues found in all myosins and the conserved IQ motifs required for anchorage to regulatory chains are also absent [36]. Structurally, Myosin A is composed of a motor domain and light chain binding domain. The motor domain is composed of 4 sub-motor- domains connected through short stretches called connectors.

As part of the interactive and assisting proteins, Myosin A interacts with two known light chains: Essential Light Chain (ELC) and Myosin A Tail Interacting Protein (MTIP).

ELC binds to Myosin A at the neck region, at the site adjacent to MTIP binding site on Myosin A [26]. Functionally, ELC has been shown to induce secondary structural changes in Myosin A. ELC binds to calcium and may be important for regulation of the complex through calcium [26,27]. ELC has also been shown to be essential for invasion [37], thus acting as a potential drug target.

MTIP was identified in *P.yeolli* as the MyoA interacting partner via yeast two-hybrid studies [38] and was found to be localised with MyoA. In the same study, through deletion analysis and β-galactosidase activity assay it was found that only the neck domain of Myosin A is involved in the interaction. Co-localisation assays using Myosin A and MTIP specific antibodies also confirmed that the two proteins interact. Further studies revealed the secondary structure of MTIP as an alpha-helical protein [39]. MTIP expression is also tightly regulated in all invasive stages and during host to vector transition. MTIP's localization may be HSP20 dependent in the *P.bergei* model [40]. The following section highlights the interaction dynamicity of MyoA and MTIP.

1.5.4 Myosin A-MTIP interaction dynamicity

The interaction between MyoA and MTIP is through the C-terminal domain of MTIP (60 amino acids) making direct contact with 20 amino acid MyoA tail domain (799-818 residues) [41,42] through ionic and hydrophobic interactions. These interacting regions are also conserved across Apicomplexan species. The two partners associate with a high affinity; the dissociation constant 235 nM and the interaction has been shown to be independent of calcium ions [39]. Specifically, it is known that only the tail domain of MyoA is sufficient for the whole protein's interaction with MTIP (Figure 1.6). At MTIP's end, changes occur only in the C terminal, and N terminal

remains structurally unchanged and is not involved when the tail of MyoA fits in it [43,44].

MyoA-MTIP interaction is highly specific yet dynamic. For example, in *P. knowlesi* the interaction is susceptible to hydrogen ion concentrations, with a critical hydrogen bond between Aspartate (MyoA)-Histidine (MTIP) being formed at basic pH only [45,46]. Another crucial interaction occurs via salt bridge formation between Serine-108 (MTIP) with Aspartate-173 (MyoA) [46]. With reference to conformation, MTIP exists in three different conformations and MyoA exists as a complex only in one of these three conformations [46,47]. The MTIP Histidine should also be de-protonated for Myo A/MTIP compact structure formation. The above studies have together revealed the interaction dynamics between the two glideosome proteins. Given the crucial role of these proteins and their interaction, MyoA-MTIP interaction is a well-established drug target.

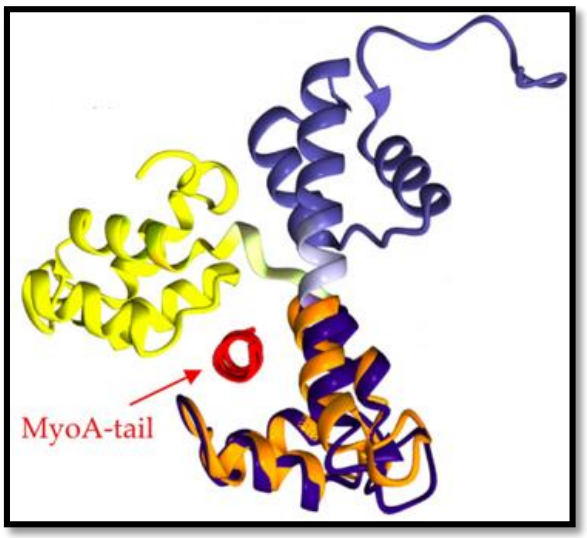

Figure 1.6: Interacting regions of Myosin A tail and MTIP (Adapted from Bosch et al., 2006) [46].

1.6 Antimalarial therapy

Antimalarials have been the most crucial weapon for treatment as well as inhibiting transmission through disrupting the life-cycle of *Plasmodium* since the 19th century. Starting from the first anti-malarial drug, Quinine isolated from the chinchona tree (Figure 1.7), malaria therapeutics has seen the discovery of potent antimalarials like chloroquine and artemisinin isolated from *Artemisia annua*.

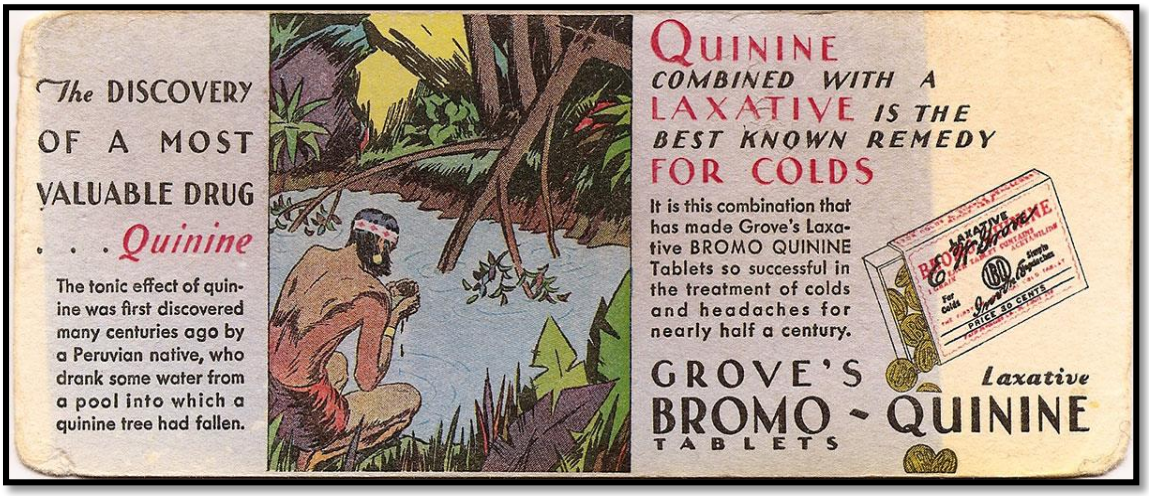

Figure 1.7: Advertising brochure depicting Quinine discovery (showing Pedro drinking from a pond that had Chinchona tree fallen, upon drinking, his fever subsided).

These drugs have been extensively used for treatment individually until they were observed to be redundant and ineffective for parasite clearance (mainly chloroquine, sulfadoxine, pyrimethamine) (Figure 1.8). Individual ineffectiveness led to the administration of a combination of antimalarials through ACT [15]. ACT combines a fast acting and a slow acting anti-malarial to ensure a greater barrier against resistance development ensuring complete parasite clearance. Administration of ACTs were highly effective in reducing disease burden and fastening elimination efforts up until 2015, after which studies directing towards ACT ineffectiveness has been on the rise. In the case of *Pv*, primaquine is the only effective drug.

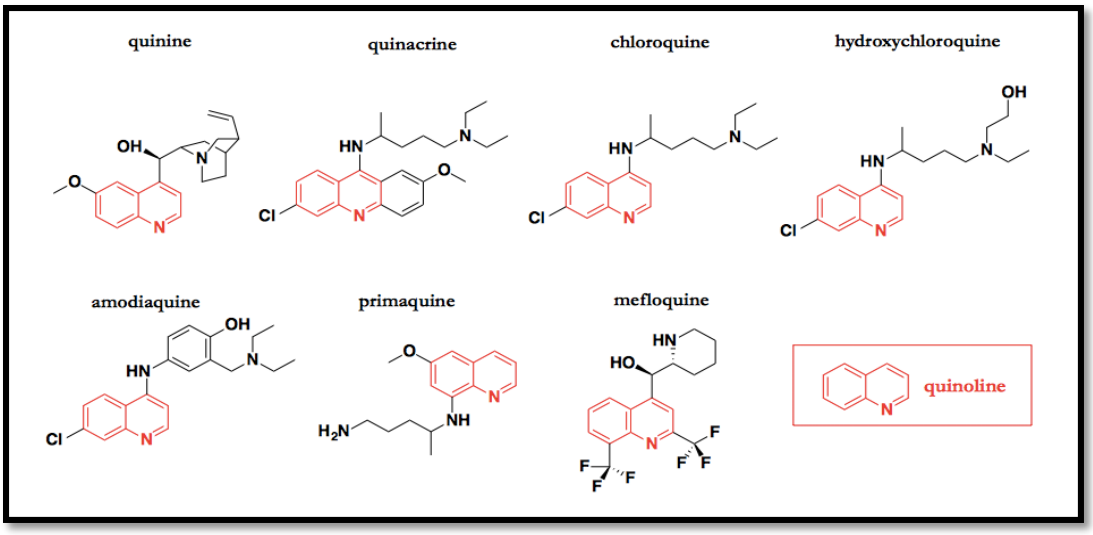

Figure 1.8: Antimalarial Quinolone and its derivatives.

1.7 Peptide based antimalarials

Anti-malarial peptides have been an area of active research since the early 1990s. Most known anti-plasmodial peptides are of natural origin – fungal [48–51], sponges [52], sea hare [53], and *Bacilli* [54]. Anti-plasmodial peptides most commonly act by membrane lysis, disturbance of parasite, and host cell homeostasis. Some known antimalarial peptides act by specifically blocking *P. falciparum* cysteine proteinase [55], histone deacetylase [48], mitochondrial bio-processes [49], actin stabilisation [56], tubulin-binding inhibition [53], interferon-gamma [57] through selective toxicity. On the other side, synthetic peptides are another class of anti-plasmodial peptides that offer the possibility of large-scale easy synthesis of parasite-specific therapeutics. Chemically synthesized amphipathic peptides have been shown to be active in the micro-molar range [52]. Chemically derived peptides from host RBC proteins like ankyrin have also shown to be potent in blocking *Plasmodium* egress [58]. Recently, the ability of peptide-based probes that interact with Myosin A with nM affinity has been shown [59]. Though not many anti-malarial peptides have been

unearthed, their potential of acting in a potent and specific manner remains huge. Altogether, peptide-based antimalarials offer immense untapped potential.

1.8 Bottlenecks for Malaria treatment

Timely and faithful diagnosis, asymptomatic case management, insecticide resistance, complex parasite life-cycle and drug non-responsiveness are by far the biggest hiccups in malaria treatment [3,60].

A rebuttal for drug-resistant parasites by having novel anti-malarial therapies have been the biggest saviour in reducing mortality since 1997 [1]. However, the antimalarial drug pipeline is exhausted with Chloroquine, the go-to drug for decades for treatment turning ineffective. After chloroquine resistance, the sulfoxine-pyrimethamine combination was also used [10]. The parasites till now remain less-unresponsiveness to this combination. On the other hand, mefloquine resistance also continues to develop.

Arising initially due to spontaneous single and/or multiple point mutations, changes that lead to the favorable mutations give parasites an upper hand in surviving even at a susceptible concentration. Thereafter, these mutated parasites multiply eventually establishing a drug-resistant population [61]. The parasite has also been able to employ multiple mechanisms that lead to drug resistance including change in drug-binding/affinity, usage of efflux pumps for throwing the drug out, and cleavage of drugs leading to reduced half-life [10]. Presently, WHO recommends artemether-lumefantrine, artesunate-amodiaquine, artesunate-mefloquine, artesunate-sulfadoxine-pyrimethamine, and dihydroartemisinin-piperaquine ACTs [62]. However, the activity of ACT is also fast-reducing [63,64].

1.9 Scope of the current work

1.9.1 Pressing need for new antimalarials

While the presently available drugs are effective in most parts of the world, the available first-line therapy has a bleak future. The parasite and human evolution has resulted in tandem through fine-tuned, well-rehearsed and deftly executed disease.

The origin of anti-malarial resistance in Cambodia and Myanmar-Thailand border followed by fast spreading resistance in other parts of the world is being tracked 2015 onwards. We need to have ACT replaceable drug combinations in the pipeline to replace both ART and second the partner. Malaria being a disease on elimination agenda of the world, novel therapeutics for its treatment are needed now more than ever. This is because if the parasite circumvents, the presently available drugs won't be sufficient. This will lead to a major health outbreak and countries that were once endemic may stand on the verge of becoming endemic again. Hence, in order to direct the progress in the right direction it is utmost important that the world has new therapies.

Risk to malaria infection is lifelong. The host does not acquire immunity even after multiple re-infections, hence drug based treatment is the dictating factor in containment and cure. Malaria still remains a major contributor of child death and suffering in resource-poor countries [11]. Till date no vaccine for mass usage is available.

Overall, to sustain the gains made since its origin, the world needs to pay utmost attention on new antimalarials both through discovery of novel antimalarials and repurposing drugs already in use for treatment of other diseases.

1.9.2 Myosin A/MTIP Interaction as drug target

Owing to their direct and indispensable role in invasion and egress, many actinomysoin components have been proven to be good drug targets. Myosin gene knockouts have proven the role of the protein as a central player in parasite life-cycle [34,35]. Apart from this, direct inhibitor of Myosin A, BDM blocks parasite locomotion [38]. With reference to perturbation of the Myosin A/MTIP interaction, studies using MyoA mimicking peptides block invasion and growth [39,46]. Further on, urea based inhibitors [43,65], hydrogen bond surrogate peptides [65], anti - MTIP nanobody [45] mimics targeting this PPI, have also shown similar effects.

All these studies have hinted at a common platform of interaction between Myosin A/MTIP which if blocked, stalls *P. falciparum* invasion in host RBC (Figure 1.9). With this premise, we chose targeting Myosin A/MTIP interaction.

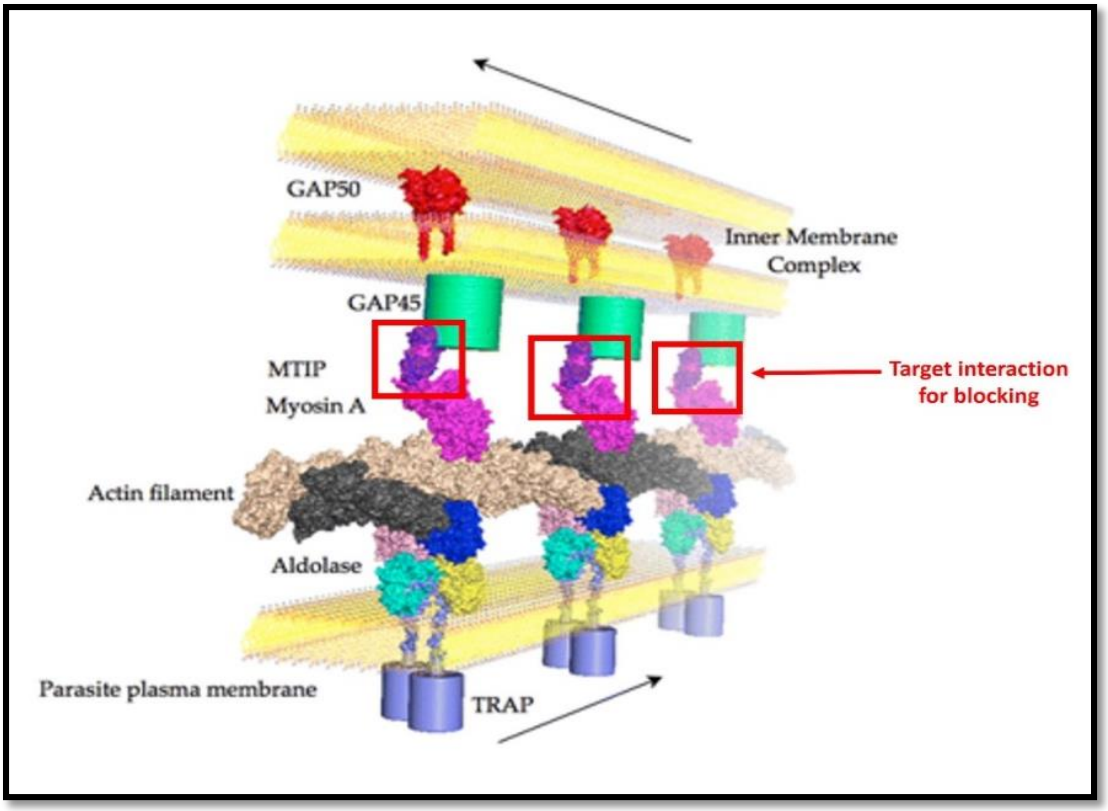

Figure 1.9: Target protein-protein interaction for disruption selected in this study (Adapted and modified from Thomas et al., 2010) [42]

1.10 Bacterial-two hybrid for finding novel interacting partners

1.10.1 High throughput screening through bacterial two-hybrid system

Protein-protein interactions (PPI) play a skeletal role in cellular processes. Understanding the interactors, their regulation, and effect of interaction can not only help in understanding cellular biology and processes, this knowledge can directly be applied to devise blockage mechanisms in case of disease causing organisms. To add to this, PPI can be regulated at multiple levels – transcriptional, translational, and post-translational. Presently used methods to study PPI are interdisciplinary in nature. Major methods include pull-down assays, gel filtration chromatography, ITC, SPR, two-hybrid assay, Circular Dichorism Spectroscopy, Nuclear Magnetic Resonance, Cryo-electron microscopy, Foster Resonance Energy Transfer (FRET), Reflectometric Interference Spectroscopy (RIFS), and Luminescent Oxygen Channelling Assay [66]. In each case, the method chosen to study PPI largely depends on the setup, sample preparation, kinetics of reactions, feasibility.

In context to novel drug discovery, high-throughput screening is one of the most effective ways enabling parallel screening drastically reducing time. The efficiency of drug discovery is also increased manifold through high-throughput screening. Alongside, the method applied for high throughput screening is also a crucial factor mimicking cellular milieu, scalability and technical considerations.

Disrupting PPI offers a crucial point of intervention against disease-causing pathogens. However, due to their large and flat interacting surfaces blocking PPI is a challenging task. Hence, in order to find PPI disruptors, the choice of method is critical. Bacterial two-hybrid system is an *E.Coli* based system that can be applied for screening PPI. The host *E.coli* system ensures easy growth with high transformation efficiency and rapid detection. At the same time, this system allows large scale target

to library hitting and screening. Hence, we chose bacterial two hybrid system for finding novel peptide based binders against established drug targets: Myosin A tail domain and Myosin A interacting domain of MTIP.

Bacterial two-hybrid allows PPI detection *in vivo* [67]. Mechanistically, the detection is based on transcriptional activation of reporter gene that leads to blue coloured colonies on X-gal indicator plates. In order to detect PPI, each pair is cloned in one of the bacterial two hybrid vectors: pBT and pTRG. The pBT vector has lamda-repressor cloned upstream to the cloned bait. Lamda-repressor has the DNA binding domain and the dimerisation domain. A fusion protein product is made during the bacterial two-hybrid assay; of which the DNA binding domain binds on the upstream operator sequence of the reporter gene cassette. In pTRG vector, the alpha subunit of RNA polymerase is present upstream to the cloned target protein. Similar to pBT vector, here too a fusion protein product is formed. If the two proteins in the fusion products interact with each other, a stable RNA polymerase complex that initiates transcription of β-galactosidase enzyme is formed, which results in blue coloured colonies (Figure 1.10).

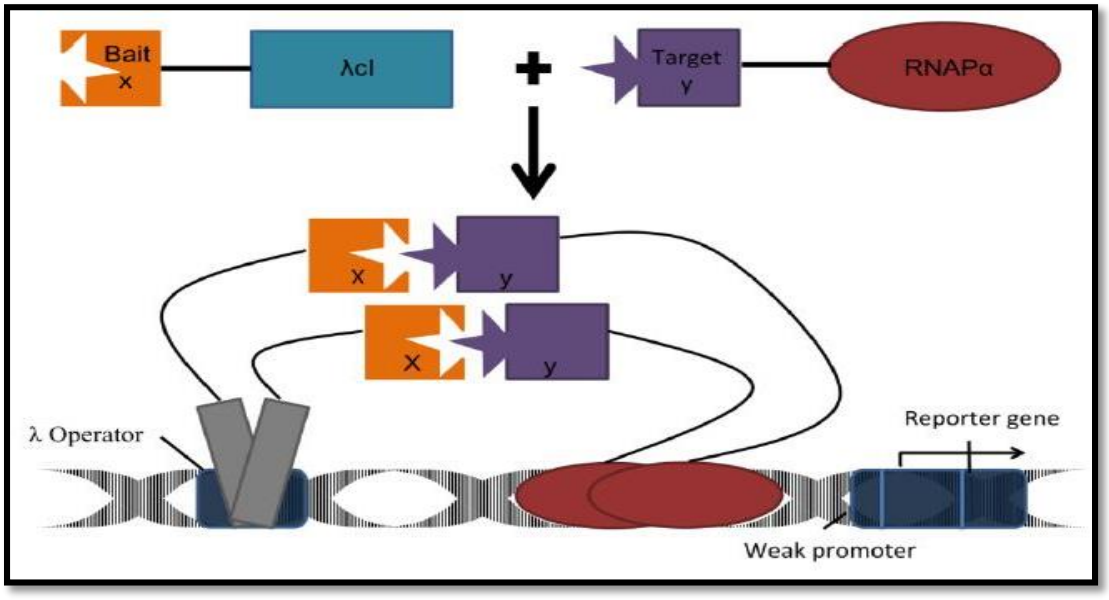

Figure 1.10: Schematic diagram representing bacterial-two hybrid assay.

1.10.2 Rationale behind bacterial three-hybrid assay

Bacterial three-hybrid is a follow-up method of the bacterial two-hybrid assay to detect the blockage of a specific PPI [68]. Apart from the native bacterial two-hybrid vectors pBT and pTRG, bacterial three-hybrid uses a third vector pMTSA. For the bacterial three-hybrid assay, the interacting proteins are cloned in pBT and pTRG vectors. In addition, the third binding partner/peptide to be tested for disruption is cloned in pMTSA. The assay works on arabinose based induction that results in the third protein cloned in pMTSA being synthesised. In the absence of arabinose, the two interacting partners interact resulting in blue coloured colonies on X-gal indicator plates due to the synthesis of β-galactosidase. For testing the blockage of this blue coloured PPI complex, arabinose is given. The colour of the colonies now formed indicates if the disruption is successful or not, thereby helping in studying the ternary complex and the interaction dynamics. Blue coloured colonies indicate the two-protein complex is formed even in the presence of the third protein/peptide. Contrastingly, white coloured colonies indicate the disruption of the initial complex due to binding of the third partner with either of the initial protein complex members (Figure 1.11).

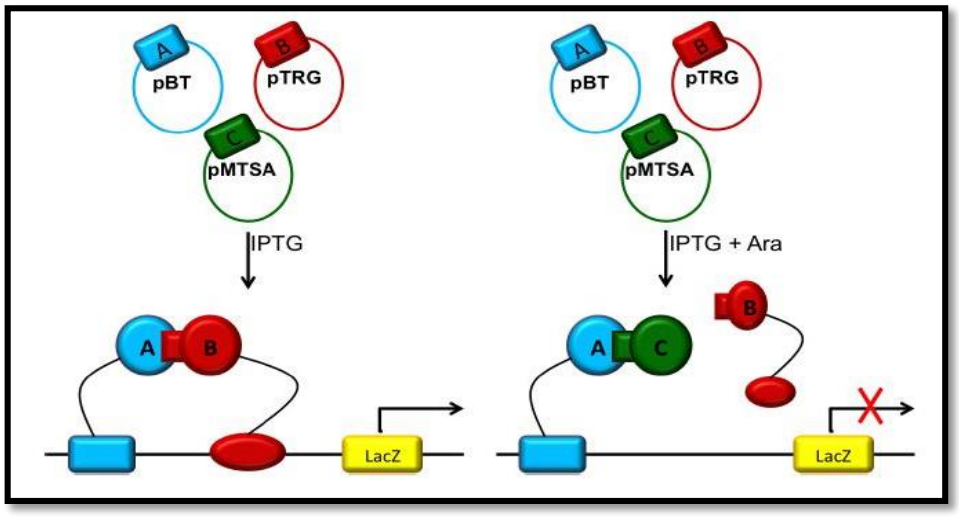

Figure 1.11: Schematic diagram representing bacterial-three hybrid assay (Adapted from Tharad et al., 2011) [68].

1.10.3 Protein evolution by codon shuffling and *de novo* dicodon library synthesis

Evolution is defined as a gradual change in a species or population helping in adapting better to the environment. Evolution through natural selection was first defined by Charles Darwin and often results in the 'origin of new species.' The change primarily results due to underlying genetic changes in the DNA of organisms that is inherited generation after generation.

Laboratory evolution of proteins by generating a plethora of peptides/proteins of defined chemical or/and functional properties allows accelerated evolution in a directed manner. The library of proteins/peptides synthesised through this is degenerate at the protein level and its members can be screened for specific properties like target binding, sequence differences/similarities, enzymatic activity, etc.

Codon Shuffling is an approach for directed evolution that comprises random joining of DNA hexamers or dicodons [69,70]. The dicodons are a result of spontaneous joining between single stranded palindromic DNA hexamers that after end to end joining are blunt ended (Table 1.4). 14 dicodons cover all 20 amino acids (excluding the stop codons, to ensure an open reading frame). The 14 dicodons are ligated in a random manner resulting in generation of codon-shuffled peptides/proteins of varying physical, chemical and biological properties. Another layer to this approach is attained while choosing the molar ratios of dicodons during library synthesis. In other words, by judiciously adding the amount of positively charged, negatively charged, hydrophobic dicodons; screwed peptide/protein libraries can be attained. These skewed libraries can be used to isolate peptides with common characteristics. This approach is part rational as it allows random oligomerisation of dicodons that are

chosen in a pre-defined manner allowing the end library to have specific characteristics. The ligated dicodons further joined to hair pins at both ends, digested and used for cloning in specific vectors.

Oligonucleotide	Duplex	DC	Oligonucleotide	Duplex	DC
5′-GAGCTC-3′	5′-GAGCTC-3′ 3′-CTCGAG-5′	EL	5′-CCCGGG-3′	5′-CCCGGG-3′ 3′-GGGCCC-5′	PG
5′-GATATC-3′	5′-GATATC-3′ 3′-CTATAG-5′	DI	5′-ATGCAT-3′	5′-ATGCAT-3′ 3′-TACGTA-5′	MH
5′-AAGCTT-3′	5′-AAGCTT-3′ 3′-TTCGAA-5′	KL	5′-CAGCTG-3′	5′-CAGCTG-3′ 3′-GTCGAC-5′	QL
5′-AACGTT-3′	5′-AACGTT-3′ 3′-TTGCAA-5′	NV	5′-TGGCCA-3′	5′-TGGCCA-3′ 3′-ACCGGT-5′	WP
5′-GGCGCC-3′	5′-GGCGCC-3′ 3′-CCGCGG-5′	GA	5′-TACGTA-3′	5′-TACGTA-3′ 3′-ATGCAT-5′	YV
5′-AGTACT-3′	5′-AGTACT-3′ 3′-TCATGA-5′	ST	5′-TTCGAA-3′	5′-TTCGAA-3′ 3′-AAGCTT-5′	FE
5′-TGCGCA-3′	5′-TGCGCA-3′ 3′-ACGCGT-5′	CA	5′-CGTACG-3′	5′-CGTACG-3′ 3′-GCATGC-5′	RT

Amino acids are listed as single letter codes. DC, dicodon.

Table 1.4: DNA hexamers forming dicodons used for library synthesis (Adapted from Rao et al., 2005) [70].

For using dicodon libraries for screening through bacterial two-hybrid, the hairpin ligated-digested-dicodons are ligated to SnaBl cut pTRG or pBT vectors. The ligated mix is subsequently transformed in XL-1 Blue *E.Coli* strain to get bacterial colonies representing cloned *de novo* synthesised dicodon library.

With this background, we aimed to block the principal glideosome powering interaction, by unearthing novel peptide inhibitor(s) using dicodon peptide library and bacterial-two hybrid screening approach.

RESEARCH OBJECTIVES

2 RESEARCH OBJECTIVES

Objectives of the study are:

1. Validation of gliding motility complex interaction Myosin A/MTIP in a bacterial two-hybrid setup.
2. Estimation of relative strength of Myosin A/MTIP interaction.
3. Validation of Myosin A/MTIP interaction through *in vitro* PPI techniques.
4. Synthesis of *de novo* dicodon libraries.
5. Finding of potent binder of Myosin A or MTIP.
6. Assessment of relative strength of interaction between binder and target.
7. *In vitro* validation of interaction between binder and target.
8. Study of disruption of Myosin A/MTIP complex *in vivo*.
9. Study of disruption of Myosin A/MTIP complex *in vitro*.
10. *In silico* studies between binder and target.
11. Study the effect of *de novo* binder on *P.falciparum* growth and invasion.

MATERIALS AND METHODS

3 MATERIALS AND METHODS

3.1 Materials

3.1.1 Chemicals and Media

Materials used in the present work were purchased from the following sources. Materials not mentioned here are mentioned with their sources as and where throughout this section.

Material	Source
Fine chemicals	Sigma Aldrich, USA; Ameresco/ VWR Life Sciences, USA; Merck, USA; Thermo Fischer Scientific, USA; G-Biosciences, USA; Roche, Switzerland.
Enzymes, DNA Polymerases	New England Biolabs, USA; Thermo Fischer Scientific, USA
LB, LA media	HiMedia Laboratories, USA
Bacteriomatch Two-Hybrid Reporter kit with plasmids, reporter and cloning strains	Stratagene, USA
Plasmid mini prep and gel elution kit	Qiagen, Germany
RPMI-1640, Albumax, Serum	Gibco/ Thermo Fischer Scientific, USA

Table 3.1: List of chemicals and media with their sources used in this study.

3.1.2 Bacterial strains

Two bacterial two-hybrid strains R1 and XL1- Blue appropriate for propagation and harbouring bacterial-two hybrid vectors pBT and pTRG were used in this study. *lacI*^{q} gene suppresses the synthesis of bait and target proteins in the absence of IPTG. For cloning and expression in other vectors, common laboratory cloning and expression strain were used. The genotypes and source of all bacterial strains is mentioned below.

***E.Coli* strain**	**Genotype**	**Source**
R1	Bacterial two-hybrid reporter strain *lacI*^{q} gene on the F´ episome, Kanamycin^{r}	Stratagene, USA
XL1- Blue	Bacterial two-hybrid cloning strain *lacI*^{q} gene on the F´ episome, *supE44*, Kan^{r}	Stratagene, USA
DH5α	*fhuA2 lac(del)U169 phoA glnV44 Φ80'* *lacZ(del)M15 gyrA96 recA1 relA1 endA1 thi-1* *hsdR17*	Invitrogen Life Sciences, USA
BL21 (DE3)	*E. coli* str. B F^{-} *ompT gal dcm lon hsdS*$_{B}$($r_{B}^{-}m_{B}^{-}$) λ(DE3 [*lacI lacUV5-T7p07 ind1 sam7 nin5*])	Novagen, Germany

Table 3.2: List of bacterial strains used in this study.

3.1.3 Vectors for cloning and expression

The following is the list of vectors used in the present study for bacterial two/three-hybrid assays, cloning and expression with their characteristics and vector maps.

S. No.	Plasmid	Relevant characteristics
1	pBT	p15A origin of replication, *lac-UV5* promoter, λ cI ORF, Chloramphenicol^r
2	pTRG	ColE1 origin of replication, *lpp* promoter, *lac-UV5* promoter, RNAPα ORF, Tetracyclin^r
3	BlaI-cut-pET 28-a	Kanamycin^r
4	pMTSA	CDF origin of replication, pBAD promoter, AraC inducer, Streptomycin^r

Table 3.3: List of vectors used in this study.

The bacterial two-hybrid vectors pBT and pTRG were procured from Agilent's BacterioMatch II two-hybrid vector kit. Both the plasmids are low copy number plasmids with pBT 5-10 copies per cell and pTRG 20-30 copies per cell. pBT is a 3.2 kb vector harbouring chloramphenicol resistance, while pTRG a 4.4 kb plasmid has tetracycline resistance.

Both the vectors are designed so as to produce fusion constructs of bait and target respectively. In pBT, the lamda repressor is followed by the target gene. This construct is cloned at SnaBl site. In pTRG, RNA Polymerase α subunit and the target gene are cloned sequentially together. The modified forms of pBT and pTRG, pBT_{nn}

and $pTRG_{nn}$ have been derived from original vectors by inserting SnaBl site (Figure 3.1, 3.2).

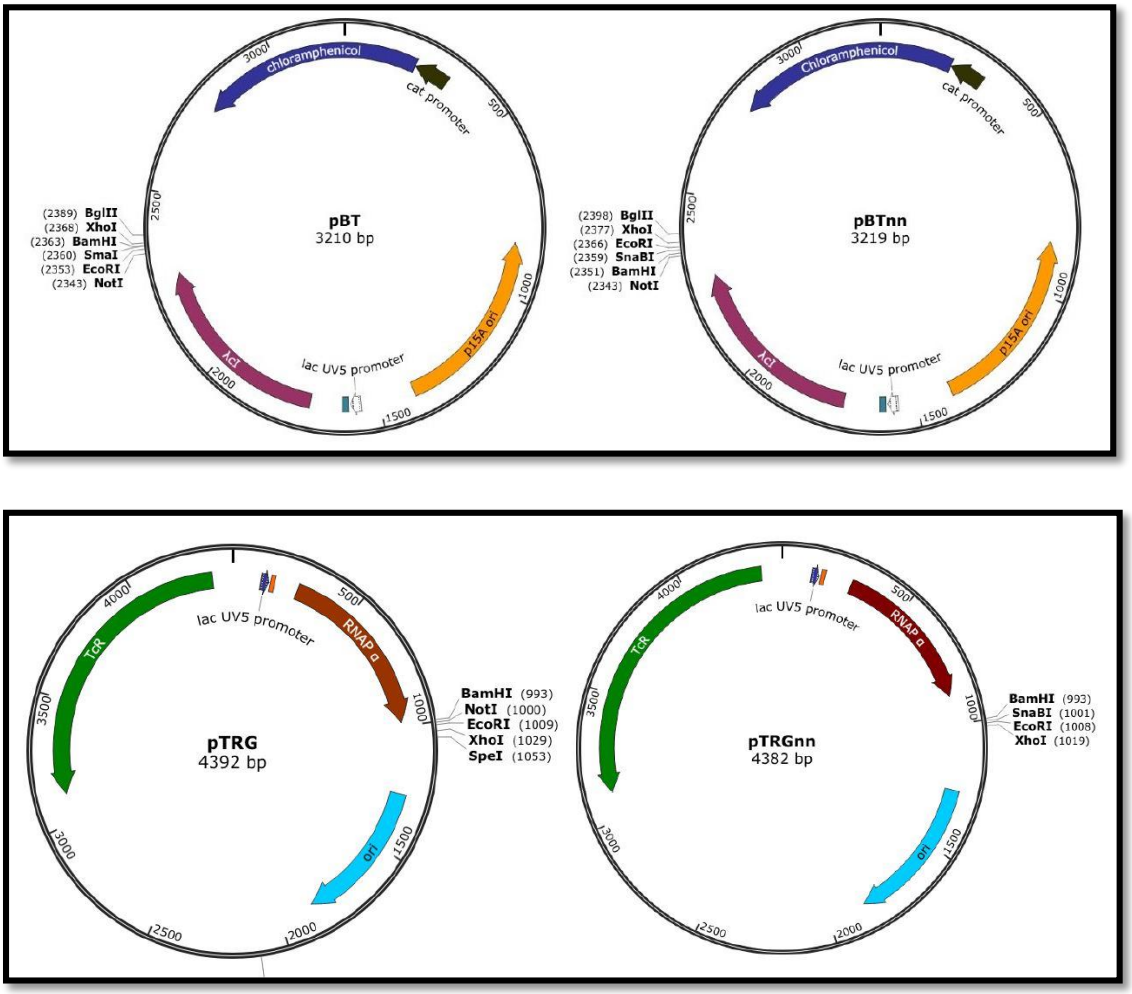

Figure 3.1: Original and modified versions of bacterial-two hybrid vectors pBT and pTRG

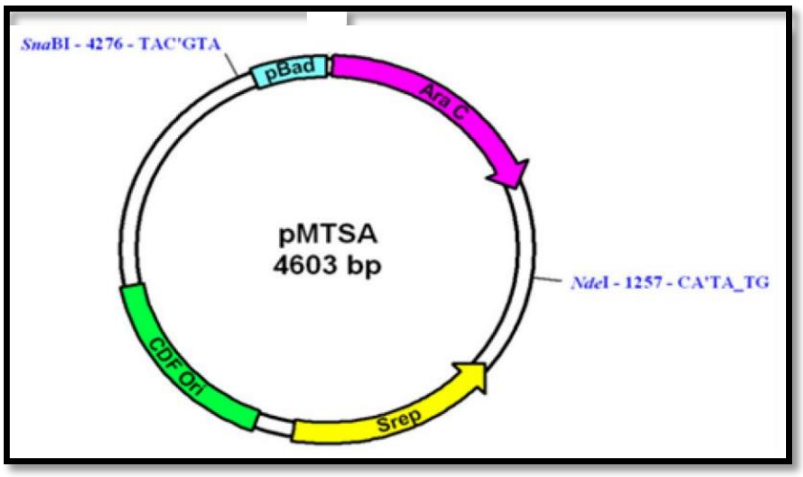

Figure 3.2: pMTSA vector used for expression and bacterial-three hybrid studies

3.1.4 Antibiotics and other stock solutions

S. No.	Name	Stock concentration	Solvent	Working concentration
1	Kanamycin	50 mg/ml	DDW	50 µg/ml
2	Tetracycline	12.5 mg/ml	Ethanol/DDW 50% (v/v)	12.5 µg/ml
3	Chloramphenicol	30 mg/ml	100% Ethanol	30 µg/ml
4	Streptomycin	50 mg/ml	DDW	50 µg/ml
5	Ampicillin	100 mg/ml	DDW	100 µg/ml
6	X-gal	80 mg/ml	N, N'- dimethyl formamide	80 µg/ml
7	X-gal inhibitor	200 mM	N, N'- dimethyl formamide	200 µM
8	IPTG	1 M	DDW	25 µM
9	L- arabinose	20% (w/v)	DDW	1% (w/v)

Table 3.4: List of antibiotics, their stock and working concentrations with solvent.

3.1.5 Oligonucleotides

Following is the list of primers used for dicodon library synthesis, MyoA tail, MTIP and ZA1 cloning. All primers were procured from Eurofins Pvt. Ltd. The primer sequences are listed below.

S. No.	Name of the primer	Oligonucleotide sequence (5' to 3')
1	Hairpins (HP)	TTTAAACACGTGGCGGCCGCTCTAGAGGCCCGCG CGGGCCTCTAGAGCGGCCGCCACGTGTTTAAA
2	HP2P	AGCGGCCGCCACGTGTTTAAA–5' end phosphorylated
3	HP2	AGCGGCCGCCACGTGTTTAAA
4	Myo A For	TCATCTAGATATCAAAAACATTCCGAGCCTGC
5	MTIP For	ATTTATTACGTAAGTGTTGCTGATATTCAGC
6	MTIP Rev	TTATATACGTATTGCAGGATGTCTTCGC
7	pTRG Rev	TAGAGGATCTCACTAGTTCATTAATTAATTA
8	pBT Rev	CCACAGGGTAGCCAGCAGCATCCT
9	pMTSA For	TCCATAAGATTAGCGGATCCTACCTGACGC
10	pMTSA or pET Rev	AGCAGCCAACTCAGCTTCCTTTCGGGCTTT

Table 3.5: List of oligonucleotides used for cloning.

3.1.6 Antibodies

All antibodies used in the present study along with their relevant details are mentioned below.

S. No.	Antibody	Protein detected	Animal used	Dilution used	Antibody profile in WB	Source
1	anti-MTIP	MTIP	Mice	1:15000	17.4 kDa	In-house
2	anti-MTIP	MTIP	Rabbit	1:10000	17.4 kDa	In-house
3	anti-His	MTIP	Mice	1:2000	17.4 kDa	Qiagen
4	anti-biotin	Myo A peptide	Mice	1:500	-	Santa Cruz Biotechnology
5	anti-His	ZA1	Mice	1:2000	10.3 kDa	Qiagen
6	anti-CFP-10	CFP-10	Rabbit	1:5000	-	Abcam

Table 3.6: List of antibodies used in this study.

3.1.7 Solutions for β – galactosidase assay

Z-Buffer: Following are the components for 50 ml Z-Buffer preparation, pH 7. The buffer is stored at 4 ^{o}C. β- mercaptoethanol is added just before use.

S. No.	Component	Working concentration	Amount
1	$Na_2HPO_4.7H_2O$	60 mM	0.8 g
2	$NaH_2PO_4.H_2O$	40 mM	0.28 g
3	KCl	10 mM	0.5 ml of 1 M stock
4	$MgSO_4$	1 mM	50 µl of 1 M stock
5	β- mercaptoethanol	50 mM	0.135 ml

Table 3.7: List of constituents and their concentrations used for Z-Buffer preparation.

Substrate: ONPG (O-nitrophenyl-β-D-pyranogalactoside) is dissolved to a concentration 1 mg/ml in Z-Buffer having β- mercaptoethanol (should be added just before use in order to avoid oxidation of the thiol group). The solution is prepared freshly and kept at 30 ^oC for the assay.

Quenching/stop solution: 1M Na_2CO_3 stored at 4 ^oC.

3.1.8 Solutions for ELISA

Following are the components for ELISA based interaction assay. Coating buffer/ Carbonate-Bi-Carbonate buffer or coating buffer was stored at 4 ^oC. For coating of peptide/proteins Nunk Maxisorb ELISA plates with plate sealer were used.

The optical density reading were taken using Tecan Spectrophotometer at 450 nm.

S. No.	Name	Constituents
1	Coating buffer/ Carbonate-Bi-Carbonate buffer	50 mM each Na_2CO_3, $NaHCO_3$ pH 9.6. For 50 ml, 1 ml 0.2 M Na_2CO_3 and 11.5 ml 0.2 M $NaHCO_3$
2	Blocking buffer	5% BSA/PBST
3	Wash buffer	1X PBS, 0.05% Tween-20
4	Binding buffer	1X PBS, pH 7.4
5	Stop solution	2N H_2SO_4

Table 3.8: List of buffers used for ELISA

3.1.9 Solutions for Gel Electrophoresis

TBE buffer 10X: 890 mM Tris, 890 mM Boric acid, 20 mM EDTA.

TE buffer: 10 mM (pH 7.5), 1 mM EDTA

DNA loading dye 6X: 30% (v/v) Glycerol, 0.25% (w/v) bromophenol blue, 0.25% (w/v) xyalene cyanol.

Wash buffer for paper elution of DNA: 100 mM NaCl in TE (pH 8)

Elution buffer for eluting DNA: 1 M NaCl in TE (pH 8)

3.1.10 Solutions for Western Blot

SDS-PAGE gel

The recipe used for preparation of 15% SDS-PAGE gel is described below.

Component	Resolving for 15% gel	Stacking
DDW	2.3 ml	3.1 ml
100% Glycerol	100 µl	50 µl
30% Acrylamide	5 ml	650 µl
1.5 M Tris (pH 8.8)	2.5 ml	-
0.5 M Tris (pH 6.8)	-	1.25 ml
10% SDS	100 µl	50 µl
40% APS	25 µl	12 µl
TEMED	4 µl	6 µl

Table 3.9: List of constituents and their volumes used for preparation of 15% SDS-PAGE gel

30% Acrylamide: 290 g acrylamide and 10 g bisacrylamide are dissolved in 600 ml DDW. After dissolution the volume is made upto 1 L. The stock solution is stored in a dark bottle at 4 ^{o}C.

SDS-PAGE Running Buffer 10X: 30.2 g Tris-base, 144 g glycine, 10 g SDS, is dissolved in 900 ml DDW. The pH is adjusted to 8.3 and volume was made upto 1 L.

The final concentration of salt is 250 mM Tris, 1.92 M Glycine, 1% SDS. Before using, the buffer is diluted to final 1X concentration.

Sample Loading Buffer 5X: 5% β- mercaptoethanol, 0.02% bromophenol blue, 30% glycerol, 10% SDS, 250 mM Tris-HCl (pH 6.8)

Tris-Tricine gels

For visualization and western blotting of low molecular weight proteins (<10 kDa) tris-tricine gels are used, whose recipe is given below.

Component	Resolving	Spacer	Stacking
49.5% T, 6% C	3.32 ml	-	-
49.5% T, 3% C	-	1.01 ml	0.5 ml
Gel Buffer	3.32 ml	1.66 ml	1.55 ml
100% Glycerol	1.05 ml	-	-
DDW	2.29 ml	2.32 ml	4.2 ml
40% APS	9 µl	5 µl	12.5 µl
TEMED	4 µl	2 µl	5 µl

Table 3.10: List of constituents and their volumes used for preparation of tris-tricine gel

49.5% T, 6% C: 46.5 g acrylamide and 3 g bisacrylamide are dissolved in 80 ml DDW. After dissolution the volume is made upto 100 ml. The solution is stored in a dark bottle at 4 ^{o}C.

49.5% T, 3% C: 48 g acrylamide and 1.5 g bisacrylamide are dissolved in 80 ml DDW. After dissolution the volume is made upto 100 ml. The solution is stored in a dark bottle at 4 ^{o}C.

Gel Buffer 3X: 36.4 g Tris bas, 0.3 g dissolved in 80 ml DDW. The pH is adjusted to 8.45 and volume is made upto 100 ml. The stock is stored at RT.

Anode Buffer 10X: 60.5 g Tris base (pH 8.9) is dissolved in 250 ml DDW. Before using, the buffer is diluted to final 1X concentration.

Cathode Buffer 10X: 30.3 g Tris base, 44.5 g Tricine, 2.5 g SDS are dissolved in 200 ml DDW. The pH is adjusted to 8.25 and volume is made upto 250 ml. Before using, the buffer is diluted to final 1X concentration.

Transfer and Western Blotting

PBS 1X: 137 mM NaCl, 2.7 mM KCl, 10 mM NaH_2PO_4, 2 mM K_2HPO_4 are dissolved and pH 7.4 is maintained. The buffer is autoclaved and stored at RT.

Wash Buffer (PBST): 0.1% Tween-20 in PBS.

Transfer Buffer: 200 mM Glycine, 24 mM tris base, 20% methanol are dissolved together. The buffer is chilled before use.

Blocking Buffer: 5% (w/v) skimmed milk in PBST.

Markers

DNA markers 1 kb DNA ladder or 1 kb plus DNA ladder from Thermo Scientific, USA were used in the study. Protein based multi-colour markers from BioRad, USA were used for SDS-PAGE. The low molecular weight markers for SDS-PAGE were procured from GeneDireX, USA.

3.1.11 Solutions for Surface Plasmon Resonence

Immobilization buffer: 1X PBS pH 7.4

Running Buffer: 10 mM Phosphate buffer

Regeneration Buffer: 1 M NaCl

3.1.12 Parasite strain

For parasite growth inhibition assay, *P. falciparum 3D7* strain (chloroquine sensitive) was used.

For RPMI media preparation, RPMI power packet is dissolved in 900 ml autoclaved DDW. To this, 2.3 g HEPES, 1.46 g L-glutamine and 2 g sodium bicarbonate is added (final pH 7.4). The volume is made up to 1 L.

3.2 Methods

3.2.1 Bacterial-two hybrid experiments

3.2.1.1 Dicodon library synthesis

De novo dicodon library was synthesised as described previously. For this, a ligation reaction of 20 µl was set up using 100 ng of each DNA hexamer or dicodon member (refer table 1.4) and 7.5 % polyethylene glycol. The mix was heated slowly to 55 ^{o}C and then gradually cooled to 4 ^{o}C and incubated at 4 ^{o}C for 24 hours. 100 pmol of 5'-phosphorylated double stranded hairpins were self-annealed separately and added to the incubated ligation mixture. After mixing these two, the whole mixture was incubated at 16 ^{o}C for another 12 hours. Following this, the DNA in the mixture was precipitated and purified by phenol: chloroform precipitation and re-suspended in nuclease free Tris-EDTA buffer. Following precipitation, the DNA was digested with XbaI at 37 ^{o}C for 4 hours. From this digested mix, 1 µl was used as a template for

PCR amplification using HP2P primers that acted both and forward and reverse primer. Subsequently, the amplified PCR fragments ranging from 100-500 bp were eluted using DEAE membrane and purified again by phenol: chloroform precipitation. These fragments were used as inserts for cloning into SnaBl cut dephosphorylated vectors $pTRG_{nn}$ and pBT_{nn} in XL-1 cells.

3.2.1.2 Cloning of Myosin A tail domain, MTIP and ZA1 in bacterial-two hybrid vectors

The known interacting regions of *Pf*Myosin A (798-818 amino acids) and MTIP (61-265 amino acids) were codon optimised and got synthesised in pUC57 from Genescript. For MyoA tail, MTIP cloning and ZA1 re-cloning, the inserts were prepared by PCR amplification using gene specific primers (MyoA For/pTRG Rev, MTIP For/pBT Rev) and HP2P primers followed by restriction digestion and blunt end cloning in pTRG and pBT. Positive clones were confirmed by sequencing.

3.2.1.3 Bacterial two-hybrid screening experiments

Bacterial two-hybrid screening experiments were performed as per manufacturer's description. Precisely, both pTRG and pBT plasmids were co-transformed in equal amounts (250 ng each) into R1 reporter cells. Transformed cells were plated on X-gal indicator plates containing kanamycin (50 µg/ml), tetracyclin (12.5µg/ml), chloramphenicol (30 µg/ml), x-gal (80 µg/ml), X-gal inhibitor 2-Phenylethyl-β-D-thiogalactoside (200 µM), Isopropyl β-D-1-thiogalactopyranoside (25 µM) and incubated at 30 ^{o}C for 48 hours.

The screening was done visually, with blue coloured colonies indicating a positive interaction. A well-established protein-protein interaction positive of *Mycobacterium*

tuberculosis proteins ESAT6/CFP10 was used as a positive control and ESAT6/empty pBT_{nn} was used as a negative control.

For dicodon library screening bacterial two-hybrid experiments, MyoA-pTRG and negatively charged DIEL library cloned in pBT were co-transformed. Initial screening was done by visual blue-white screening, followed by re-transformation, segregation and re-co-transformation in order to confirm the interactions. The sequence of novel dicodon partner was obtained from sequencing.

3.2.1.4 β-galactosidase reporter assay

For quantitatively assessing the strength of positive interactions a colorimetric reporter enzyme assay was performed [71]. Statistical significance was tested using Student's t-test, by comparing all values to the negative control along with Welch's correction.

3.2.2 Protein synthesis and purification

3.2.2.1 Cloning of MTIP and ZA1 in expression vectors

MTIP was cloned in BlaI-cut pET28a for protein synthesis. The MTIP insert was prepared by restriction digestion using SnaBl followed by ligation in SnaBl cut-Blal-cut pET28a. The ligated mix was transformed in R1 competent cells followed by screening of clones using gene and vector specific primers (MTIP For/pET Rev). After confirming the positive clones, sequencing was performed to confirm cloning.

ZA1 insert was prepared using HP2P primers from the original ZA1-pBT library clone and ligated in pMTSA vector by blunt end cloning. The orientation of positive clones was confirmed by sequencing. ZA1-pMTSA clone was used for expression of ZA1 and bacterial three-hybrid studies.

3.2.2.2 Expression and purification of MTIP and ZA1

For expression, MTIP-pET 28a plasmid was transformed in *E.Coli* BL21 (DE3) cells and induced at various concentrations of IPTG, at different temperatures. The amount of MTIP protein synthesised in various conditions was checked by SDS-PAGE gel. For large scale purification, MTIP expression was induced at 0.6 mM IPTG for 3 hours at 37 ^{o}C. MTIP was obtained in the supernatant. The induced cell pellet was re-suspended in PBS pH 7.4 and sonicated till a clear solution was obtained. The solution was subsequently centrifuged at 13000 rpm for an hour to obtain a clear cell lysate. The lysate was allowed to bind Ni-NTA beads overnight at 4 ^{o}C and the protein was subsequently purified by slowly increasing imidazole concentration in PBS. The eluted fractions were ran on 15% SDS-PAGE and fractions having high concentrations of the protein were pooled and subsequently dialysed against PBS pH 7.4. The purified protein was ran on 15% SDS-PAGE and confirmed by western blot analysis using anti-MTIP antibody (1:5000 dilution).

For ZA1 protein, the expression was checked in *E.Coli* BL21 (DE3) by arabinose based induction. ZA1 protein was found in inclusion bodies. Standardization similar to MTIP was done to check maximal expression at various concentrations of ZA1. For large scale purification, BL21 cells carrying ZA1-pMTSA plasmid was grown in liquid culture overnight at 37 ^{o}C with streptomycin (50 µg/ul). Secondary culture was inoculated with 1% inoculum and grown till mid-log phase in the presence of streptomycin and induced with 1% arabinose for 3 hours at 37 ^{o}C. The cell pellet was sonicated in re-suspension buffer (10 mM Tris HCl, 150 mM NaCl pH 7.4) in the presence of PIC (1X) and PMSF (2mM) until a clear solution was obtained. The pellet was solubilized in solubilisation buffer (10 mM Tris HCl, 300 mM NaCl 8M Urea, 10 mM imidazole pH 7.4) and the resulting supernatant containing proteins was bound to

Ni-NTA resin at room temperature. The bound proteins were eluted by sequential increase of imidazole in solubilisation buffer. The eluted fractions were ran on tris-tricine PAGE and fractions carrying the protein were pooled and dialyzed in10 mM Tris HCl, 150 mM NaCl pH 7.4 along with gradual decrease in urea to gradually removal the denaturant enabling refolding of the protein. The purified protein was ran on tris-tricine PAGE and confirmed by western blot analysis using anti-His antibody.

3.2.2.3 Antibody generation

Purified MTIP protein was resolved by SDS-PAGE and checked for purity. Approx. 100µg of this was mixed with Complete Freund's adjuvant for the 1st dose and incomplete Freund's adjuvant for booster dose after 7 days. The mixture was administered into mice sub-cutaneously and the bleed was collected after 7 days of 1st booster. Pre-immune sera were collected before immunizing the mice**.** Mice were administered several booster doses and sera were collected every 7th day of the injection.

3.2.2.4 Ethics Statement

Animal studies were performed following CPCSEA guidelines and approved by Institutional Animal Ethics Committee (IEAC) of JNU. Female BALB/c mice were obtained from Central Laboratory Animal Resources, JNU, New Delhi and maintained under standard conditions and. For experiments, donor blood was obtained from Rotary blood bank (RBB), New Delhi, India.

3.2.3 *In vitro* protein-protein interaction assays

3.2.3.1 Enzyme-linked immunosorbant assay

ELISA based protein-protein interaction assay was carried out as described previously [19,72] with slight modifications. Briefly, 500 ng MyoA peptide was coated in 0.1 M Carbonate/Bicarbonate Buffer (SPL Maxisorb ELISA plates) for 2 hours at 37 ^{o}C and blocked at 4 ^{o}C overnight in blocking buffer (5% skimmed milk in PBST). Subsequently, the plates were washed three times with washing buffer (1x PBS, 0.05% Tween-20) and overlaid with increasing concentrations of the second interacting protein partner (0 µM, 0.1 µM, 0.25 µM, 0.5 µM, 1 µM and 2.5 µM) in test wells. In the negative control wells, an unrelated mycobacterial protein ESAT-6 was overlaid at same concentrations. The proteins were allowed to bind for 2 hours at 37 ^{o}C after which the wells were washed. Next, the overlaid bound protein was detected using specific primary antibody (rabbit anti-MTIP antibody 1:10000 dilution, mouse anti-His antibody 1:2000 dilution) in all wells except antibody control wells. A non-specific antibody anti-CFP-10 (1:5000 dilution) was used in these wells. After binding for 2 hours and washing, HRP conjugated secondary antibody (anti-rabbit and anti-mouse 1:5000 dilution) was allowed to bind to the washed plates for 2 hours at 37 ^{o}C. The ELISA plates were washed followed by addition of TMB substrate and incubated at 37 ^{o}C for 15-30 min until colour development. The reaction was stopped by 2 N H_2SO_4 and absorbance was taken at 450 nm. All wells were put up in triplicates.

3.2.3.2 Isothermal titration calorimetry

ITC experiments were performed using ITC_{200} Microcalorimeter (Malvern, UK) at 25 ^{o}C in phosphate buffer. The cell and syringe volumes were kept 310 µl and 40 µl

respectively. The syringe was loaded with 100 µM MyoA tail for MyoA/MTIP interaction study and 150 µM for MyoA/ZA1 interaction study. Sample cell was loaded with 10 µM each of MTIP and ZA1. MTIP and ZA1 were titrated using MyoA tail in injections of 2 µl each except for the first injection that was 0.4 µl. In between each titration, a 150 sec interval for stirring was kept to ensure that the signal returns to baseline. Throughout the experiment, constant stirring of 300 rpm was maintained to ensure proper mixing of reaction components. For both the experiments, a corresponding buffer control was also set up in which PBS was taken in syringe. The enthalpy changes of titrations were measured and baseline values were subtracted from test samples. Data analysis was done using Origin software and curve was fitted to obtain stoichiometry (N), binding constant (K_a) and enthalpy change (ΔH).

3.2.3.3 Surface plasmon resonance

SPR assays were performed using Auto Lab Espirit SPR. 1.03 ng/mm^2 MyoA peptide was immobilized on the surface of the sensor chip. PBS pH 7.4 was used as immobilization and running buffer. For kinetic measurements, increasing concentrations of MTIP (1 µM, 5 µM, 15 µM, 20 µM, 25 µM and 40 µM) and ZA1 (0.6 µM, 0.8 µM, 1 µM, 2.5 µM, 5 µM, 7.5 µM and 10 µM) were injected respectively over MyoA tail as well as reference flow cell at a flow rate of 16.7 µl/sec. The association and dissociation timings were 300 sec and 200 sec respectively. The surface of the chip was regenerated using 1M NaCl solution at the end of each injection cycle. Data fitting was done using Auto Lab SPR Kinetic evaluation software provided with the instrument.

3.2.3.4 Far-western dot blot assay

For Far-western dot-blot assay, 5 µg each of ZA1S peptide, BSA and non-specific peptide (N'- *p*SDNG*p*SGDD -C') was immobilised on nitrocellulose membrane strip. Subsequent to the drying of the membrane, blocking was carried out overnight at 4 ^{o}C, following which the second peptide Myosin A was overlaid in 5 µg/ml of binding solution (1% BSA/PBST) on the strip for 2 hours at room temperature. The strip was washed stringently and the bound Myosin A peptide detected using anti-biotin antibody (1:500 dilution) and HRP conjugated secondary antibody.

3.2.4 *In vivo* disruption studies

3.2.4.1 Bacterial-three hybrid assay

For bacterial three-hybrid experiments, MyoA-pTRG and MTIP-pBT were co-transformed in R1 competent cells. The resulting co-transformants were checked for the presence of both the plasmids by PCR using gene and vector specific primers (MyoA For/pTRG Rev, MTIP For/pBT Rev). The resulting blue colonies were used to prepare competent cells which were subsequently transformed with ZA1-pMTSA or control pMTSA vector only plasmid and plated on X-gal indicator plates both in the presence or absence of L-arabinose (2% w/v). The plates were incubated at 30 ^{o}C for 48 hours. The colour of the colonies blue/white indicated the formation or disruption of Myosin A/MTIP complex. The background and validation of bacterial three hybrid assay has been described previously.

3.2.4.2 Arabinose gradient liquid β-galactosidase assay

An arabinose gradient assay in liquid culture was performed as described previously [73]. Briefly, the mid-log phase grown culture was induced with varying concentrations of L-arabinose (0-4 mM) for 3 hours at 37 ^{o}C. The cells were pelleted

and the levels of β-galactosidase were measured. *E.Coli* BL21 (DE3) cells were induced with varying concentrations of L-arabinose (as used in arabinose gradient assay). Whole cell lysates of 10 ml culture were used of analyse the expression of ZA1 using anti-His antibody (1:2000 dilution).

3.2.5 *In vitro* disruption studies

3.2.5.1 Competitive ELISA

For ELISA based inhibition of interaction between MyoA/MTIP complex using ZA1, 500 ng peptide was coated on Maxisorb ELISA plates followed by overnight blocking at 4 ^{o}C. The bound peptide was overlaid with MTIP (1 µM) for 2 hours at 37 ^{o}C. The plates were washed with wash buffer (1x PBS, 0.05% Tween-20) thrice and overlaid with increasing concentrations of ZA1 (0, 0.5, 1, 2, 5 µM) for 2 hours at 37 ^{o}C. The plates were again washed and the amount of bound MTIP was detected using anti-MTIP antibody (1:10000 dilution) followed by HRP conjugated secondary antibody. Optical density was taken at 450 nm. All wells were put up in triplicates.

3.2.5.2 Competitive ITC

For Competitive ITC experiment, a pre-bound complex of MyoA-MTIP in equal molar ratio (150 µM each) was taken in syringe. The complex was used to titrate ZA1 (10 µM) present in the cell. As a control, pre-bound MyoA-MTIP complex was titrated in buffer only. All the parameters were kept same as the one on one ITC experiment. Origin software was used for data analysis and binding parameters like N, K_a and ΔH were calculated.

3.2.6 *In silico* studies

3.2.6.1 Model construction and Ramachandran plot analysis

X-Ray diffraction structure of MyoA was obtained from protein data bank (PDB ID: 1QAC). For *ab initio* modelling of ZA1 and ZA1S, I-tasser tool was employed. Quality of the resulting model was validated using Ramachandran plot analysis tool PROCHECK.

3.2.6.2 Docking studies

For protein-protein docking of ZA1 and ZA1S with MyoA tail, ClusPro tool was used with default settings. For analysis of the docking results, Pymol, PDBSUM and Ligplot+ tools were used.

3.2.7 Malaria culture studies

3.2.7.1 Parasite culture

P. falciparum 3D7 strain was thawed and cultured *in vitro* in human O+ erythrocytes at 4% haematocrit using the method described previously. Briefly, parasites were cultured in medium containing RPMI 1640 (Invitrogen), supplemented with 2 g/L $NaHCO_3$ (Sigma), 5 g/L Albumax (Invitrogen), 50 mg/L Hypoxanthine (Sigma) and 10 µg/mL gentamicin sulphate (Invitrogen) at a pH of 7.2 under mixed gas condition (5% CO_2, 5% O_2, 95% N_2) at 37 ℃.

3.2.7.2 Growth inhibition assay

For the growth inhibition assay, parasites were synchronized using 5% sorbitol (Sigma) and cultured at 18-20 hour ring-stage in a 24-well plate in triplicates for 72 hours in a total 500 µl volume/well. Initial parasitemia and haematocrit were adjusted to 1% and 2% respectively. ZA1S peptide was added at a final concentration of 10, 20, 40 µM. Control wells without any peptide or inhibitor were set to validate the

normal growth rate of parasite. After every 24 hours, a smear was made. Smears were fixed in methanol and stained 10% Giemsa (Sigma) for 10 min. Percent of infected erythrocytes containing different stages of parasite were counted using light microscope under 100X oil-immersion. Percent growth inhibition was calculated using the following formula, and data was plotted graphically.

$$\% \text{ Growth Inhibition } = \frac{(\text{Control} - \text{treated})}{\text{Control}} \times 100$$

RESULTS

4 RESULTS

4.1 Validation of Myosin A/MTIP interaction

4.1.1 Bacterial-two hybrid studies between Myosin A and MTIP

4.1.1.1 Sequence analysis of chosen targets

*Pf*Myosin A and MTIP are crucial proteins that help drive the insertion of the parasite in the host RBC. Both these proteins form a major component of glideosome complex tethering the whole machinery to the IMC of *P. falciparum*. The interacting regions of *Pf*Myo A and MTIP have been mapped by previous studies [39,42,46]. The interaction of Myo A to MTIP is via the 20 amino acid long C terminal tail of Myo A that makes direct contacts with the C terminal domain of MTIP. First, the protein sequence of the interacting regions was analysed using Expasy ProtParam tool. The isoelectic point or pI of Myo A tail was found to be 12.02 while of MTIP was found to be 4.37 (Figure 4.1). Due to highly basic and acidic nature of both these proteins, the interaction is majorly charged-based.

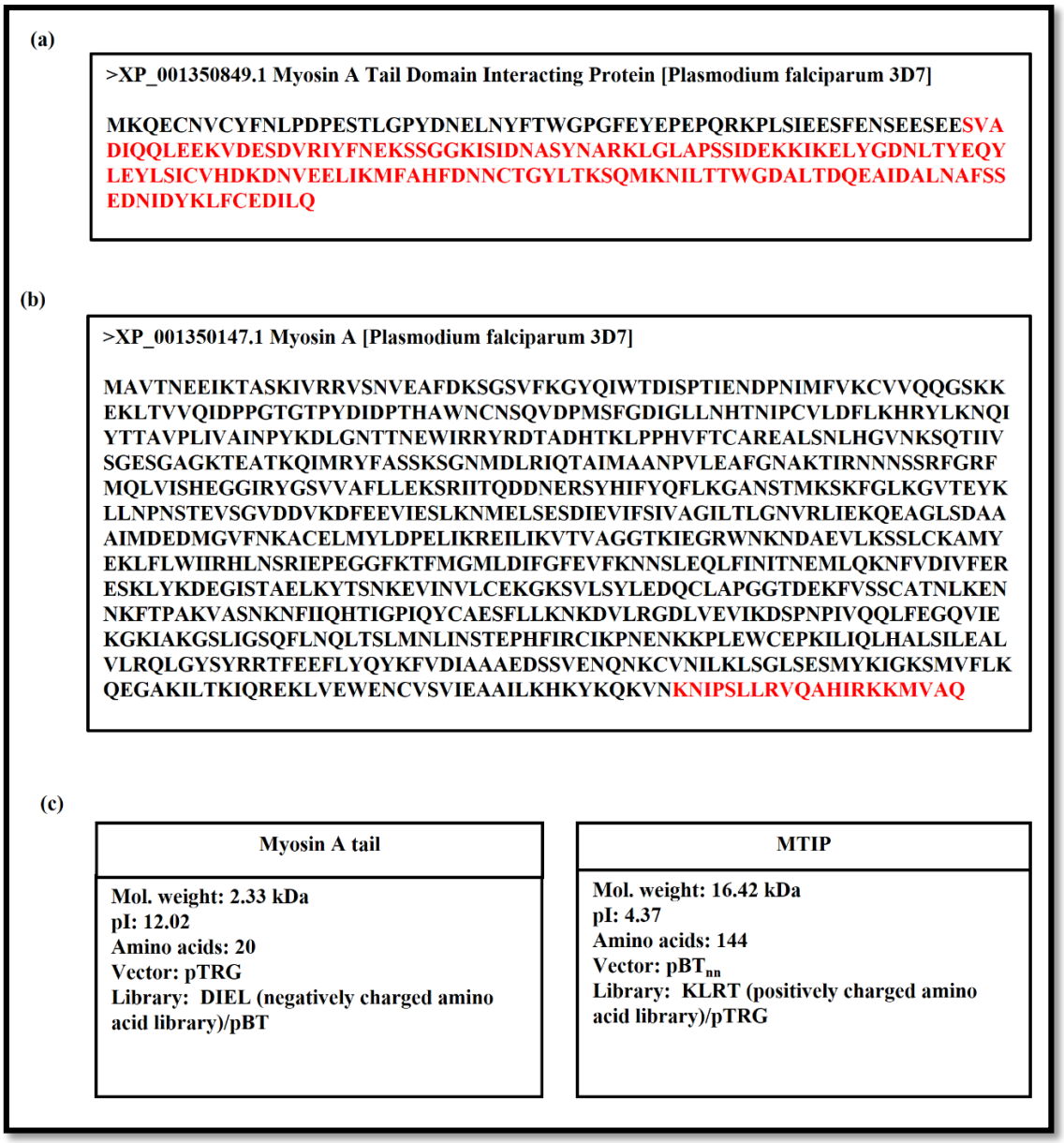

Figure 4.1: Sequences of MTIP and Myosin A. Complete sequence of (a) *Pf*MTIP 204 amino acids and (b) *Pf*Myosin A 818 amino acids long. Sequence in red indicates the interacting regions of the two proteins that are used for the present study. (c) Analysis of the interacting regions of Myo A and MTIP.

4.1.1.2 Cloning of interacting members in bacterial-two hybrid vectors

In order to ascertain this interaction in our system, the interacting domains of *Pf*MyoA (798-818 residues) and MTIP (61-204 residues) were codon optimised and cloned in bacterial two-hybrid vectors pTRG and pBT_{nn}. MTIP-pBT was obtained from Genescript, further it was cloned in pTRG. Myo A tail domain was cloned in pTRG

vector. The presence of insert was confirmed by gene and vector specific primers through colony PCR followed by restriction digestion. A 432 base pair fall-out of MTIP in MTIP-pTRG was observed (Figure 4.2a, 4.2b). For Myosin A tail 101 base pair PCR amplified fragment and positive clones through PCR were obtained (Figure 4.2c, 4.2d). All clones were thereafter sequenced for confirmation.

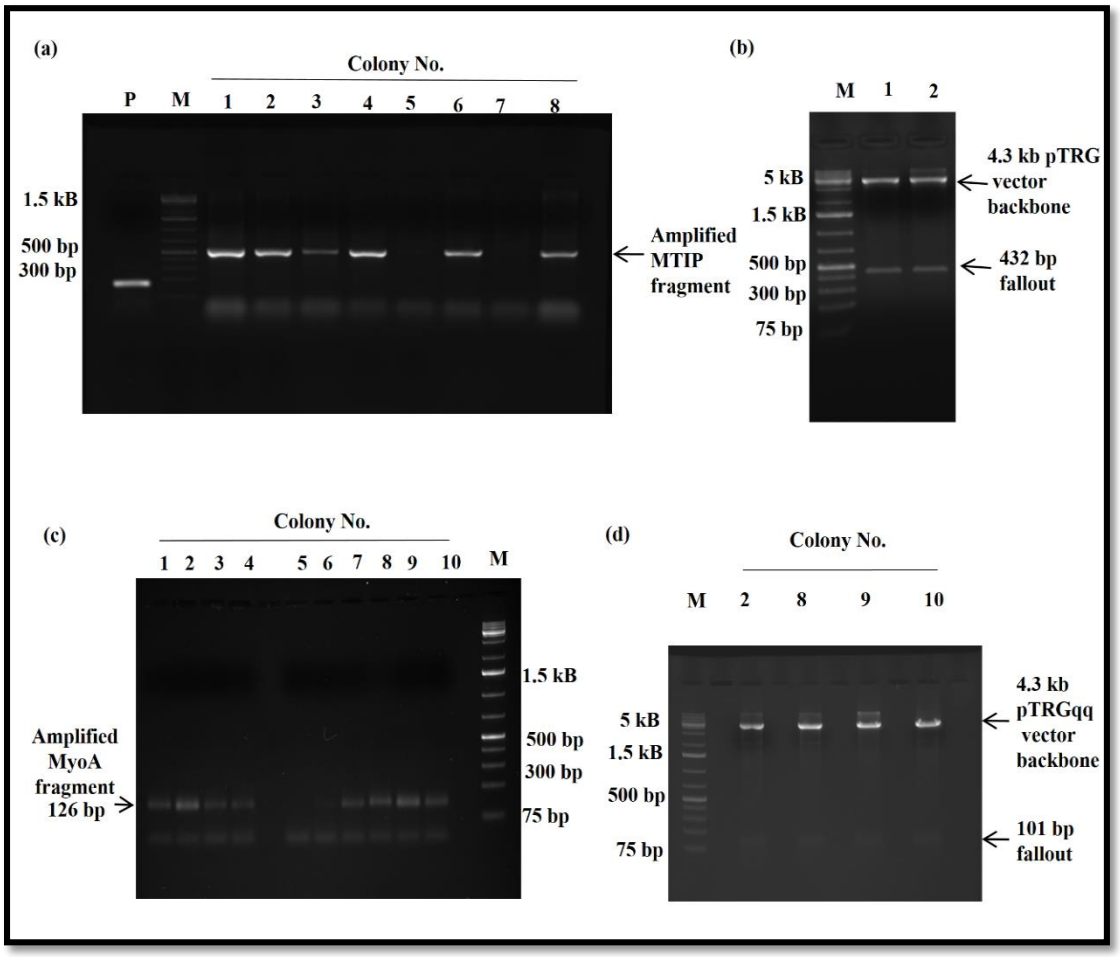

Figure 4.2: Cloning of MTIP and MyoA. (a) Colony PCR showing positive colonies having the MTIP insert after ligation. (b) MTIP fallout of 432 bp after SnaBl enzyme digestion from positive colonies. (c) Colony PCR showing positive colonies having the Myo A insert after ligation. (d) Myo A fall-out of restriction digestion from positive colonies.

4.1.1.3 Bacterial-two hybrid based Myosin A/MTIP interaction validation

The co-transformed R1 competent cells to be used to bacterial-two hybrid assay were checked for the presence of Myo A-pTRG and MTIP-pBT plasmids using gene and vector specific primers. Bands at 127 bp and 526 bp denoting Myo A and MTIP respectively confirmed the presence of both genes in the right orientation (Figure 4.3a).

Using Myosin A-pTRG and MTIP-pBT plasmids, a bacterial two-hybrid assay was set up. A strong interaction between Myosin A tail and MTIP was observed owing to the blue coloured colonies obtained on X-gal indicator plates (Figure 4.3b). Alongside, a well-documented interaction between *Mycobacterial* proteins ESAT-6 and CFP-10 [68,74,75] was used as the positive control and ESAT-6 and empty vector pBT_{nn} was taken as the negative control.

4.1.1.4 Relative strength assessment between Myosin A/MTIP

The relative strength of the interaction between Myosin A tail domain and MTIP was quantified using liquid β-galactosidase assay. The assay is a calorimetric assay based on the amount of reporter enzyme β-galactosidase that is in turn dependent on the number of lacZ reporter transcript copies [19,72]. The relative Miller's units of MyoA/MTIP were found to be 96.14 ± 3.45, even more than the positive control ESAT-6/CFP-10 whose Miller's units were found to be 79.17 ± 1.67 (Figure 4.3c). As negative control ESAT-6/empty pBT was used whose Miller's units were found to be 5.73 ± 0.62.

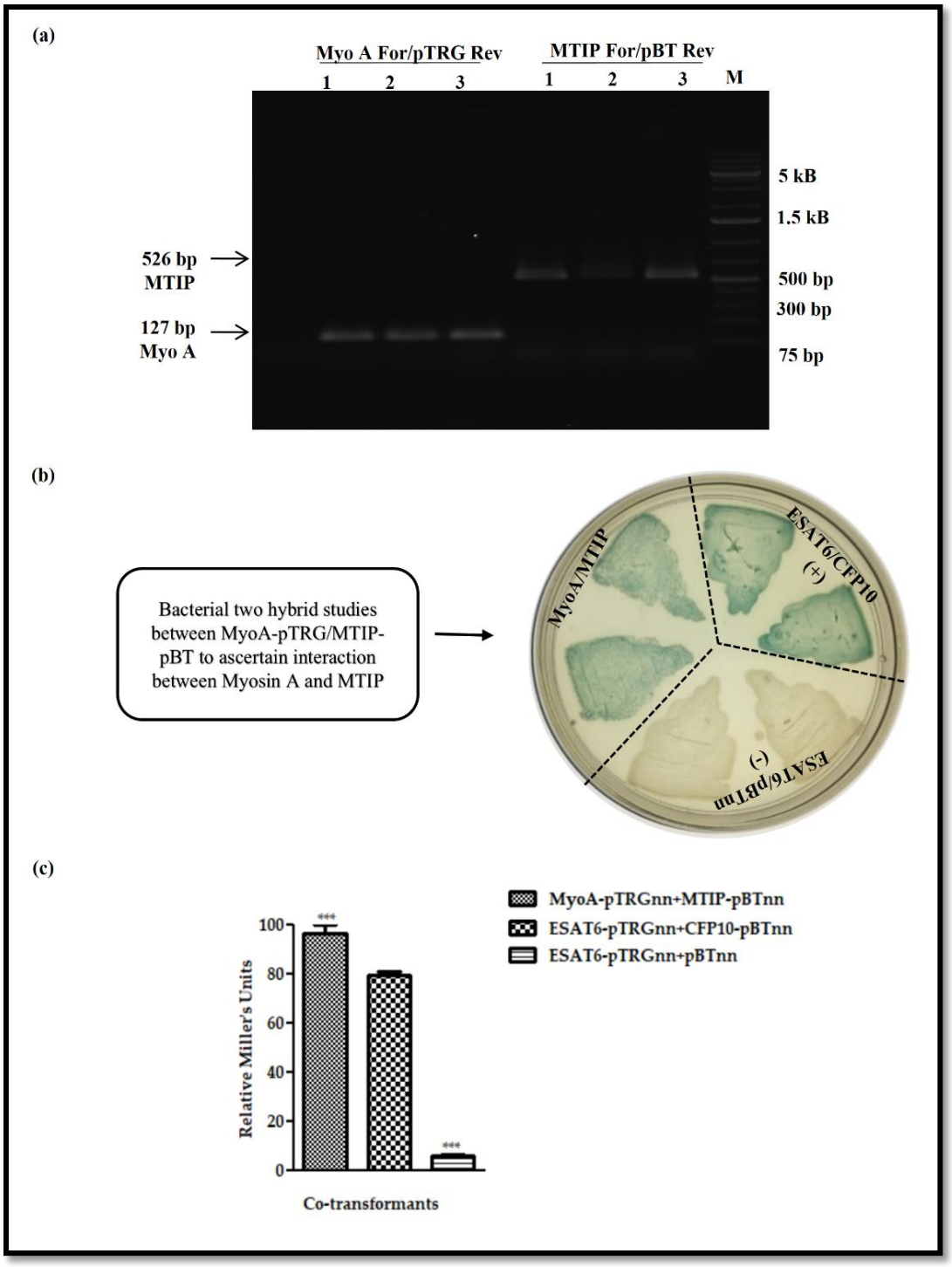

Figure 4.3: Myosin A/MTIP interaction validation. (a) The presence of both interacting partner plasmids MyoA-pTRG and MTIP-pBT after co-transformation in R1 cells confirmed via directional PCR using gene and vector specific primers. Band at 526 bp is of MTIP and 127 bp is of Myo A. (b) X-gal indicator plates showing liquid patching of bacterial two hybrid assay between Myosin A/MTIP (native interaction) (c) Liquid β-galactosidase assay to quantitate the relative enzyme activity (Miller Units) for co-transformant pairs: Myosin A-pTRGnn versus MTIP- pBT 96.14±3.45, ESAT6-pTRGnn versus CFP10-pBTnn 79.17±1.67 (positive control), ESAT6-pTRGnn versus empty pBTnn 5.73±0.62 (negative control).

These findings confirmed the interaction of interacting domains of *Plasmodium* proteins Myo A and MTIP. The results also confirmed that that both these domains maintained structural nativity to associate together as they do inside the parasite.

With this premise, we proceeded to find bindings from dicodon library against any of the chosen targets that would ultimately block this crucial motor interaction.

4.1.2 *In vitro* studies for Myosin A/MTIP interaction characterisation

4.1.2.1 Cloning, expression and purification studies of targets

In order to purify the interacting region of MTIP, MTIP encoding codon-optimised gene was cloned in pET28-a expression vector via blunt end cloning at SnaBl sites. The positive clones were screened via colony PCR followed by restriction digestion to obtain a 432 base pair MTIP fall-out (Figure 4.4a, 4.4b). Finally, the insert sequence was confirmed by sequencing.

For expression analysis, MTIP-pET28-a plasmid was transformed in *E.coli* BL21 (DE3) cells. The vector pET28-a is constructed to add six histidine residues to the C terminal end of the protein that can be used as a tag for purifying the protein via affinity purification. The expression of MTIP was confirmed upon comparing IPTG induced and un-induced cell pellet. A band in IPTG induced lane at the expected size of 16.4 kDa was observed. Next, analysis of MTIP interacting region in bacterial cell pellet or supernatant was carried for purification. Most protein was found to be going in supernatant (Figure 4.4c). Hence, for large scale purification, MTIP was purified from supernatant after sonication.

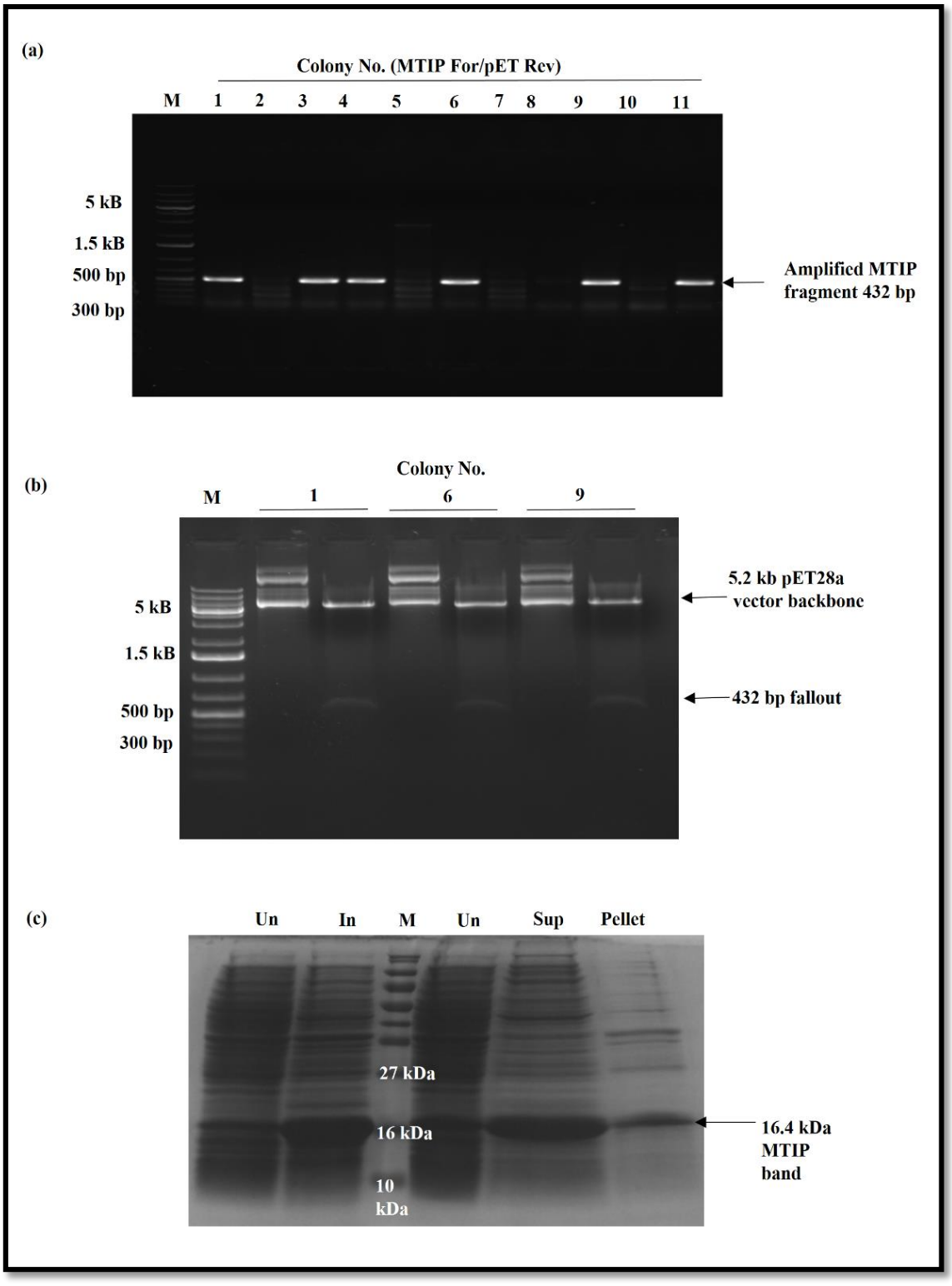

Figure 4.4: Cloning and expression of MTIP. (a) Positive colonies showing the presence of MTIP insert in BlaI-cut-pET28-a vector. (b) MTIP 432 bp fallout after SnaBl digestion of the isolated plasmid. (c) The expression of MTIP in BL21 (DE3) checked. In induced (In) lane a band at 16.4 kDa was observed when compared to un-induced (Un) lane. Most of MTIP protein goes in Supernatant (Sup) pool as indicated with the MTIP band.

Recombinant MTIP-His (61-204 residues) was purified from *E.coli* BL21 (DE3) supernatant. 17.4 kDa MTIP was purified under native conditions by gradually increasing the concentration of imidazole as described in detail in the methods section. The purified MTIP protein was dialysed against PBS for removing imidazole and ran on 15% SDS-PAGE gel and western blotting using *Pf*anti-MTIP antibody (1:15000, rabbit polyclonal) (Figure 4.5a).

Analysis of Myosin A tail peptide: Myosin A tail (798-818 residues) was commercially synthesised and acquired from Genescript. The peptide identity was confirmed by running it on tris-tricine gel to obtain a 2.5 kDa peptide band upon commasie staining (Figure 4.5b).

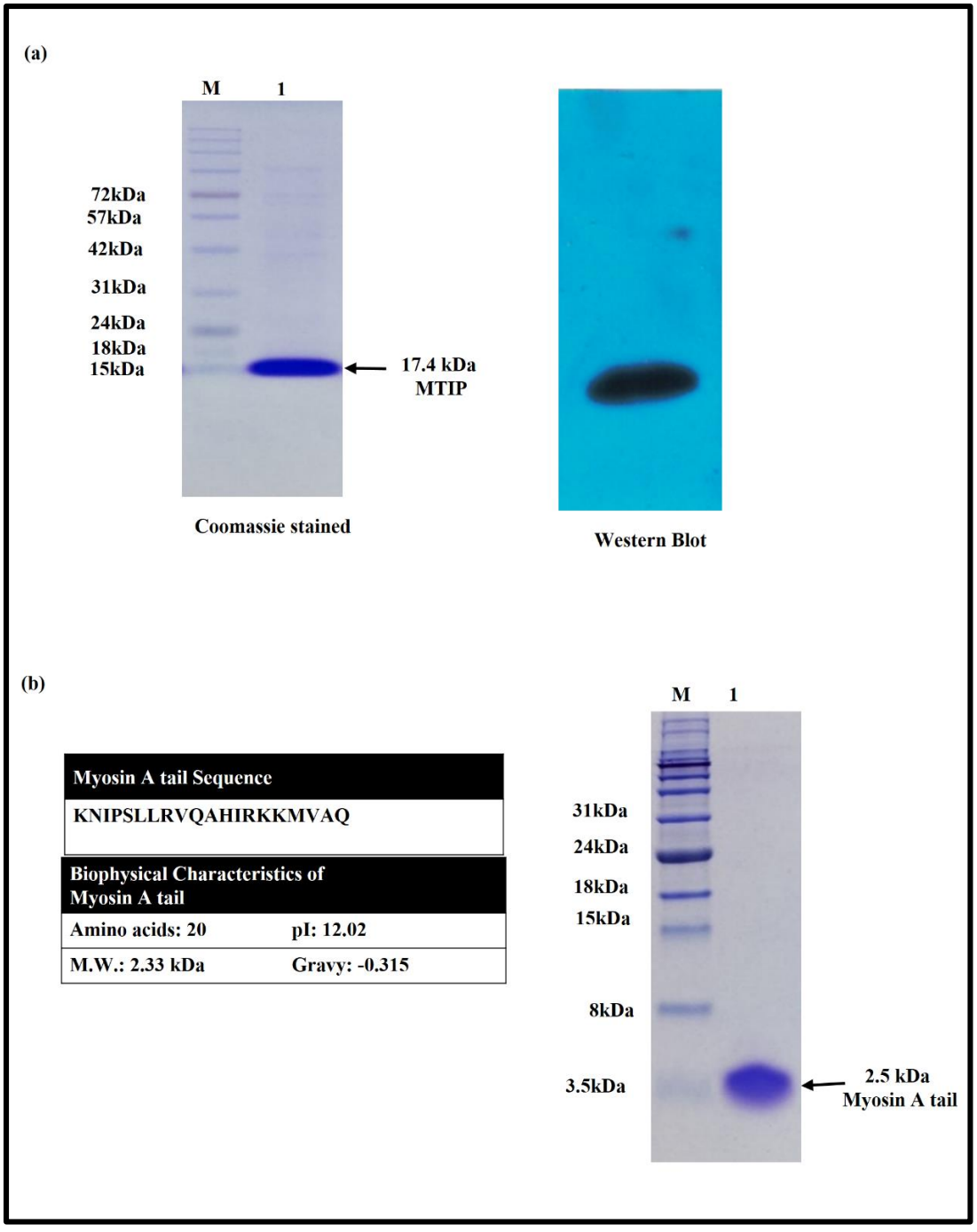

Figure 4.5: Expression of MTIP and Myosin A. (a) Purified MTIP-His by Ni-NTA Column chromatography. Commassie stained 15% polyacrylamide gel. Lane M: Marker, Lane 1: Purified MTIP. (17.4 kDa). Western blot of purified MTIP-His using anti-MTIP (rabbit). (b) Amino acid sequence and biophysical characteristics of MyoA tail. Synthesized Myosin A tail peptide (2.5 kDa) resolved on tris-tricine polyacrylamide gel.

4.1.2.2 ELISA based Myosin A/MTIP interaction study

An ELISA based interaction assay was performed to test the interaction [19,72]. For ELISA, Myo A tail was coated on the ELISA plates and MTIP was overlaid. After stringent washing, the binding of MTIP was detected using anti-MTIP antibody. We found a concentration dependent increase in between Myo A/MTIP interaction (Figure 4.6a). The specificity of the interaction was tested by testing the ELISA based interaction of MTIP with an unrelated protein ESAT-6 in which no interaction was found (Figure 4.12b).

4.1.2.4 SPR based Myosin A/MTIP interaction study

As a proof of concept, the interaction of Myo A tail with MTIP was checked by SPR. For this, Myo A peptide was immobilised on the sensor chip surface followed by injection of MTIP at increasing concentrations. A clear association and dissociation curve upon injection and exhaustion of MTIP was observed confirming the interaction. The response units or degree to shift in the angle due to Myo A tail-MTIP interaction was also found to be directly proportional to the concentration of MTIP (Figure 4.6b). The K_d for the interaction was found to be 22.7 µM.

4.1.2.3 ITC based Myosin A/MTIP interaction study

The interaction of Myo A tail and MTIP was also studied by ITC [76]. The binding of Myo A to MTIP showed negative enthalpy (binding enthalpy change ΔH: -4.7 kcal/mol) and positive entropy (TΔS: 3.8 kcal/mol) suggesting that the reaction was both enthalpy and entropy driven. The dissociation constant for Myo A/MTIP was found to be 450 nM (Figure 4.6c, 4.6d). A sigmoidal curve ending near the zero base line indicated the saturation of all binding sites.

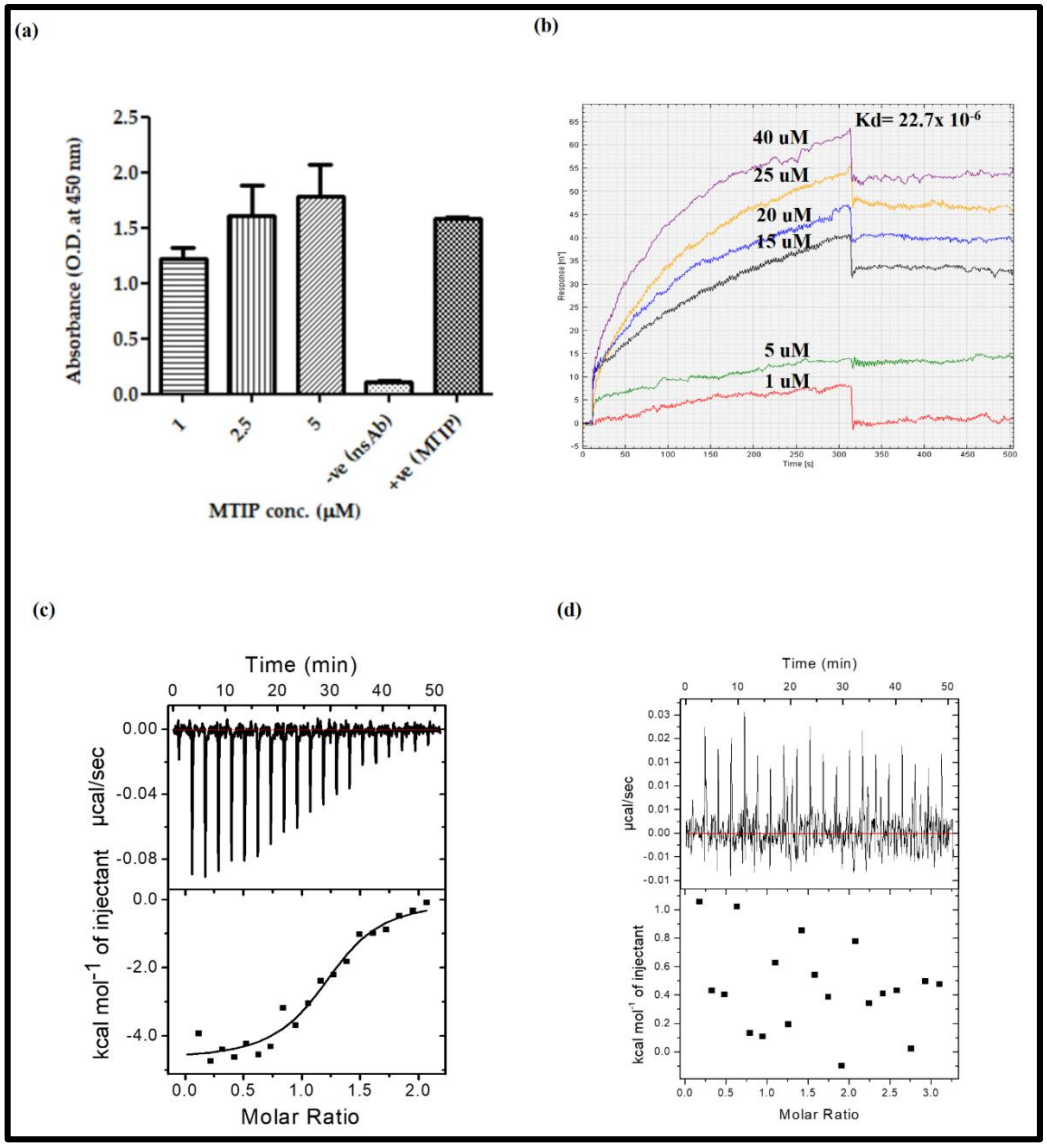

Figure 4.6: *In vitro* protein-protein interaction studies between Myosin A/MTIP. Validation of interaction between MyoA and MTIP tail protein by (a) ELISA based interaction assay, (b) Surface Plasmon Resonance analysis and (c) Isothermal Titration Calorimetry (ITC) studies. ITC data upper panel depicts the raw calorimetric values denoting the amount of heat (exothermic peaks) produced following sequential injection of Myosin A into MTIP. The amount of heat generated per injection as a function of molar ratio of Myosin A to MTIP is depicted in the lower panel. K_d of Myosin A/MTIP interaction was found to be 0.45 x 10^{-6}. (d) Buffer control for ITC experiment. Final ITC data was obtained by subtracting the data with background heats. For ELISA based assay, Myosin A was coated on ELISA plates. MTIP was overlaid at increasing concentrations as shown and detected by anti-MTIP (rabbit) antibody followed by detection using HRP conjugated secondary antibody. A non-specific antibody (anti-CFP10) was used as the antibody control. MTIP coated on plates was used as the positive control. Negative control for the ELISA experiment is shown Figure 4.12b. The ELISA for all interactions was performed in triplicates and each bar represents mean ± standard deviation represented by error bars. For Surface Plasmon Resonance analysis, the indicated concentrations of MTIP were overlayed on immobilized Myosin A and biophysical parameters were computed using 1:1 binding model. K_d of Myosin A/MTIP interaction was found to be 22.7 x 10^{-6}.

4.2 Identification of binder(s)

4.2.1 Synthesis of dicodon library

The dicodon *de novo* library was synthesised using part-rational approach [69,77]. In this approach, various dicodon were mixed in screwed ratios to obtain preferentially charged library. For this, KL, RT; DI, EL were the dicodons added in skewed ratios. The ligated dicodons were then ligated with HP2P primers and the ligated PCR amplified inserts were checked on agarose gel. Inserts smaller than 1000 bp were eluted since only small molecule binders against targets need to be identified (Figure 4.7a). The eluted inserts were ligated with de-phosphorylated pBT and pTRG vectors and finally the obtained library was checked on agarose gel (Figure 4.7b).

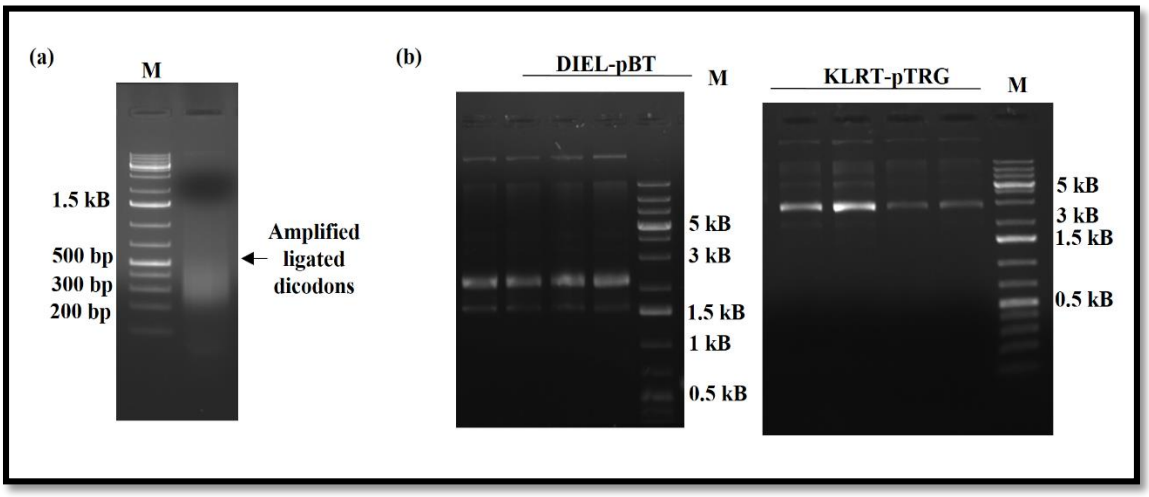

Figure 4.7: Synthesis of *denovo* dicodon library. (a) Amplified dicodons to be ligated in bacterial-two hybrid vectors. (b) Dicodon libraries DIEL-pBT and KLRT-pTRG after ligation and plasmid isolation.

4.2.2 *De novo* binder screening through bacterial two-hybrid

4.2.2.1 Unearthing Myosin A tail binders

The interaction of Myo A to MTIP is indispensable for successful parasite invasion. Previous studies have shown the C terminal tail of Myo A is sufficient and is the only region that interacts with MTIP [46,46]. Also, the interacting regions of Myo A and MTIP are shown to be drug targets with inhibitors targeting the interaction successfully blocking *P. falciparum* entry in host RBC [43,78,79]. Hence, *de novo* peptide library was screened with the aim to unearth potent peptide binders of Myo A tail. For this, a bacterial two-hybrid assay was set up using Myo A-tail-pTRG and the library of opposite charge (negative) DIEL-pBT to increase the chances of finding charged based interaction binder of Myo A tail. Four binders ZA1, ZA2, ZA3, and ZA4 were found to interacting with Myosin A after repeated rounds of transformation, segregation and re-co-transformation (Figure 4.8a). Of these ZA1 and ZA4 showed stronger binding based on intensity of blue colour on X-gal indicator plate. After sequencing all the binders, ZA1 and ZA4 were found to have same sequence (Figure 4.8b).

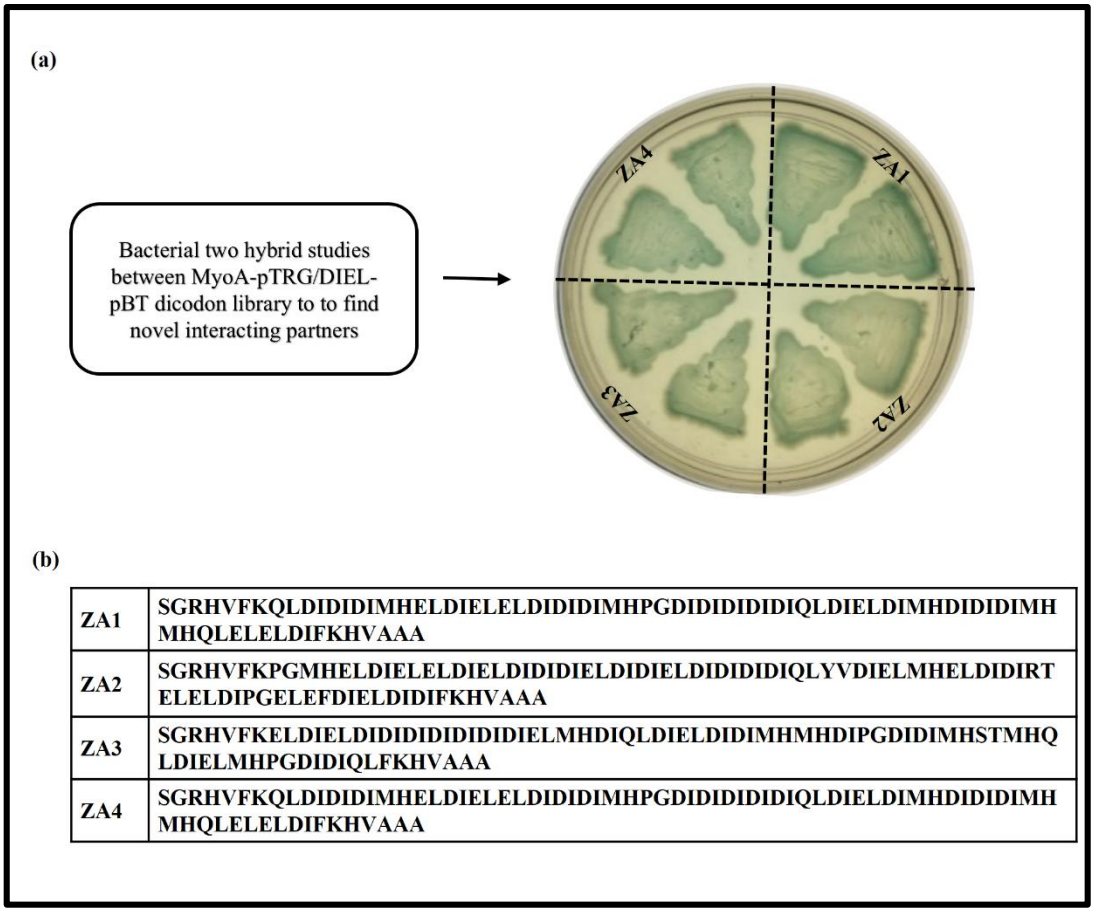

ZA1	SGRHVFKQLDIDIDIMHELDIELELDIDIDIMHPGDIDIDIDIDIQLDIELDIMHDIDIDIMH MHQLELELDIFKHVAAA
ZA2	SGRHVFKPGMHELDIELELDIELDIDIDIELDIDIELDIDIDIDIQLYVDIELMHELDIDIRT ELELDIPGELEFDIELDIDIFKHVAAA
ZA3	SGRHVFKELDIELDIDIDIDIDIDIDIDIELMHDIQLDIELDIDIMHMHDIPGDIDIMHSTMHQ LDIELMHPGDIDIQLFKHVAAA
ZA4	SGRHVFKQLDIDIDIMHELDIELELDIDIDIMHPGDIDIDIDIDIQLDIELDIMHDIDIDIMH MHQLELELDIFKHVAAA

Figure 4.8: Binders of Myosin A tail. (a) X-gal indicator plate showing binders of Myosin A obtained upon screening against DIEL dicodon library. The intensity of blue colour indicates strength of interaction. (b) Sequence analysis of various Myosin A tail binders.

4.2.2.2 Bacterial-two hybrid based Myosin A/ZA1 interaction study

The interaction between the chosen most potent binder of Myo A tail was confirmed by bacterial two-hybrid assay wherein Myo A was cloned in pTRG and ZA1 was re-cloned in pBT bacterial two-hybrid vector. Blue-coloured colonies gave a qualitative analysis of the interaction between Myo A tail and ZA1 (Figure 4.9a). Alongside, ESAT-6/CFP-10 and ESAT-6/empty pBT were used as positive and negative controls respectively.

4.2.2.3 Relative strength assessment between Myosin A/ZA1

The quantitative analysis of interaction was done using β-galactosidase assay with the same controls. The relative strength of Myosin A/ZA1 was found to be at least 80% of the positive interaction, confirming a strong significant interaction (Figure 4.9b).

4.2.2.4 Sequence analysis of ZA1

Sequencing of ZA1 showed it to be an 80-amino acid long novel polypeptide. Further analysis was performed using Expasy's ProtParam tool. GRAVY value of ZA1 was found to be 0.146 and the pI was found to be 4.01 (Figure 4.9c). A highly acidic nature of ZA1 further hinted on charged based interaction with Myosin A tail whose pI is 12.02.

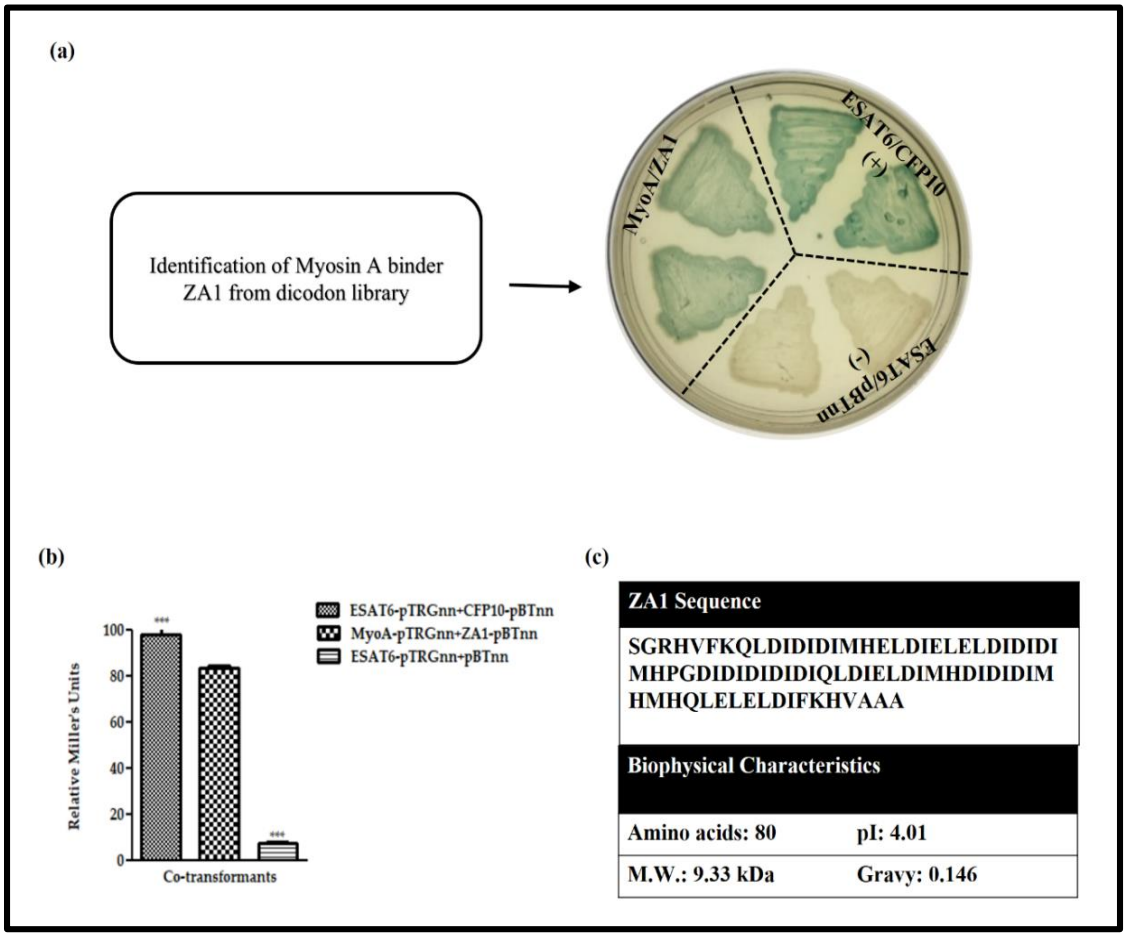

Figure 4.9: Identification of a *de novo* peptide ZA1 binding partner for *P. falciparum* MyoA tail. (a) X-gal indicator plates showing liquid patching of bacterial two-hybrid assay between Myosin A/ZA1 peptide (b) Liquid β-galactosidase assay to quantitate the relative enzyme activity (Miller Units) for co-transformant pairs: Relative Miller Units: Myosin A-pTRGnn versus ZA1-pBTnn 83.48±0.82, ESAT6-pTRGnn versus CFP10-pBTnn 98.02±2.07 (positive control), ESAT6-pTRGnn versus empty pBTnn 7.10±0.77 (negative control). All streaks are labelled to represent genes cloned in pTRGnn/pBTnn. ESAT6-pTRGnn/CFP10-pBTnn and ESAT6-pTRGnn/empty pBTnn are the positive and negative controls respectively. Graphs depict the representative of one of the three independent biological replicates (technical triplicates) and error bars represents the standard deviation. (c) Amino acid sequence and biophysical characteristics of ZA1 polypeptide identified from *denovo* codon-shuffled library. Expasy's ProtParam tool (https://web.expasy.org/protparam/) was used to find the molecular weight, isoelectric point and hydropathicity of ZA1.

4.2.3 *In vitro* studies for Myosin A/ZA1 interaction characterisation

4.2.3.1 Cloning, expression and purification studies of Myosin A binder

The cloning of ZA1 for expression, purification and bacterial three-hybrid assays was done in pMTSA vector at SnaBl restriction enzyme site via blunt end cloning. The presence of ZA1 insert was confirmed in the obtained colonies by colony PCR using pMTSA For/Rev primers and HP2P primers. A band at the expected site confirmed cloning (Figure 4.10a). In case of pMTSA For/Rev primers, the band at a higher position was obtained owing to the additional amplified pMTSA vector sequence (Figure 4.10a). The orientation and sequence was lastly confirmed by sequencing the plasmid. Next, for expression check ZA1-pMTSA was transformed in *E.coli* BL21 (DE3) and the expression of ZA1 was checked supernatant and pellet. ZA1 protein was found to be completely going in pellet (Figure 4.10b). Hence, pellet culture pellet was subsequently used for large scale ZA1 purification.

Large scale purification of ZA1 was carried out from *E.Coli* pellet under-denaturing conditions of urea. The protein was later refolded and checked using tris-tricine gel. A band at 10.33 kDa of ZA1 was obtained. The identity of the protein was further

confirmed by a western blot using anti-His antibody that indicated a band at the same position (Figure 4.10c).

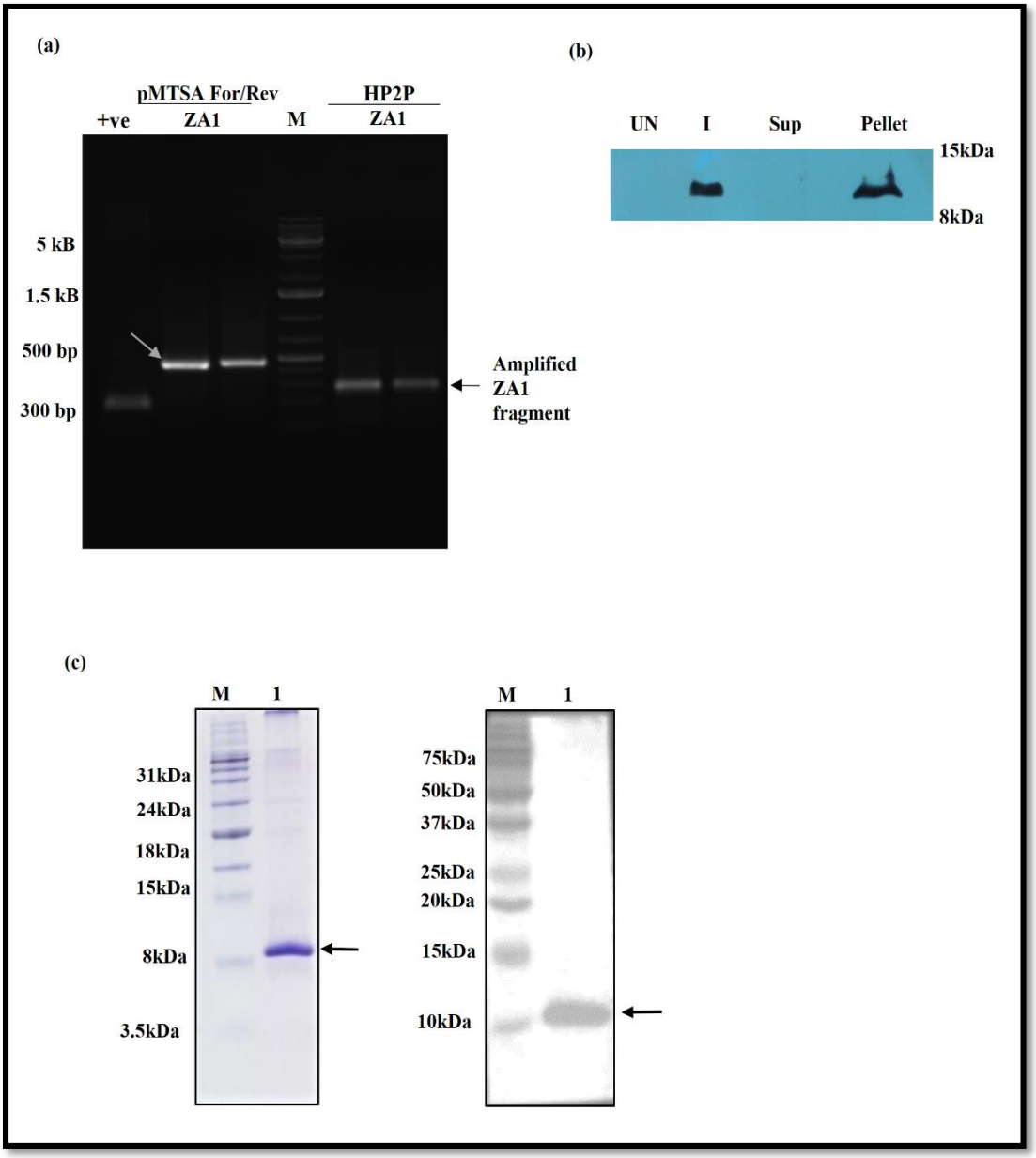

Figure 4.10: Cloning and expression of ZA1 polypeptide. (a) Confirmation of the presence of ZA1 insert in pMTSA vector after ligation using vector specific and HP2 primers. (b) Expression analysis confirming the expression of ZA1 cloned in pMTSA and transformed in R1 cells. A band near 10 kDa in induced (I) well and not in un-induced well confirmed ZA1 expression. ZA1 polypeptide completely goes to pellet pool as observed from the band. (c) Purification of His-tagged ZA1 by Ni-NTA column chromatography under denaturing conditions, followed by a refolding step. Coomassie stained tris-tricine gel. Lane M: Marker, Lane 1: Purified C-terminal His tagged ZA1 (10.33 kDa). Western blot of ZA1 using anti-His (mouse) antibody followed by detection using HRP conjugated anti-mouse secondary antibody.

4.2.3.2 ELISA based Myosin A/ZA1 interaction study

In order to test if ZA1 interacted with Myo A tail *in vitro,* various protein-protein interaction assays were performed. For ELISA, the interaction between the two was checked by coating Myo A tail on ELISA plate well followed by an overlay coating of ZA1-His *de novo* peptide. The amount of ZA1 binding to Myo A tail was detected using an anti-His antibody. The results showed a gradual concentration dependent increase in the intensity of interaction between Myo A tail and ZA1 as the overlaying concentration is increased, as observed by calorimetric OD measurement at 450 nm (Figure 4.11a). Alongside, the un-coated plate showed baseline absorbance. The specificity of this interaction was also confirmed with a parallel control to test the interaction of ZA1 with an unrelated protein ESAT-6 with which no interaction was found Figure 4.12b.

4.2.3.3 ITC based Myosin A/ZA1 interaction study

The assessment of Myo A-tail-ZA1 interaction and biophysical characterisation was next performed by ITC. For this, Myo A was titrated into ZA1. A sigmoidal curve that is typical to binding isotherm indicated a positive interaction between the two peptides. The curve reaching zero baseline indicated saturation of all ZA1 molecules (Figure 4.11b). Data fitting was done using single site model. The binding interaction resulted in 1:1 stoichiometry suggesting that one molecule of Myo A binds with one molecule of ZA1. The binding was observed to be enthalpically opposed (ΔH: +2.4 kcal/mol) and entropically favourable ($T\Delta S$: +10.9 kcal/mol) resulting in a strong binding affinity with a dissociation constant, K_d of 660 nM. In order to rule out the possibility of heat changes simply due to Myo A, a parallel control experiment was run in which Myo A was sequentially added into buffer was performed and it showed

no heat changes (Figure 4.12a). The results confirmed the interaction of novel polypeptide ZA1 with Myo A tail.

4.2.3.4 SPR based Myosin A/ZA1 interaction study

As a proof of concept, the interaction of Myo A tail with ZA1 was investigated by SPR. In a manner similar to Myo A-MTIP interaction testing, Myo A peptide was immobilised on the sensor chip surface followed by injection of MTIP at increasing concentrations. A clear association and dissociation curve upon injection and exhaustion of ZA1 proved the interaction between the two. The K_d for the interaction was found to be 5.11 µM (Figure 4.11c).

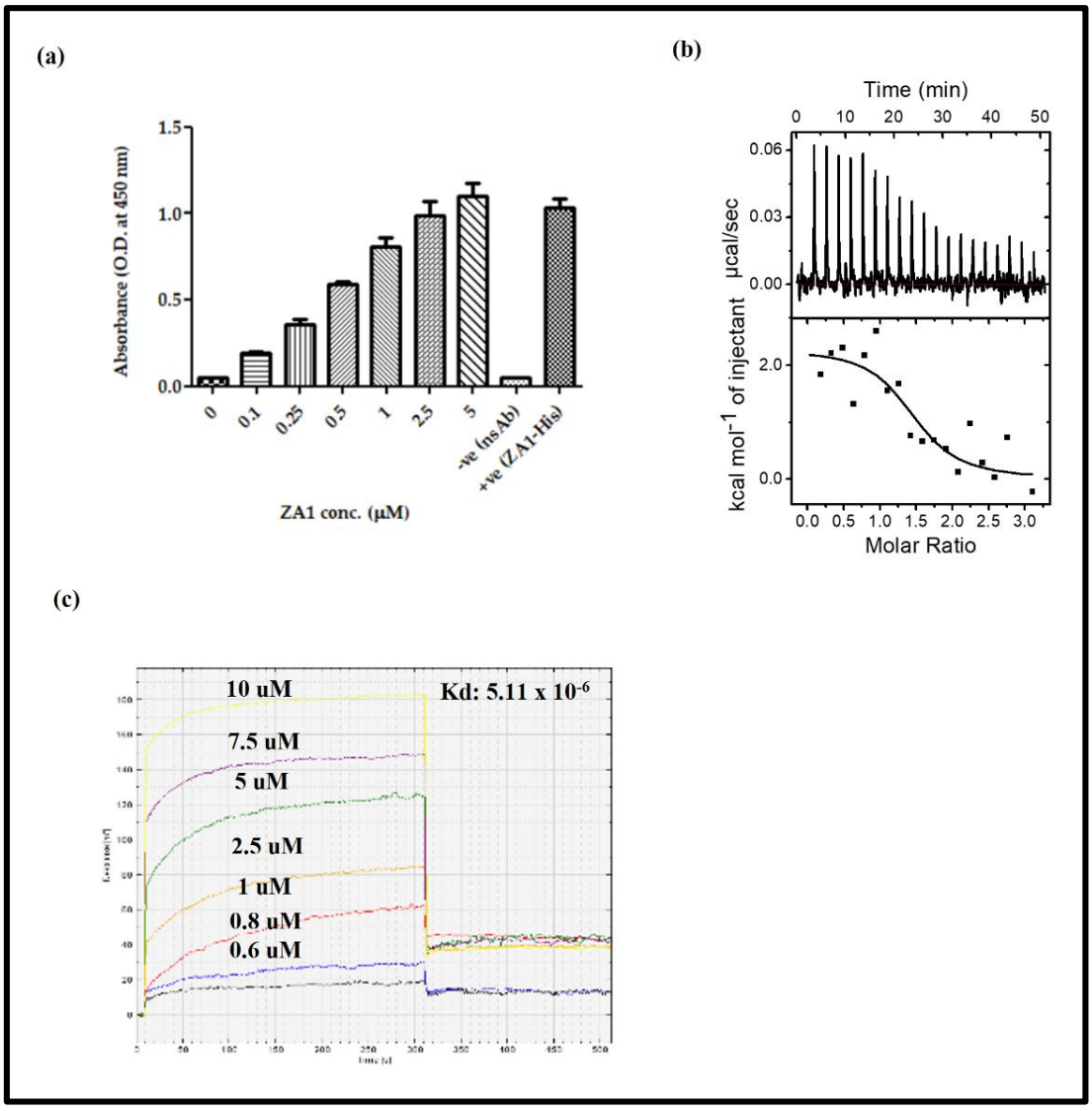

Figure 4.11: *In vitro* protein-protein interaction studies between Myosin A/ZA1. Validation of interaction between MyoA and ZA1 peptide by (a) ELISA based interaction assay (b) Isothermal Titration Calorimetry (ITC) studies (c) Surface Plasmon Resonance analysis. ITC data upper panel depicts the raw calorimetric values denoting the amount of heat (endothermic peaks) produced following sequential injection of Myosin A into ZA1. The amount of heat generated per injection as a function of molar ratio of Myosin A to ZA1 is depicted in the lower panel. K_d of Myosin A/ZA1 interaction was 1.9 x 10^{-6}. Buffer control for ITC experiment is shown in Figure 4.12a. Final ITC data was obtained by subtracting the data with background heats. For ELISA based assay, Myosin A was coated on ELISA plates. ZA1 was overlaid at increasing concentrations as shown and detected by or anti-His (mouse) antibody respectively followed by detection using HRP conjugated secondary antibody. A non-specific antibody (anti-CFP10) was used as the antibody control. ZA1 coated on plates was used as the positive control. Negative control for the ELISA experiment is shown in Figure 4.12b. The ELISA for all interactions was performed in triplicates and each bar represents mean ± standard deviation represented by error bars. For SPR analysis, the indicated concentrations of ZA1 were overlaid on immobilized Myosin A and biophysical parameters were computed using 1:1 binding model. K_d of Myosin A/ZA1 interaction was 5.11 x 10^{-6}.

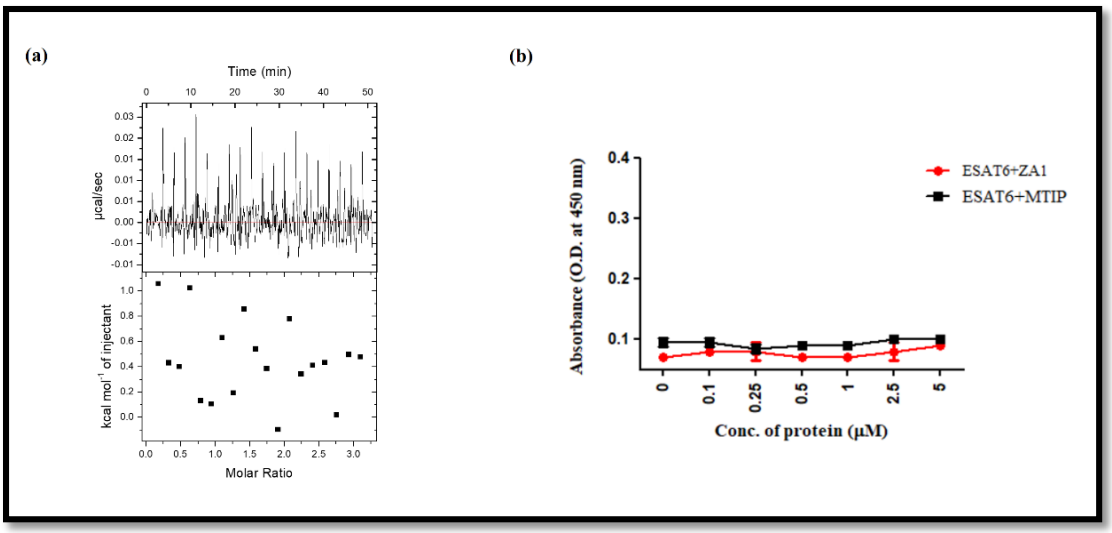

Figure 4.12: Negative control for ITC and ELISA experiments. (a) The raw calorimetric data denoting the amount of heat produced following each injection of Myosin A from syringe into cell containing buffer only. No heat changes were observed when Myosin A was added into buffer. (c) 500 ng non-specific Mycobacterial protein ESAT-6 was coated on ELISA plates and indicated concentrations of ZA1 and MTIP were overlaid respectively. No interaction was observed between the coated and overlaid proteins.

4.3 Myosin A/MTIP complex disruption studies

4.3.1 *In vivo* studies for inhibition of Myosin A/MTIP

4.3.1.1 Bacterial-three hybrid studies

Myo A/MTIP exist as a complex initiating *P. falciparum*'s entry in human RBC. Upon electrostatic, covalent and ionic interaction establishment between the tail amino acids of Myo A and MTIP C-terminal domain the motor domain of Myo A hydrolysis ATP thereby producing the propulsive force. With this background and a potent binder of Myo A tail, ZA1 in hand, it was prudent to assess ZA1's capacity to disrupt Myo A-MTIP complex. For this ZA1 cloned in pMTSA vector earlier was transformed in R1 cells harbouring Myo A-tail-pTRG and MTIP-pBT and plated on X-gal indicator plates containing arabinose. The plasmids were also plated on X-gal arabinose negative plates. Arabinose acted as an inducer of ZA1. As a control, a parallel transformation using empty pMTSA vector was done in R1 cells harbouring Myo A-tail-pTRG and MTIP-pBT. The 'test' showed blue coloured colonies in arabinose minus plate asserting the successful Myo A/MTIP complex formation while white R1 colonies where observed in arabinose plus X-gal plate. The white colonies indicated that Myosin A/MTIP complex where unable to form in the presence of ZA1 (Figure 4.13a). Parallely, in the 'control' cells the complex was formed both in presence and absence of arabinose.

4.3.1.2 Arabinose gradient liquid β-galactosidase assay

To test if the amount of ZA1 has a direct effect on Myo A/MTIP complex formation, L-Arabinose gradient β-galactosidase assay was performed. In this, R1 cells harbouring Myo A-tail-pTRG and MTIP-pBT plasmids were transformed with either ZA1-pMTSA or pMTSA only. The expression of ZA1 was tightly regulated with

pBAD promoter that unlike IPTG inducible promoters do not show leaky expression of the downstream gene. Additionally, the expression of the downstream gene can be regulated over a wide range of arabinose concentrations and subsequent levels of lacZ expression. Upon induction, the test showed an arabinose dependent depletion of lacZ expression corroborating to less interaction of Myo A tail with MTIP due to increased ZA1 expression (Figure 4.13b). Simultaneously, control pMTSA did not show any disruption of Myosin A/MTIP complex at any L-arabinose concentration due to empty pMTSA vector. A gradual increase in the levels of ZA1 upon increasing arabinose was confirmed by western blot analysis by detecting the amount of ZA1 expressed at various arabinose concentrations.

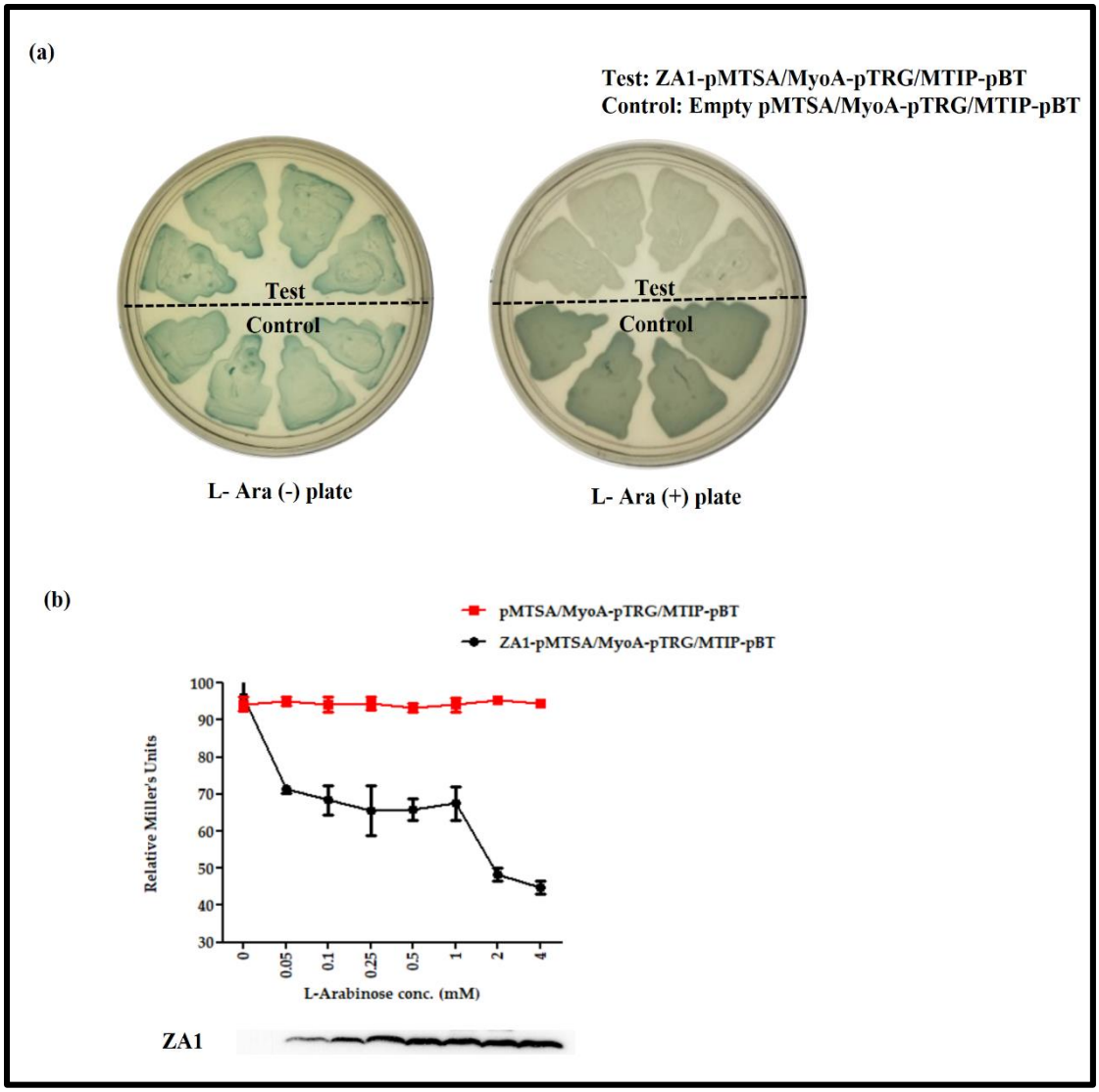

Figure 4.13: Disruption of MyosinA/MTIP interaction by bacterial three-hybrid assay (*in vivo*). Bacterial three-hybrid assay to study the disruption of Myosin A/MTIP complex by ZA1 in the absence and presence of L-Arabinose. (a) *E.coli* triple co-transformant containing ZA1-pMTSA, Myosin A-pTRGnn and MTIP- pBT (test) and Triple co-transformant containing empty pMTSA, Myosin A-pTRGnn and MTIP- pBT (control) on LB agar with 2% L-Arabinose (b) L-Arabinose gradient liquid β-galactosidase assay. Relative Miller Units of triple co-transformant pairs empty pMTSA, Myosin A-pTRGnn, MTIP- pBT (red line) and ZA1-pMTSA, Myosin A-pTRGnn, MTIP- pBT (black line) plotted against a range of L-Arabinose concentrations. The graph is an average of three independent assays and standard deviation is represented by error bars. Below it is the western blot of *E.coli* whole cell lysates to analyse the expression of ZA1 with increasing concentrations of L-Arabinose using anti-His (mouse) antibody followed by detection using HRP conjugated secondary antibody.

4.3.2 *In vitro* studies for inhibition of Myo A/MTIP

4.3.2.1 Complex disruption via competitive ELISA

In order to ascertain the binding of ZA1 with Myosin A tail in the presence of MTIP, we performed competitive binding experiments by ITC and ELISA. Myo A tail was coated on ELISA plates followed by equimolar ratio of MTIP to allow Myo A/MTIP complex formation. The complex was overlaid with ZA1 in increasing concentrations and after stringent washing the amount of MTIP bound to Myo A tail was detected using specific antibody. The binding of Myo A to MTIP was found to be negatively dependent on ZA1 concentrations. The amount of MTIP bound to Myo A tail reduced with increasing ZA1 confirming the preferential binding of Myo A to ZA1 in the presence of MTIP (Figure 4.14a).

4.3.2.2 Complex disruption via competitive ITC

The ability of ZA1 to disrupt the Myo A/MTIP complex was further tested by competitive binding analysis using ITC. Here, a MTIP-bound Myo A was titrated into ZA1. If the Myo A/MTIP complex is able to bind ZA1, that will prove the ability of ZA1 to interfere with the Myo A-MTIP complex. The result in Figure 4.14b shows that MTIP-bound Myosin binds to ZA1 but with weaker affinity (K_d: 47 µM) compared to free Myosin A binding to ZA1. The interactions are driven by unfavourable enthalpy (ΔH: 53 kcal/mol) and favourable entropy (TΔS: 59.3 kcal/mol; ΔG= 6.3 kcal/mol) Thus, 80 times decrease in the binding strength clearly indicates competition between ZA1 and MTIP for Myosin A. However, no complete elimination of binding strength suggests two possibilities 1) ZA1 binds partially to a MTIP site and thus interfere with Myosin-MTIP complex 2) ZA1 has additional binding site on Myosin A apart from MTIP-site. The graph showed an endothermic binding curve (in contrast to exothermic binding curve of Myo A/MTIP complex with positive enthalpy and entropy in agreement to binding characteristics observed for Myo A/ZA1 binding (Figure 4.14b). A parallel ITC experiment showing near zero

heat changes upon injection of Myo A/MTIP complex in PBS confirmed that the heat changes were due to Myo A/MTIP complex disruption and Myo A/ZA1 complex formation (Figure 4.14c).

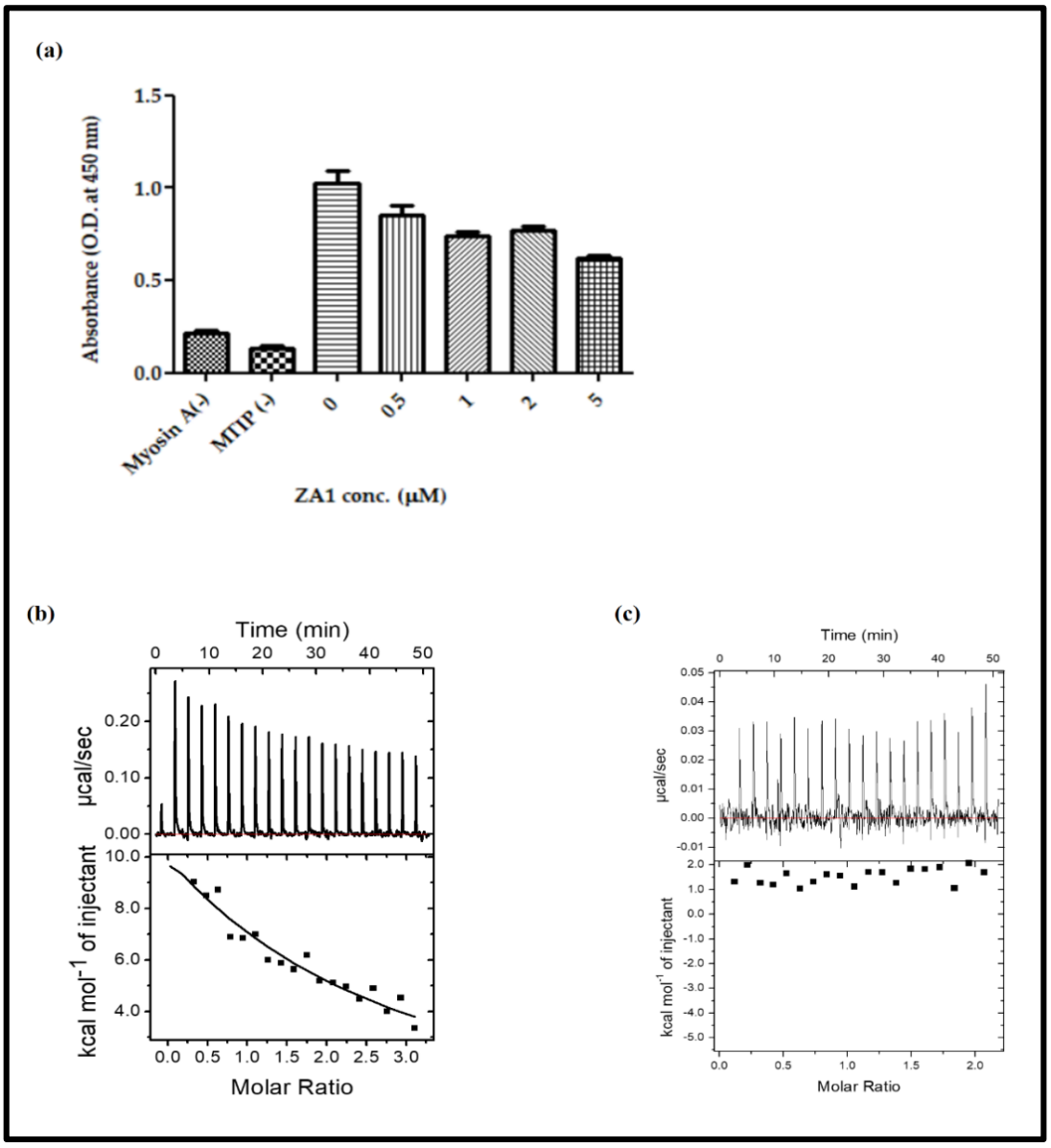

Figure 4.14: Disruption of Myosin A/MTIP interaction in presence of ZA1 *in vitro*. (a) ELISA based inhibition of interaction between Myosin A and MTIP using the inhibitor ZA1. Myosin A was coated on ELISA plates followed by overlaying of MTIP. Next, ZA1 protein was overlaid at the indicated concentrations followed by detection by anti-MTIP (rabbit) antibody and by detection using HRP conjugated anti-rabbit secondary antibody. As negative controls, in a subset of wells Myosin A and MTIP was not coated. (b) Isothermal Titration Calorimetry competitive binding for titration of pre-bound Myosin A-MTIP complex to ZA1. With each injection of the complex from syringe into the cell heat changes due to Myosin A-ZA1 interaction are plotted against time (upper panel). The amount of heat generated as a function of molar ratio of Myosin to ZA1 is represented (lower panel). (c) Control for the competitive binding experiments for ITC.

4.4 Elucidation and interaction studies of shorter peptide

4.4.1 Bioinformatics studies for identification of short peptide

4.4.1.1 Myosin A/ZA1 *in silico* studies

In order to fully understand the residue by residue interaction between Myo A/ZA1 *in silico* studies were performed. The Myo A/ZA1 complex interacts via eleven hydrogen bonds and the binding was found to be favourable with a minimum binding energy of -586.4 kCal/mol. Interestingly, most polar contacts lay along a stretch of amino acids from Aspartate-10 to Glutamate-18. This encouraged us to study the binding of Myo A tail with a shortened ZA1: ZA1S (DIDIDIMHE). Ramachandran plot of Myo A tail/ZA1 structure derived from homology modelling showed the residues in the favourable region, thus validating the *in silico* predicted model for interaction (Figure 4.15a).

4.4.1.2 Myosin A/ZA1S *in silico* studies

Docking studies between Myo A tail and ZA1S were performed in a manner similar to Myo A/ZA1 *in silico* studies. The results revealed a favourable interaction with a minimum binding energy -447.3 kCal/mol and eleven hydrogen bonds. Ramachandran plot of Myo A tail/ZA1S structure derived from homology modelling showed the residues in the favourable region, thus validating the *in silico* predicted model for interaction (Figure 4.15b).

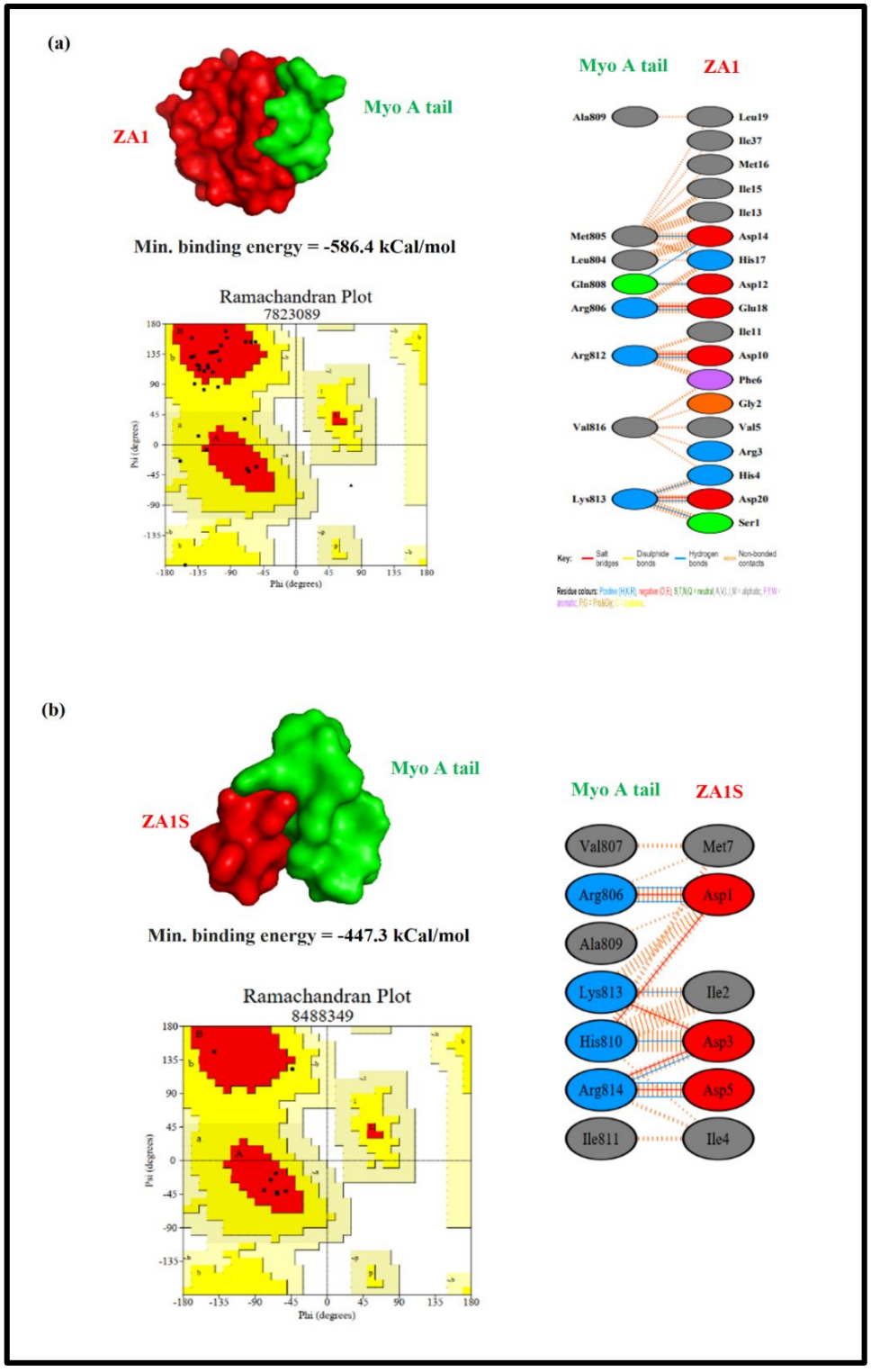

Figure 4.15: *In silico* studies for identification of a shorter peptide. (a) The 3D structure of ZA1 (red) interacting with Myosin A tail (green) obtained through Pymol. The space filling model and pictorial representation of residues involved in interaction. Ramachandran plot of Myo A tail/ZA1 structure derived from homology modelling (black dots: residues in the favourable region). (b) The 3D structure of ZA1S (red) interacting with Myosin A tail (green) obtained through Pymol. The space filling model and pictorial representation of hydrogen bond interface is shown. Ramachandran plot of Myo A tail/ZA1S structure derived from homology modelling (black dots: residues in the favourable region).

4.4.2 *In vitro* Myosin A/ZA1S interaction studies

4.4.2.1 Myosin A/ZA1S interaction via dot blot assay

The direct interaction between ZA1S and Myo A tail was tested by dot-far western analysis. For this, ZA1S peptide was immobilised on a strip of nitrocellulose membrane followed by an overlay with biotinylated Myo A tail. After stringent washing, the bound Myo A tail was detected using anti-biotin antibody. Myosin A was detected in the spot corresponding to ZA1S and not BSA, thus confirming the interaction (Figure 4.16a).

4.4.2.2 Myosin A/ZA1S interaction via ELISA

The interaction of Myo A/ZA1S was also validated by ELISA. For this, ZA1S was coated ELISA wells followed by overlaying with increasing concentrations of Myo A tail peptide. The amount of Myo A peptide bound to ZA1S was detected using anti-biotin antibody after stringent washing. Myo A tail showed significant binding to ZA1S as seen by a proportionate increase in OD_{450} with increasing the overlaid Myo A tail (Figure 4.16b). These results confirmed that ZA1S binds to Myo A tail.

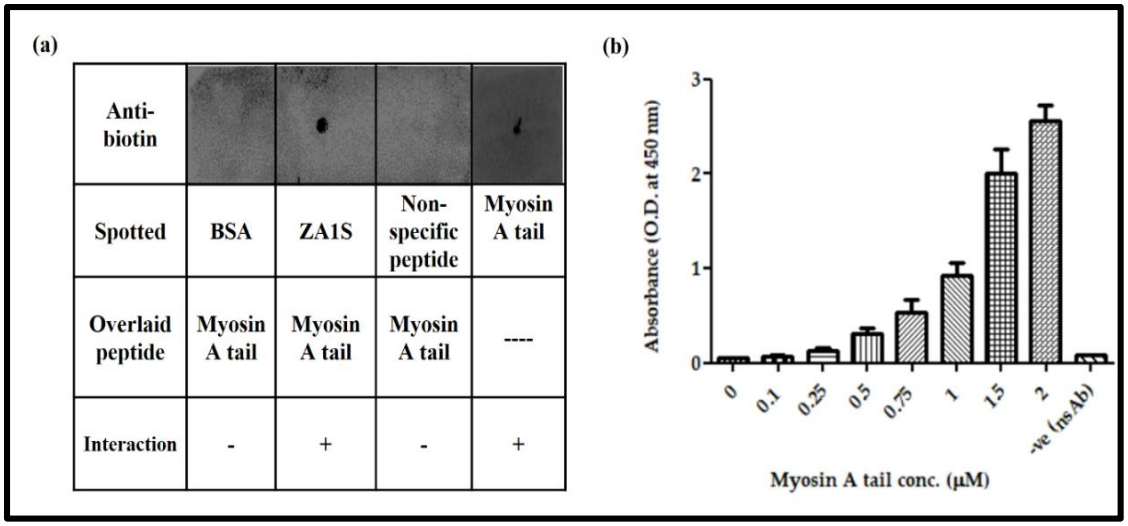

Figure 4.16: Interaction studies for Myosin A tail/ZA1S. (a) Far western-dot blot assay and (b) ELISA to access the interaction between Myosin A tail and ZA1S. For far western, 5µg of each ZA1S peptide, BSA and non-specific peptide was immobilised on strip and strip was incubated with 5µg/ml biotinylated Myosin A tail followed by detection using anti-biotin (mouse) antibody. Myosin A peptide spotted directly on membrane was used to check the antibody. For ELISA, the indicated concentrations of Myosin A tail were overlaid on immobilized ZA1S and interaction was detected by anti-biotin (mouse) antibody after stringent washing.

4.5 Malaria growth and invasion inhibition assay

To examine the effect of ZA1S peptide on *P. falciparum* 3D7 growth, a growth inhibition assay was performed. The assay was set up taking untreated assay wells as positive control and treating parasites with increasing concentrations of ZA1S. A concentration-dependent increase in invasion inhibition was observed upon treatment with ZA1, though there was no change in the parasite morphology (Figure 4.17). In control wells, normal parasite invasion was observed however in ZA1S treated wells decreased invasion was observed. These results confirmed the inhibitory effect to novel ZA1S peptide on *P.falciparum* invasion/growth in RBCs.

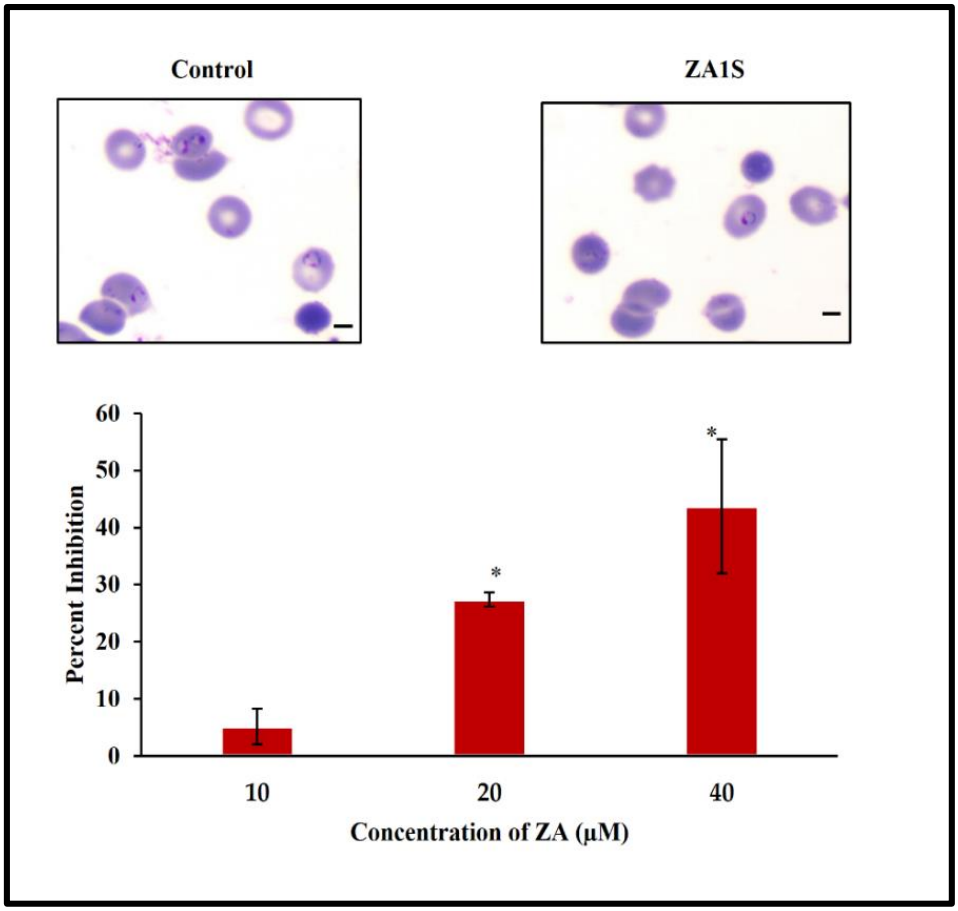

Figure 4.17: The effect of ZA1S on *P. falciparum* 3D7 growth. *Pf*3D7 parasites in smears representing control and treated sets at 24 hpi (Scale bars: 5 µm). Staging in control and treated sets of 1000 erythrocytes (infected + uninfected) at different concentrations of ZA1S.

DISCUSSION

5 DISCUSSION

Myosins are motor proteins that couple the chemical energy to mechanical energy by ATP hydrolysis, generating the force allowing movement [80]. Myosin A belongs to an atypical class of myosins and has been shown to be crucial for motility and invasion in *Plasmodium* species [35] and other Apicomplexa [20,34]. The motor complex proteins generate locomotive force by myosin pulling back actin with assistance of other proteins [23,25,81]. Hence, myosins are central to invasion machinery. The tail region of Myosin A is also conserved across species [31,82] and uniquely present in the parasite. Hence, we sought to inhibit this interaction via the tail domain of Myosin A.

In the current study we have found a new peptide binder against the Myosin A Apicomplexan motor protein in order to block its interaction with its physiological binder MTIP, an interaction shown to be crucial for *Plasmodium* invasion [46]. We began by authenticating the already identified protein-protein interaction of Myosin A and MTIP [38,39,46] while taking only the interacting regions of the two proteins in the *in vivo* bacterial two-hybrid screening system. This served three purposes: 1) provided a proof-of-concept that not the whole proteins but only the residues 799-818 of Myosin A and 79-204 of MTIP are sufficient for a strong interaction between the two proteins; 2) this gave us confidence that only the interacting regions can be further used for inhibitor screening thus helping in unearthing highly domain targeted binders against *P. falciparum* Myosin A; and 3) Myosin A/MTIP interaction has never been previously validated through a bacterial two-hybrid. Since we planned to use bacterial two-hybrid as a screening approach, it was prudent to check the original interaction that we aimed to disrupt in the same backdrop of screening. Our

Myosin A/MTIP bacterial two-hybrid assay showed intense blue colour and interaction. Quantitative assessment revealed the strength of interaction to be even higher (20% higher) than the positive control used for the experiment: ESAT6/CFP10. ESAT-6/CFP-10 is a well-documented PPI with a K_d of 1.1 x 10^{-8} M [74,75,83]. With this we understood that we are setting up to block a relatively very strong PPI.

As we set out the peptide screening, we first studied the interacting domain characteristics' of Myosin A tail (target). While the overall Myosin A protein was neither too acidic nor too basic, its tail domain is highly basic enriched in positively charged amino acids hence giving it a pI of 12.02. Charged based PPI are well-documented [84] and are a crucial force behind strong PPI interactions [85,86]. Hence, we used preferentially charged libraries in order to find new binders against Myosin A tail domain. We have previously found novel peptide binders against various pathogen and host proteins using the similar approach [19,72,83]. The Myosin A tail being basic, an acidic library having greater amounts of negatively charged amino acids was used for peptide screening.

We used using a part-rational approach [69,70,77] that allowed the synthesis of a myriad of proteins in test-tube. With this high-throughput bacterial two-hybrid screening approach, we found 4 potent binders ZA1, ZA2, ZA3 and ZA4 that showed potent interaction with Myosin A tail in the initial assay, re-transformation assay, segregation and re-co-transformation assay. Upon sequencing the four binders and studying the biophysical characteristics, we found all binders to be acidic in nature (pI near to 4). This confirmed the identity and nature of the interaction between our target and novel binders obtained from the peptide library. The approach used allowed directed evolution by codon shuffling, resulting in large variety of proteins distinct in

sequence, secondary structure and binding capacities against the bait Myosin A tail. The strength of each PPI is a function of charge between two proteins and structural complementarity apart from other attributes [84]. With the aim to find the most potent binder amongst these, we chose ZA1, which showed maximum blue colour intensity (an indication of a greater strength of interaction between two proteins) on X-gal indicator plate. Through *in vivo* quantitative assessment, we found Myosin A-ZA1 interaction to be highly significant (80% of the positive control ESAT-6/CFP-10). As a proof of concept, the novel interaction between Myosin A-ZA1 was checked by *in vitro* PPI techniques: ELISA, SPR, and ITC. The interaction between the two peptides was found to be significant in all of these thus confirming the binding.

While individual PPI is possible, it was also important to check if this novel binding (Myosin A-ZA1) also takes place in the presence of the target's physiological binder (MTIP). For this, we performed qualitative and quantitative *in vitro* and *in vivo* assays. Competitive ELISA and competitive ITC confirmed disruption of the already formed Myosin A-MTIP complex. *In vivo*, bacterial three-hybrid and arabinose gradient assays confirmed native complex disruption.

Myosin A/MTIP is part of the bigger glideosome complex residing in the IMC of the parasite [24,25,82,87]. The peptide binder ZA1 is 80 amino acids long. Hence, it cannot enter the parasite. New Permeability Pathways are uptake pathways in *Plasmodium* which have been shown to act as channels for anions, carbohydrates, and peptides [88]. With the aim to shorten the original peptide without compromising target binding, we studied Myosin A/ZA1 interaction on a residue to residue basis. *In silico* studies revealed that almost all ZA1 residues involved in interaction with Myosin A tail lay in a continuous stretch of ZA1 from Asp10 to Glu18. The peptide

ZA1 was shortened to 9 amino acids length ZA1S, whose structure was docked with Myosin A tail. Bioinformatically, we found the Myosin A/ZA1S complex to be stable. Opposite charges of Myosin A tail and ZA1S also hinted at a strong interaction. Hence, ZA1S peptide was synthesized and its *in vitro* interaction was confirmed by ELISA and dot blot assay. Lastly, this novel ZA1S peptide was added to *P.falciparum* culture to study the direct effect of ZA1S on parasite growth and invasion. The shorter peptide ZA1S also abrogated *P.falciparum* invasion in RBCs (Figure 5.1). However, we did not obtain a complete disruption in our *in vivo* liquid culture studies (60% disruption) and *P. falciparum* invasion culture studies (45% disruption). This could be due to the inherent tightness of Myosin A/MTIP complex along with closed nature of the complex [39]. Alongside, the time of addition of the peptide depending on the stage of *P. falciparum* will also effect inhibition capacity. Another very recent study [59] has used peptides as Myosin A binding probes. The study has also examined peptide uptake and found that uptake varies with the life stage of *Plasmodium.* In the future course, peptide permeability studies along with targeted sequence modifications and charge enhancement can increase the invasion blocking efficiency.

Overall, this study has allowed discovery of novel peptide based inhibitors, ZA1 and ZA1S, which can be used as templates and scaffolds for developing better therapeutics and peptidomimetic studies against defined targets allowing parasite specific targeting. The peptide inhibitors can also be used in combination with other drugs for better anti-malarial efficacy.

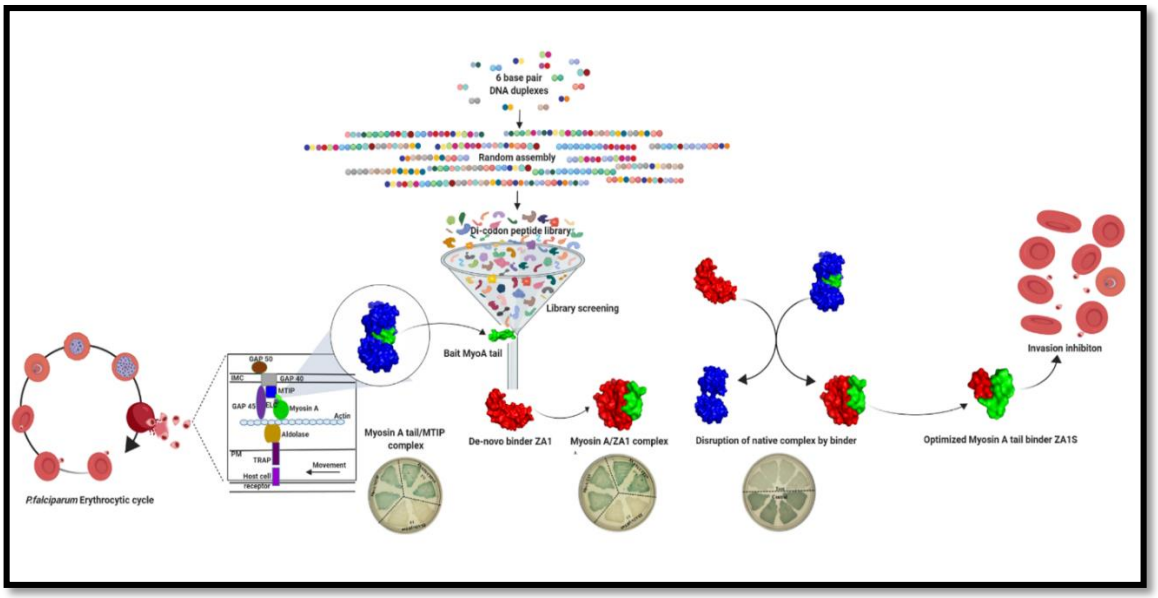

Figure 5.1: Model depicting the overall study flow.

SUMMARY, CONCLUSION

AND

FUTURE PERSPECTIVES

6 SUMMARY, CONCLUSION AND FUTURE PERSPECTIVES

Malaria has been an age old challenge since 2700 B.C. The causative agent of malaria in humans, *Plasmodium falciparum* has devised defence mechanisms that allow it to escape presently available malaria drugs. Additionally, resistance to these drugs is spreading at a rapid pace with every passing year new regions are reporting drug resistance. Overall, years of progress in malaria will be at stake if we do not have new therapeutics for treatment. If the situation persists and worsens, the world's malaria elimination goal will be a lost cause. The number of lives we lose added to the economic loss caused by the disease attracts attention and scientific studies to continually discover new, effective, and irreplaceable drugs which the parasite cannot evade.

The present study is an attempt to paralyze the parasite by stalling its gliding motility. The glideosome complex is responsible for *P .falciparum*'s invasion and egress. The central protein of the glideosome complex, Myosin A is used as a target in the study to stall parasite movement. *Pf*Myosin A is an 818 amino acid protein. The target being absolutely essential for motility and invasion, we expect that the parasite will not develop resistant against this binder. The hypothesis was to specifically block a crucial, non-redundant interaction between Myosin A tail domain and MTIP. This study has discovered best fit binders to critical *P. falciparum* target Myosin A using part rational approach of directed evolution and codon shuffling.

The main conclusions derived from this study are as follows:

- Myosin A tail regions and MTIP were found to be drug targets through literature review, and the two proteins were taken as targets for unearthing potent binders.
- Myosin A (residue 700-818)-MTIP (residue 79-204) mapped interacting regions bind with high affinity to each other *in vivo* in bacterial two-hybrid system. These regions are sufficient for the strong interaction and complex formation. The interaction was validated qualitatively and quantitatively *in vivo*.
- Myosin A-MTIP mapped interacting regions interacted *in vitro* with strong affinity, as validated by protein-protein interaction techniques.
- By applying 'codon-shuffling', the study found peptide binders from *de novo* synthesized libraries for Myosin A tail based on charge and structural fit.
- Of all the binders obtained, the strongest one was ZA1. ZA1 bound to Myosin A tail domain both *in vivo* and *in vitro*. The interaction was checked qualitatively and quantitatively *in vivo*.
- As a proof of concept, Myosin A-ZA1 interaction was confirmed to be positive through protein-protein interaction techniques.
- The interaction between Myosin A-ZA1 modulated the interaction between Myosin A-MTIP negatively. In the presence of MTIP, Myosin A binds to ZA1 *in vitro* and *in vivo.* Hence, the novel Myosin A binder ZA1 could successfully break the already formed Myosin A-MTIP complex due to preferential binding.
- The residue to residue interaction between Myosin A-ZA1 revealed that the interaction between the two peptides is due to hydrogen bonding and ionic

bonds. The bonding between Myosin A-ZA1 was through residues lying at a continuous stretch in the two peptides.

- A shorter peptide ZA1S was deduced from longer ZA1 through bioinformatics studies and the binding model found it to be stable and in favourable regions.
- ZA1S-Myosin A tail interacted with each other *in vitro*.
- ZA1S peptide decreased *P. falciparum* invasion in erythrocytes.

In summary, the present work puts forward new knowledge in the area of drug discovery and malaria therapeutics thereby giving clues to targeting the indispensable *P. falciparum* process of gliding motility. By applying the already existing lab-based high throughput screening method of codon shuffling through directed evolution, this study is a step forward in applicative biology for novel therapies. We have built a foundation on which further improvisations through peptidomemitic, peptide delivery and improvisations for better activity studies are needed. Furthermore, the peptide-based binders obtained in this study can be used in one or in combination with other drug candidates to develop an all-round malaria therapy.

REFERENCES

7 REFERENCES

1. Talapko J, Škrlec I, Alebić T, Jukić M, Včev A. Malaria: The past and the present. Microorganisms. 2019;7.

2. Akanksha Gupta AKS and AQ. Evaluating Ancient Indian History and Culture towards Malaria Control Measures Based on Traditional Knowledge System. 2014;1:181–90. Available from: http://www.ijims.com

3. Global Malaria Programme: WHO Global. World malaria report 2019 [Internet]. WHO Reg. Off. Africa. 2019. Available from: https://www.who.int/news-room/fact-sheets/detail/malaria

4. Dhiman S. Correction to: Are malaria elimination efforts on right track? An analysis of gains achieved and challenges ahead (Infectious Diseases of Poverty DOI: 10.1186/s40249-019-0524-x). Infect Dis Poverty. Infectious Diseases of Poverty; 2019;8:1–19.

5. Manuscript A. Europe PMC Funders Group Spread of Artemisinin Resistance in Plasmodium falciparum Malaria. 2015;371:411–23.

6. Mishra N, Prajapati SK, Kaitholia K, Bharti RS, Srivastava B, Phookan S, et al. Surveillance of artemisinin resistance in Plasmodium falciparum in India using the kelch13 molecular marker. Antimicrob Agents Chemother. 2015;59:2548–53.

7. Amato R, Pearson RD, Almagro-Garcia J, Amaratunga C, Lim P, Suon S, et al. Origins of the current outbreak of multidrug-resistant malaria in southeast Asia: a retrospective genetic study. Lancet Infect Dis [Internet]. The Author(s). Published by Elsevier Ltd. This is an Open Access article under the CC BY 4.0 license; 2018;18:337–45. Available from: http://dx.doi.org/10.1016/S1473-3099(18)30068-9

8. Ménard D, Clain J, Ariey F. Multidrug-resistant Plasmodium falciparum malaria in the Greater Mekong subregion. Lancet Infect Dis. 2018;18:238–9.

9. Takala-Harrison S, Jacob CG, Arze C, Cummings MP, Silva JC, Dondorp AM, et al. Independent emergence of artemisinin resistance mutations among Plasmodium falciparum in Southeast Asia. J Infect Dis. 2015;211:670–9.

10. Sinha S, Medhi B, Sehgal R. Challenges of drug-resistant malaria. Parasite. 2014;21.

11. Maier AG, Matuschewski K, Zhang M, Rug M. Plasmodium falciparum. Trends Parasitol [Internet]. Elsevier Ltd; 2019;35:481–2. Available from: https://doi.org/10.1016/j.pt.2018.11.010

12. Milner DA. Malaria pathogenesis. Cold Spring Harb Perspect Med. 2018;8:1–11.

13. Cowman AF, Tonkin CJ, Tham W, Duraisingh MT. Review The Molecular Basis of Erythrocyte Invasion by Malaria Parasites. Cell Host Microbe [Internet]. Elsevier Inc.; 2017;22:232–45. Available from: http://dx.doi.org/10.1016/j.chom.2017.07.003

14. Herrera R, Anderson C, Kumar K, Molina-Cruz A, Nguyen V, Burkhardt M, et al. Reversible conformational change in the plasmodium falciparum circumsporozoite protein masks Its adhesion domains. Infect Immun. 2015;83:3771–80.

15. Cowman AF, Healer J, Marapana D, Marsh K. Malaria: Biology and Disease. Cell [Internet]. Elsevier Inc.; 2016;167:610–24. Available from: http://dx.doi.org/10.1016/j.cell.2016.07.055

16. Lin CS, Uboldi AD, Epp C, Bujard H, Tsuboi T, Czabotar PE, et al. Multiple plasmodium falciparum merozoite surface protein 1 complexes mediate merozoite binding to human erythrocytes. J Biol Chem. 2016;291:7703–15.

17. Weiss GE, Gilson PR, Taechalertpaisarn T, Tham WH, de Jong NWM, Harvey KL, et al. Revealing the Sequence and Resulting Cellular Morphology of Receptor-Ligand Interactions during Plasmodium falciparum Invasion of Erythrocytes. PLoS Pathog. 2015;11:1–25.

18. Singh S, Alam MM, Pal-bhowmick I, Brzostowski JA, Chitnis CE. Distinct External Signals Trigger Sequential Release of Apical Organelles during Erythrocyte Invasion by Malaria Parasites. 2010;6.

19. Prakash P, Zeeshan M, Saini E, Muneer A, Khurana S, Kumar Chourasia B, et al. Human Cyclophilin B forms part of a multi-protein complex during erythrocyte invasion by Plasmodium falciparum. Nat Commun [Internet]. Springer US; 2017;8. Available from: http://dx.doi.org/10.1038/s41467-017-01638-6

20. Besteiro S, Dubremetz JF, Lebrun M. The moving junction of apicomplexan parasites: A key structure for invasion. Cell Microbiol. 2011;13:797–805.

21. King CA. Cell motility of sporozoan protozoa. Parasitol Today. 1988;4:315–9.

22. Frénal K, Dubremetz J, Lebrun M, Soldati-favre D. Gliding motility powers invasion and egress in Apicomplexa. Nat Publ Gr [Internet]. Nature Publishing Group; 2017;15:645–60. Available from: http://dx.doi.org/10.1038/nrmicro.2017.86

23. Kumpula EP, Kursula I. Towards a molecular understanding of the apicomplexan actin motor: On a road to novel targets for malaria remedies? Acta Crystallogr Sect FStructural Biol Commun. International Union of Crystallography; 2015;71:500–13.

24. Baum J, Richard D, Healer J, Rug M, Krnajski Z, Gilberger TW, et al. A conserved molecular motor drives cell invasion and gliding motility across malaria life cycle stages and other apicomplexan parasites. J Biol Chem. 2006;281:5197–208.

25. Frénal K, Polonais V, Marq JB, Stratmann R, Limenitakis J, Soldati-Favre D. Functional dissection of the apicomplexan glideosome molecular architecture. Cell Host Microbe. 2010;8:343–57.

26. Green JL, Wall RJ, Vahokoski J, Yusuf NA, Mohd Ridzuan MA, Stanway RR, et al. Compositional and expression analyses of the glideosome during the Plasmodium life cycle reveal an additional myosin light chain required for maximum motility. J Biol Chem. 2017;292:17857–75.

27. Pazicky S, Dhamotharan K, Kaszuba K, Mertens HDT, Gilberger T, Svergun D, et al. Structural role of essential light chains in the apicomplexan glideosome. Commun Biol [Internet]. Springer US; 2020;3:1–14. Available from: http://dx.doi.org/10.1038/s42003-020-01283-8

28. Boucher LE, Bosch J. The apicomplexan glideosome and adhesins - Structures and function. J Struct Biol. 2015;190:93–114.

29. Kappe SHI, Buscaglia CA, Bergman LW, Coppens I, Nussenzweig V. Apicomplexan gliding motility and host cell invasion : overhauling the motor model. 2004;20:13–6.

30. Alexander DL, Arastu-kapur S, Dubremetz J, Boothroyd JC. Plasmodium falciparum AMA1 Binds a Rhoptry Neck Protein Homologous to TgRON4 , a Component of the Moving Junction in Toxoplasma gondii. 2006;5:1169–73.

31. Chaparro-Olaya J, Dluzewski AR, Margos G, Wasserman MM, Mitchell GH, Bannister LH, et al. The multiple myosins of malaria: The smallest malaria myosin, Plasmodium falciparum myosin-B (Pfmyo-B) is expressed in mature schizonts and merozoites. Eur J Protistol. 2003;39:423–7.

32. Yusuf NA, Green JL, Wall RJ, Knuepfer E, Moon RW, Schulte-Huxel C, et al. The Plasmodium class XIV Myosin, MyoB, has a distinct subcellular location in invasive and motile stages of the malaria parasite and an unusual light chain. J Biol Chem. 2015;

33. Pinder JC, Fowler RE, Dluzewski AR, Bannister LH, Lavin FM, Mitchell GH, et al. Actomyosin motor in the merozoite of the malaria parasite, Plasmodium falciparum: Implications for red cell invasion. J Cell Sci. 1998;111:1831–9.

34. Meissner M, Schlüter D, Soldati D. Role of Toxoplasma gondii myosin a in powering parasite gliding and host cell invasion. Science (80-). 2002;298:837–40.

35. Robert-Paganin J, Robblee JP, Auguin D, Blake TCA, Bookwalter CS, Krementsova EB, et al. Plasmodium myosin A drives parasite invasion by an atypical force generating mechanism. Nat Commun [Internet]. Springer US; 2019;10. Available from: http://dx.doi.org/10.1038/s41467-019-11120-0

36. Heintzelman MB, Schwartzman JD. A novel class of unconventional myosins from Toxoplasma gondii. J Mol Biol. 1997;271:139–46.

37. Moussaoui D, Robblee JP, Auguin D, Krementsova EB, Haase S, Blake TCA, et al. Full-length plasmodium falciparum myosin a and essential light chain pfelc structures provide new anti-malarial targets. Elife. 2020;9:1–24.

38. Bergman LW, Kaiser K, Fujioka H, Coppens I, Daly TM, Fox S, et al. Myosin A tail domain interacting protein (MTIP) localizes to the inner membrane complex of Plasmodium sporozoites. J Cell Sci. 2003;116:39–49.

39. Green JL, Martin SR, Fielden J, Ksagoni A, Grainger M, Yim Lim BYS, et al. The MTIP-myosin A complex in blood stage malaria parasites. J Mol Biol. 2006;355:933–41.

40. Siden-Kiamos I, Goosmann C, Buscaglia CA, Brinkmann V, Matuschewski K, Montagna GN. Polarization of MTIP is a signature of gliding locomotion in Plasmodium ookinetes and sporozoites. Mol Biochem Parasitol [Internet]. Elsevier; 2020;235:111247. Available from: https://doi.org/10.1016/j.molbiopara.2019.111247

41. Douse CH, Green JL, Salgado PS, Simpson PJ, Thomas JC, Langsley G, et al. Regulation of the plasmodium motor complex: Phosphorylation of myosin a tail-interacting protein (MTIP) loosens its grip on MyoA. J Biol Chem. 2012;287:36968–77.

42. Thomas JC, Green JL, Howson RI, Simpson P, Moss DK, Martin SR, et al. Interaction and dynamics of the Plasmodium falciparum MTIP-MyoA complex, a key component of the invasion motor in the malaria parasite. Mol Biosyst. 2010;6:494–8.

43. Kortagere S, Welsh WJ, Morrisey JM, Daly T, Ejigiri I, Sinnis P, et al. Structure-based design of novel small-molecule inhibitors of plasmodium falciparum. J Chem Inf Model. 2010;

44. Kortagere S, Mui E, McLeod R, Welsh WJ. Rapid discovery of inhibitors of Toxoplasma gondii using hybrid structure-based computational approach. J Comput Aided Mol Des. Springer; 2011;25:403–11.

45. Khamrui S, Turley S, Pardon E, Steyaert J, Fan E, Verlinde CLMJ, et al. The structure of the D3 domain of Plasmodium falciparum myosin tail interacting protein MTIP in complex with a nanobody. Mol Biochem Parasitol [Internet]. Elsevier B.V.; 2013;190:87–91. Available from: http://dx.doi.org/10.1016/j.molbiopara.2013.06.003

46. Bosch J, Turley S, Daly TM, Bogh SM, Villasmil ML, Roach C, et al. Structure of the MTIP-MyoA complex, a key component of the malaria parasite invasion motor. Proc Natl Acad Sci U S A. 2006;103:4852–7.

47. Delmotte A, Tate EW, Yaliraki SN, Barahona M. Protein multi-scale organization through graph partitioning and robustness analysis: Application to the myosin-myosin light chain interaction. Phys Biol. 2011;8.

48. Darkin-Rattray SJ, Gurnett AM, Myers RW, Dulski PM, Crumley TM, Allocco JJ, et al. Apicidin: A novel antiprotozoal agent that inhibits parasite

histone deacetylase (cyclic tetrapeptide¯ Apicomplexa¯ antiparasitic¯ malaria¯ coccidiosis). Med Sci. 1996;93:13143–7.

49. Nagaraj G, Uma M V., Shivayogi MS, Balaram H. Antimalarial activities of peptide antibiotics isolated from fungi. Antimicrob Agents Chemother. 2001;45:145–9.

50. Thongtan J, Saenboonrueng J, Rachtawee P, Isaka M. An antimalarial tetrapeptide from the entomopathogenic fungus Hirsutella sp. BCC 1528. J Nat Prod. 2006;69:713–4.

51. Sabareesh V, Ranganayaki RS, Raghothama S, Bopanna MP, Balaram H, Srinivasan MC, et al. Identification and characterization of a library of microheterogeneous cyclohexadepsipeptides from the fungus Isaria. J Nat Prod. 2007;70:715–29.

52. Pérez-Picaso L, Velasco-Bejarano B, Aguilar-Guadarrama AB, Argotte-Ramos R, Rios MY. Antimalarial activity of ultra-short peptides. Molecules. 2009;14:5103–14.

53. Fennell BJ, Carolan S, Pettit GR, Bell A. Effects of the antimitotic natural product dolastatin 10, and related peptides, on the human malarial parasite Plasmodium falciparum. J Antimicrob Chemother. 2003;51:833–41.

54. Rautenbach M, Vlok NM, Stander M, Hoppe HC. Inhibition of malaria parasite blood stages by tyrocidines, membrane-active cyclic peptide antibiotics from Bacillus brevis. Biochim Biophys Acta - Biomembr. 2007;1768:1488–97.

55. Rosenthal PJ, Wollish WS, Palmer JT, Rasnick D. Antimalarial effects of peptide inhibitors of a Plasmodium falciparum cysteine proteinase. J Clin Invest. 1991;88:1467–72.

56. Mizuno Y, Makioka A, Kawazu SI, Kano S, Kawai S, Akaki M, et al. Effect of jasplakinolide on the growth, invasion, and actin cytoskeleton of Plasmodium falciparum. Parasitol Res. 2002;88:844–8.

57. Charoenvit Y, Brice GT, Bacon D, Majam V, Williams J, Abot E, et al. A small peptide (CEL-1000) derived from the β-chain of the human major histocompatibility complex class II molecule induces complete protection against malaria in an antigen-independent manner. Antimicrob Agents Chemother. 2004;48:2455–63.

58. Dhawan S, Dua M, Chishti AH, Hanspal M. Ankyrin peptide blocks falcipain-2-mediated malaria parasite release from red blood cells. J Biol Chem. 2003;278:30180–6.

59. Saunders CN, Cota E, Baum J, Tate EW. Peptide probes for Plasmodium falciparum MyoA tail interacting protein (MTIP): exploring the druggability of the malaria parasite motor complex Peptide probes for Plasmodium falciparum MyoA tail interacting protein (MTIP): exploring the druggability o. 2020;

60. Ghosh SK, Rahi M. Malaria elimination in India - The way forward. J Vector Borne Dis. 2019;56:32–40.

61. A., Shafiq CWNSSJRB. 乳鼠心肌提取 HHS Public Access. Physiol Behav. 2017;176:139–48.

62. Report WM. 20 1 0.

63. World Health Organization. Malaria report 2019. Who. 2018.

64. Ashley EA, Pyae Phyo A, Woodrow CJ. Malaria. Lancet. 2018;391:1608–21.

65. Douse CH, Maas SJ, Thomas JC, Garnett JA, Sun Y, Cota E, et al. Crystal structures of stapled and hydrogen bond surrogate peptides targeting a fully buried protein-helix interaction. ACS Chem Biol. 2014;9:2204–9.

66. Miura K. An Overview of Current Methods to Confirm Protein- Protein Interactions. Protein Pept Lett. 2018;25:728–33.

67. Joung JK, Ramm EI, Pabo CO. A bacterial two-hybrid selection system for studying protein-DNA and protein-protein interactions. Proc Natl Acad Sci U S A. 2000;97:7382–7.

68. Tharad M, Samuchiwal SK, Bhalla K, Ghosh A, Kumar K, Kumar S, et al. A three-hybrid system to probe In Vivo protein-protein interactions: Application to the essential proteins of the RD1 complex of M. tuberculosis. PLoS One. 2011;

69. Chopra S, Ranganathan A. Protein evolution by "Codon Shuffling": A novel method for generating highly variant mutant libraries by assembly of hexamer DNA duplexes. Chem Biol. 2003;

70. Rao A, Chopra S, Ram G, Gupta A, Ranganathan A. Application of the "codon-shuffling" method: Synthesis and selection of de novo proteins as antibacterials. J Biol Chem. 2005;280:23605–14.

71. Miller JH. Experiments in molecular genetics. Assay of ß Galactosidase [Internet]. Cold Spring Harb. Lab. Press. Cold Spring Harbor Laboratory Press; 1972. Available from: https://openlibrary.org/books/OL5298363M/Experiments_in_molecular_genetics

72. Bhalla K, Chugh M, Mehrotra S, Rathore S, Tousif S, Dwivedi VP, et al. Host ICAMs play a role in cell invasion by Mycobacterium tuberculosis and Plasmodium falciparum. Nat Commun. Nature Publishing Group; 2015;6.

73. Miller JH. Experiments in molecular genetics. Assay of ß Galactosidase. Cold Spring Harb. Lab. Press. 1972.

74. Mener AK, Bal NC, Chary KVR, Arora A. Mycobacterium tuberculosis H37Rv ESAT-6-CFP-10 complex formation confers thermodynamic and biochemical stability. FEBS J. 2006;273:1445–62.

75. Renshaw PS, Lightbody KL, Veverka V, Muskett FW, Kelly G, Frenkiel TA, et al. Structure and function of the complex formed by the tuberculosis virulence factors CFP-10 and ESAT-6. EMBO J. 2005;24:2491–8.

76. Jain R, Gupta S, Munde M, Pati S, Singh S. Development of novel anti-malarial from structurally diverse library of molecules, targeting plant-like CDPK1, a multistage growth regulator of P. falciparum. Biochem J. 2020;477:1951–70.

77. Rao A, Ram G, Saini AK, Vohra R, Kumar K, Singh Y, et al. Synthesis and selection of de novo proteins that bind and impede cellular functions of an essential mycobacterial protein. Appl Environ Microbiol. 2007;73:1320–31.

78. Douse CH, Vrielink N, Wenlin Z, Cota E, Tate EW. Targeting a dynamic protein-protein interaction: Fragment screening against the malaria myosin a motor complex. ChemMedChem. 2015;10:134–43.

79. Singh S, Kosey D. Computational design of molecular motors as nanocircuits in Leishmaniasis. F1000Research. 2017;6:1–35.

80. Batters C, Veigel C. Myosins. 2016;

81. Boucher LE, Bosch J. The apicomplexan glideosome and adhesins – Structures and function. J Struct Biol [Internet]. Elsevier Inc.; 2015;190:93–114. Available from: http://dx.doi.org/10.1016/j.jsb.2015.02.008

82. Jones ML, Kitson EL, Rayner JC. Plasmodium falciparum erythrocyte invasion : A conserved myosin associated complex. 2006;147:74–84.

83. Samuchiwal SK, Tousif S, Singh DK, Kumar A, Ghosh A, Bhalla K, et al. A peptide fragment from the human COX3 protein disrupts association of Mycobacterium tuberculosis virulence proteins ESAT-6 and CFP10, inhibits mycobacterial growth and mounts protective immune response. BMC Infect Dis. 2014;14:1–11.

84. Kiel C, Selzer T, Shaul Y, Schreiber G, Herrmann C. Electrostatically optimized Ras-binding Ral guanine dissociation stimulator mutants increase the rate of association by stabilizing the encounter complex. Proc Natl Acad Sci U S A. 2004;101:9223–8.

85. Sinha N, Smith-Gill S. Electrostatics in Protein Binding and Function. Curr Protein Pept Sci. 2005;3:601–14.

86. Bloomfield VA. Association of proteins. J Dairy Res. 1979;46:241–52.

87. Cowman AF, Crabb BS. Invasion of red blood cells by malaria parasites. Cell. 2006.

88. Ginsburg H, Stein WD. The New Permeability Pathways Induced by the Malaria Parasite in the Membrane of the Infected Erythrocyte: Comparison of Results Using Different Experimental Techniques. J Membr Biol. 2004;197:113–22.

PUBLICATIONS AND PRESENTATIONS

8 PUBLICATIONS AND PRESENTATIONS

8.1 Publications

1. **Anam Z**, Joshi N, Gupta S, Yadav P, Chaurasiya A, Kahlon AK, Kaushik S, Munde M, Ranganathan A, Singh S. A De novo Peptide from a High Throughput Peptide Library Blocks Myosin A-MTIP Complex Formation in *Plasmodium falciparum*. International journal of molecular sciences. 2020 Jan;21(17):6158.
2. Chaurasiya A, Garg S, Khanna A, Narayana C, Dwivedi VP, Joshi N, **Anam Z,** Singh N, Singhal J, Kaushik S, Kahlon AK, Srivastava P, Marothia M, Kumar M, Kumar S, Kumari G, Munjal A, Gupta S, Singh P, Pati S, Das G, Sagar R, Ranganathan A and Singh S. Pathogen induced subversion of NAD^+ metabolism mediating host cell death: a target for development of chemotherapeutics (Manuscript ID: CDDISCOVERY-20-0997R, Cell Death Discovery, In Press).
3. Prakash P, Zeeshan M, Saini E, Muneer A, Khurana S, Chourasia BK, Deshmukh A, Kaur I, Dabral S, Singh N, **Anam Z**, Chaurasiya A, Kaushik S, Dahiya P, Kalamuddin M, Thakur JK, Mohmmed A, Ranganathan A and Malhotra P. Human Cyclophilin B forms part of a multi-protein complex during erythrocyte invasion by *Plasmodium falciparum*. Nature communications. 2017 Nov 16;8(1):1-2.
4. **Anam Z**, D.A.B. Rex, Yadav P, Sah R K, Kumari G, Chaurasiya A, Singh N, Prasad T.S., Pati S, Singh S and Ranganathan A. Complementary cross-talk between palmitoylation and phosphorylation in regulation of *Plasmodium falciparum* invasion of erythrocytes (Manuscript under preparation).

5. Chaurasiya A, Garg S, **Anam Z,** Kumari G, Joshi N, Kumari J, Singhal J, Singh N, Kaushik S, Kahlon AK, Dubey N, Srivastava P, Marothia M, Kumar M, Das G, Singh S and Ranganathan A. Repositioning of the anti-Hepatitis C Virus drug Alisporivir against Artemisinin-resistant *Plasmodium falciparum* (Manuscript under preparation).

8.2 Presentations in conferences and workshops

1. **Zill-e-Anam**, Dr. Anand Ranganathan, "Blocking Crucial Protein-Protein Interactions of *P. falciaprum* via novel peptide inhibitors" oral presentation at 8th Hong Kong University – Pasteur Cell Biology Course in March 2018.
2. **Zill-e-Anam**, Sachin Kumar Samuchiwal, Dr. Anand Ranganathan, "Disrupting Crucial Protein-Protein Interactions of *Mycobacterium Tuberculosis* via novel peptide inhibitors" poster presentation at Annual Open Day, Jawaharlal Nehru University in October, 2017.
3. **Zill-e-Anam**, Sachin Kumar Samuchiwal, Dr. Anand Ranganathan, "Disrupting Crucial Protein-Protein Interactions of *Mycobacterium Tuberculosis* via novel peptide inhibitors" poster presentation at 7th Symposium on Frontiers in Molecular Medicine, Special Centre for Molecular Medicine, Jawaharlal Nehru University in March, 2017.
4. **Zill-e-Anam**, Kuhulika Bhalla, Anand Ranganathan, "Host ICAMs: Key players for *Mycobacterium tuberculosis* invasion" poster presentation at National Conference on Understanding the Mechanism and Challenges of Complex Diseases at Shaheed Rajguru College of Applied Sciences for Women, University of Delhi in January, 2017.

International Journal of
Molecular Sciences

MDPI

Article

A De novo Peptide from a High Throughput Peptide Library Blocks Myosin A -MTIP Complex Formation in *Plasmodium falciparum*

Zill e Anam [1], Nishant Joshi [2], Sakshi Gupta [3], Preeti Yadav [1], Ayushi Chaurasiya [1], Amandeep Kaur Kahlon [1], Shikha Kaushik [1], Manoj Munde [3], Anand Ranganathan [1,*] and Shailja Singh [1,*]

1 Special Centre for Molecular Medicine, Jawaharlal Nehru University, New Delhi 110067, India; zillzz85@gmail.com (Z.e.A.); preetiyadav.bms@gmail.com (P.Y.); ayushi.chaurasiya01@gmail.com (A.C.); amangenomics@gmail.com (A.K.K.); shikhakaushik29@gmail.com (S.K.)
2 Department of Life Sciences, School of Natural Sciences, Shiv Nadar University, Greater Noida, Uttar Pradesh 201304, India; nj633@snu.edu.in
3 School of Physical Sciences, Jawaharlal Nehru University, New Delhi 110067, India; sakshi2027@gmail.com (S.G.); mundemanoj@gmail.com (M.M.)
* Correspondence: anand.icgeb@gmail.com (A.R.); shailja.jnu@gmail.com (S.S.)

Received: 14 April 2020; Accepted: 15 May 2020; Published: 26 August 2020

Abstract: Apicomplexan parasites, through their motor machinery, produce the required propulsive force critical for host cell-entry. The conserved components of this so-called glideosome machinery are myosin A and myosin A Tail Interacting Protein (MTIP). MTIP tethers myosin A to the inner membrane complex of the parasite through 20 amino acid-long C-terminal end of myosin A that makes direct contacts with MTIP, allowing the invasion of *Plasmodium falciparum* in erythrocytes. Here, we discovered through screening a peptide library, a de-novo peptide ZA1 that binds the myosin A tail domain. We demonstrated that ZA1 bound strongly to myosin A tail and was able to disrupt the native myosin A tail MTIP complex both in vitro and in vivo. We then showed that a shortened peptide derived from ZA1, named ZA1S, was able to bind myosin A and block parasite invasion. Overall, our study identified a novel anti-malarial peptide that could be used in combination with other antimalarials for blocking the invasion of *Plasmodium falciparum*.

Keywords: malaria; peptide inhibitor; myosin A; myosin A tail interacting protein (MTIP)

1. Introduction

The burden caused by a malarial parasite—*Plasmodium falciparum*—remains huge despite a recent decline in the number of malaria cases [1]. The non-responsiveness of the parasite to existing therapies calls for an urgent need for discovering new drugs that are parasite-specific. For successful transmission, the parasite must complete its life cycle in each of the sub microenvironments: gut of Anopheles mosquito, hepatocytes, and erythrocytes. Entry in erythrocytes allows asexual reproduction of the parasite, leading to rapid proliferation and an exponential increase in the number of merozoites. It is an essential step in the parasite life cycle and is also an attractive target since the merozoites are in the bloodstream and directly exposed, thereby making them vulnerable to drugs [2].

The encounter of the malarial parasite with host erythrocyte is mediated by sequential and highly dynamic processes involving initial interaction of the egressed merozoite, leading to re-orientation of the apical end, the formation of a tight junction in between the two membranes, followed by the engagement of invasion motor and entry. This is concluded by the shedding of a protein coat, the formation of the parasitophorous vacuole, resealing of red blood cell (RBC) membrane,

Chaurasiya et al. *Cell Death Discovery* _####################_
https://doi.org/10.1038/s41420-020-00366-z

Cell Death Discovery

ARTICLE Open Access

Pathogen induced subversion of NAD^+ metabolism mediating host cell death: a target for development of chemotherapeutics

Ayushi Chaurasiya[1], Swati Garg[1], Ashish Khanna[2], Chintam Narayana[2], Vedprakash Dwivedi[3], Nishant Joshi[4], Zill e Anam[1], Niharika Singh[1], Jhalak Singhal[1], Shikha Kaushik[1], Amandeep Kaur[1], Pallavi Srivastava[1], Manisha Marothia[1], Mukesh Kumar[1], Santosh Kumar[3], Geeta Kumari[1], Akshay Munjal[1], Sonal Gupta[1], Preeti Singh[1], Soumya Pati[4], Gobardhan Das[1], Ram Sagar[2], Anand Ranganathan[1] and Shailja Singh[1]

Abstract

Hijacking of host metabolic status by a pathogen for its regulated dissemination from the host is prerequisite for the propagation of infection. *M. tuberculosis* secretes an NAD^+-glycohydrolase, TNT, to induce host necroptosis by hydrolyzing Nicotinamide adenine dinucleotide (NAD^+). Herein, we expressed TNT in macrophages and erythrocytes; the host cells for *M. tuberculosis* and the malaria parasite respectively, and found that it reduced the NAD^+ levels and thereby induced necroptosis and eryptosis resulting in premature dissemination of pathogen. Targeting TNT in *M. tuberculosis* or induced eryptosis in malaria parasite interferes with pathogen dissemination and reduction in the propagation of infection. Building upon our discovery that inhibition of pathogen-mediated host NAD^+ modulation is a way forward for regulation of infection, we synthesized and screened some novel compounds that showed inhibition of NAD^+-glycohydrolase activity and pathogen infection in the nanomolar range. Overall this study highlights the fundamental importance of pathogen-mediated modulation of host NAD^+ homeostasis for its infection propagation and novel inhibitors as leads for host-targeted therapeutics.

Introduction

Intracellular pathogens have evolved strategies to manipulate host cell pathways for dissemination and infection propagation. Unlike independent organisms, intracellular pathogens depend on the activities of host cell to complete their life cycle. Some of these pathogens have evolved strategies for host manipulation to increase their survival causing detrimental effects to the host, leading to its death. Because dissemination is an essential aspect of pathogenesis, targeting or modulating host processes involved in pathogenesis can control the infection[1]. Pathogen-mediated changes in host intracellular nicotinamide adenine dinucleotide (NAD^+), an essential coenzyme and a redox factor regulating numerous cellular metabolic pathways, levels have been observed in various diseases[2,3]. In particular, host uses NAD^+ as a substrate for a group of "NAD^+-dependent" enzymes[4,5]. Q1 – Q4

Recently, *Mycobacterium tuberculosis*, the causative agent for tuberculosis, mediated modulation of host NAD^+ homeostasis has been presented as one of the most fascinating examples of a pathogen's infection strategy wherein NAD^+ depletion through TNT activates necroptosis pathways in order to facilitate growth and spread of *M. tuberculosis*[6–8]. However, the regulation of

Correspondence: Ram Sagar (ram.sagar@bhu.ac.in) or Anand Ranganathan (anand.icgeb@gmail.com) or Shailja Singh (shailja.jnu@gmail.com)
[1]Special Centre for Molecular Medicine, Jawaharlal Nehru University, New Delhi 110067, India
[2]Department of Chemistry, Institute of Science, Banaras Hindu University, Varanasi 221005 Uttar Pradesh, India
Full list of author information is available at the end of the article
These authors contributed equally: Ayushi Chaurasiya, Swati Garg, Ashish Khanna
Edited by A. Janic

nature COMMUNICATIONS

ARTICLE

DOI: 10.1038/s41467-017-01638-6 OPEN

Human Cyclophilin B forms part of a multi-protein complex during erythrocyte invasion by *Plasmodium falciparum*

Prem Prakash[1,2], Mohammad Zeeshan[1], Ekta Saini[1], Azhar Muneer[1], Sachin Khurana[1], Bishwanath Kumar Chourasia[1], Arunaditya Deshmukh[1], Inderjeet Kaur[1], Surabhi Dabral[1], Niharika Singh[1,3], Zille Anam[3], Ayushi Chaurasiya[3], Shikha Kaushik[3], Pradeep Dahiya[4], Md. Kalamuddin[1], Jitendra Kumar Thakur[4], Asif Mohmmed[1], Anand Ranganathan[2,3] & Pawan Malhotra[1]

Invasion of human erythrocytes by *Plasmodium falciparum* merozoites involves multiple interactions between host receptors and their merozoite ligands. Here we report human Cyclophilin B as a receptor for PfRhopH3 during merozoite invasion. Localization and binding studies show that Cyclophilin B is present on the erythrocytes and binds strongly to merozoites. We demonstrate that PfRhopH3 binds to the RBCs and their treatment with Cyclosporin A prevents merozoite invasion. We also show a multi-protein complex involving Cyclophilin B and Basigin, as well as PfRhopH3 and PfRh5 that aids the invasion. Furthermore, we report identification of a de novo peptide CDP3 that binds Cyclophilin B and blocks invasion by up to 80%. Collectively, our data provide evidence of compounded interactions between host receptors and merozoite surface proteins and paves the way for developing peptide and small-molecules that inhibit the protein–protein interactions, individually or in toto, leading to abrogation of the invasion process.

[1] Malaria Biology Group, International Centre for Genetic Engineering and Biotechnology (ICGEB), Aruna Asaf Ali Marg, New Delhi 110067, India. [2] Recombinant Gene Products Group, International Centre for Genetic Engineering and Biotechnology (ICGEB), Aruna Asaf Ali Marg, New Delhi 110067, India. [3] Special Centre for Molecular Medicine, Jawaharlal Nehru University, Aruna Asaf Ali Marg, New Delhi 110067, India. [4] Plant Mediator Lab, National Institute of Plant Genome Research, Aruna Asaf Ali Marg, New Delhi 110067, India. Prem Prakash and Mohammad Zeeshan contributed equally to this work. Correspondence and requests for materials should be addressed to A.R. (email: anand.icgeb@gmail.com) or to P.M. (email: pawanmal@gmail.com)

Zill-e-Anam Thesis Dec, 2020

by Zill E Anam

Submission date: 26-Dec-2020 12:06PM (UTC+0530)
Submission ID: 1481292416
File name: Zill-e-Anam_PhD_Thesis_December,_2020.docx (11.37M)
Word count: 11754
Character count: 65575

Zill-e-Anam Thesis Dec, 2020

ORIGINALITY REPORT

3%	2%	3%	1%
SIMILARITY INDEX	INTERNET SOURCES	PUBLICATIONS	STUDENT PAPERS

PRIMARY SOURCES

1	www.nature.com Internet Source	1%
2	Reetika Manhas, Smriti Tandon, Shib Sankar Sen, Neha Tiwari, Manoj Munde, Rentala Madhubala. " Parasites Are Inhibited by the Benzoxaborole AN2690 Targeting Leucyl-tRNA Synthetase ", Antimicrobial Agents and Chemotherapy, 2018 Publication	1%
3	Prem Prakash, Mohammad Zeeshan, Ekta Saini, Azhar Muneer et al. "Human Cyclophilin B forms part of a multi-protein complex during erythrocyte invasion by Plasmodium falciparum", Nature Communications, 2017 Publication	1%
4	livrepository.liverpool.ac.uk Internet Source	<1%
5	hdl.handle.net Internet Source	<1%

Bhalla, Kuhulika, Monika Chugh, Sonali

6 Mehrotra, Sumit Rathore, Sultan Tousif, Ved Prakash Dwivedi, Prem Prakash, Sachin Kumar Samuchiwal, Sushil Kumar, Dhiraj Kumar Singh, Swapnil Ghanwat, Dhiraj Kumar, Gobardhan Das, Asif Mohmmed, Pawan Malhotra, and Anand Ranganathan. "Host ICAMs play a role in cell invasion by Mycobacterium tuberculosis and Plasmodium falciparum", Nature Communications, 2015.

<1%

Publication

Exclude quotes	On	Exclude matches	< 14 words
Exclude bibliography	On		